Experimental and numerical simulation of degradation of pollutants in water by microbubble-enhanced cold plasma activation -Degradation - Effect of pollutants' initial concentration

by

Nima Shahsavari

A thesis submitted in partial fulfillment of the requirements for the degree of

Master of Science

in

Chemical Engineering

Department of Chemical and Materials Engineering
University of Alberta

Abstract

The necessity to secure reliable water resources has always been a challenge for human societies. Numerous factors contribute to heightened concerns, often resulting in serious crises for governments striving to ensure the provision of clean potable water for diverse purposes. At the same time, overpopulation, global warming, and industrial growth have motivated researchers to think about alternative ways to provide, recycle, reuse and treat water resources. Besides, increased access to social media and stricter environmental regulations compel industry sectors to find suitable, efficient, and feasible approaches to treat their wastewater, so that treated water can be safely disposed of to water bodies or reused in similar applications. There has been a myriad of conventional methods for water and wastewater treatments some of which are still frequently used. However, a more advanced approach capable of being utilized for a wide range of pollutants present in water is still an open research avenue.

First part of this thesis is devoted to coupling cold plasma activation with hydrodynamic cavitation to leverage better mass transfer between gas and liquid phases via microbubble generation and collapse. A modified Venturi tube with an opening is used to allow the self-entrainment of air as the plasma gas into the water flow. Three sample pollutants widely observed in wastewater streams are studied i.e., two antibiotics (sulfathiazole and norfloxacin) and an azo dye (methylene blue). The effects of initial concentration and water flow rate are investigated. Energy yield and degradation kinetics of experiments are also elaborated and applications are extended to larger volumes to show the ability of method to be applied in larger capacities. In the second part, Computational Fluid Dynamic (CFD) simulations are performed

to study the interactions in a three phase system. Cavitation effect is elaborated in detail along with the impact from air as the plasma activated gas. Effect of different water flow rates on the generation and expansion of cavitating bubbly flow is studied and results are validated versus experiments that were conducted in the first chapter. Transient simulations are performed in ANSYS Fluent 2020R2 commercial CFD software. Reynolds Averaged Navier-Stokes (RANS) models are utilized to capture turbulence phenomena and mixture model is considered for multiphase flow. Post processing of results are performed in CFD-Post to better understand the dynamics and physical behavior of the system.

To conclude, this thesis introduces the cold plasma discharge combined with cavitation as a novel Advanced Oxidation Process (AOP) for wastewater treatment. The applicability is shown by testing the method in a wide spectrum of pollutants and results show the successful performance even at higher water volumes. CFD simulations help better understand the complex phase interactions and how cavitation can assist in degradation of endocrine pollutants in water streams. Insights from this thesis can guide future studies on optimizing the system and testing other pollutants where other AOPs do not show effective outcomes.

Preface

This Thesis is original work done by **Nima Shahsavari**. Contents of the chapters come from the following research work: Microbubble-enhanced cold plasma activation for water decontamination: Degradation dynamics and energy yield in relation to pollutant concentration, total volume and flow rate of water (2023). N. Shahsavari, X. Zhang. I am the main author of this research paper and was responsible in doing experiments, analyzing data, developing the methodology, writing and revision of manuscript. Dr. X. Zhang is the supervisory author contributing intellectually and was involved with the manuscript composition.

Acknowledgements

I would like to express my sincere gratitude to Dr. Hao Zhang, my supervisor, who helped me with all steps during this tortuous path. It was with his assistance and guidance that I could accomplish this program. I am thankful for his allowing me to join his research group. I never forget all the moments during this MSc. program when he patiently helped me find an answer to the problems and issues. I acknowledge the funding support from Separation Technologies Ltd. under joint program of Mitacs Business Strategic Internship (BSI). I want to especially thank Dr. Joe Zhou for his support and interest in the research encouraging scientific works in this green and sustainable field. Support from Natural Science and Engineering Research Council of Canada (NSERC) Collaborative Research and Development Grants, the Canada Research Chair Program is acknowledged. This work is partially supported by the Canada Research Chairs program. I should also thank Drs. Hongbo Shi, Mingbo Li and Petr Nikrityuk for their guidance and insight during the project. Many thanks to all present and past members of the Soft Matter Interfaces group for their help, advice, support, and friendship. I am so delighted I had the chance to collaborate with them. In the end, I would like to show the most sincere thanks to my family who gave all their love to me during this program and never stopped supporting me emotionally, mentally, and financially. This thesis is written in their memory.

Table of Contents

List of Tables

List of Figures

List of Symbols

Constants

α	Convergent angle
β	Divergent angle
μ_l	Dynamic viscosity of the liquid
Ω	Unit symbol for electric resistance
ω	Turbulent dissipation rate in k-ω model
ρ_l	Density of liquid
σ	Cavitation number
σ_{est}	Standard deviation
ε	Strain
C_0	Initial concentration
d_{in}	Inlet pipe diameter
Err_{rel}	Relative error
m	Mass
n_e	Electron density
p_v	Water vapor pressure
P_∞	Pressure at open surface
Q_w	Water flow rate
R_c	Condensation rate
R_e	Evaporation rate
Re	Reynold's number
Re_{in}	Inlet Re
T_e	Electron temperature

T_g	Gas temperature
u'	Difference between average and instantaneous velocity
u_{in}	Inlet velocity
u_{th}	Average velocity in throat
v	Velocity
ε	Turbulent dissipation rate in k-ε model

Abbreviations

AC Alternate current.

AOP Advanced oxidation process.

APPJ Atmospheric pressure plasma je.

CAP Cold atmospheric plasma.

CFD Computational fluid dynamics.

DBD Dielectric barrier discharge.

DE Degradation efficieny.

ED Endocrine disruptors.

EY Energy yield.

FVM Finite Volume Method.

GLDBD Gas liquid dielectric barrier discharge.

HC Hydrodynamic cavitation.

HPLC High performance liquid chromatography.

LC Liquid chromatography.

LC-TOF-MS Liquid chromatography - time of flight - mass spectrometry.

LC-MS Liquid chromatography mass spectrometry.

LFS Low force stereolithography.

MB Methylene blue.

NOR Norfloxacin.

NTP Non-thermal plasma.

PAW Plasma activated water.

PDB Potato dextrose broth.

PMB Plasma microbubbles.

QUICK Quadratic upwind interpolation for convection kinematics.

RANS Reynolds Averaged Navier-Stokes.

RF Radio frequency.

RNG Re-Normalisation group.

RNS Reactive nitrogen species.

RONS Reactive oxygen and nitrogen species.

ROS Reactive oxygen species.

SERS Surface enhanced Raman sepctrometry.

SST shear stress transport.

STZ Sulfathiazole.

TKE Turbulence kinetic energy.

VoF Volume of fluid.

Chapter 1

Introduction

1.1 Background

1.1.1 Degradation of pollutants in water

The problem of securing reliable water resources for people has always been a challenge for communities. Population increase and unsustainable utilization of natural resources puts extra pressure on providing water supplies. Besides, global warming makes water tension inevitable and many countries in arid and semi arid regions have started to think about alternative water resources. Recycling water seems to be an efficient approach that does not stress out natural bodies of water and also reduces the wastewater released to the nature. There are many traditional methods to treat water and wastewater with the goal of reusing it either for drinking or industrial purposes. Chlorination[1], boiling and solar disinfection[2], flocculation and coagulation[3], ozonation[4–6], and photochemical treatment[7, 8] are some of the methods fairly investigated in the literature. Although many of these methods are still being used in water treatment facilities worldwide, there are considerations to be made. Solar disinfection and desalination is not effective for water supplies with high concentration of pollutants. However, it is fairly reliable for desalination and in combination with other techniques. In other words, solar disinfection alone cannot degrade many pollutants in water. Treating water with chlorine derivatives obviously adds an external chemical to water which in turn can increase the risk of having an

unhealthy water. Unreacted chlorine along with by-products of reactions can lead to residual chemical species that can harm human bodies. Flocculation and coagulation also has the down side of adding chemicals to water. Nevertheless, it is widely used in water treatment plants. According to Gomez et al. [9], ozonation cause the formation of bromate in water. Additionally, it is mentioned that ozonation is less effective in degrading antibiotic resistant genes compared with chlorination and the intensity should be controlled carefully[10]. Photochemical water treatment is an advanced promising technology for water treatment, but there are some aspects that should be taken into account. Zhao et al. [11] and Sukhatskiy et al.[12] have reviewed the disadvantages of each photochemical treatment system.

There is another major factor when trying to find a reliable solution for degrading chemicals in water. The pollutants chemistry undoubtedly has a major impact on determining which method to be used. Recently, we have faced new array of pollutants that are known as emerging contaminants. Mostly coming from hospitals or farms (due to using pesticides) these emerging contaminants require more effective degradation techniques. Khan et al. [13] states that emerging contaminants are those caused primarily by micropollutants, endocrine disruptors (EDs), pesticides, pharmaceuticals, hormones, and toxins, as well as industrially-related synthetic dyes and dye-containing hazardous pollutants. Advancements in biotechnology and environment engineering necessitates the need to look for more innovative water remediation implementations. Figure 1.1 illustrates life-cycle and distribution of some of these emerging contaminants.

More specifically, antibiotics develop as the bacteria modify and the chemicals and agents that used to be effective in the past lose their advantage. Apart from the chemical nature of pollutants, in some cases the scale of the contaminants requires other methods that are able to penetrate in small micro and nano scales. Micro plastics are one of the examples in this regard. Not only are the micro plastic resistant to many advanced oxidation processes, but also they are abundant in micro scales in

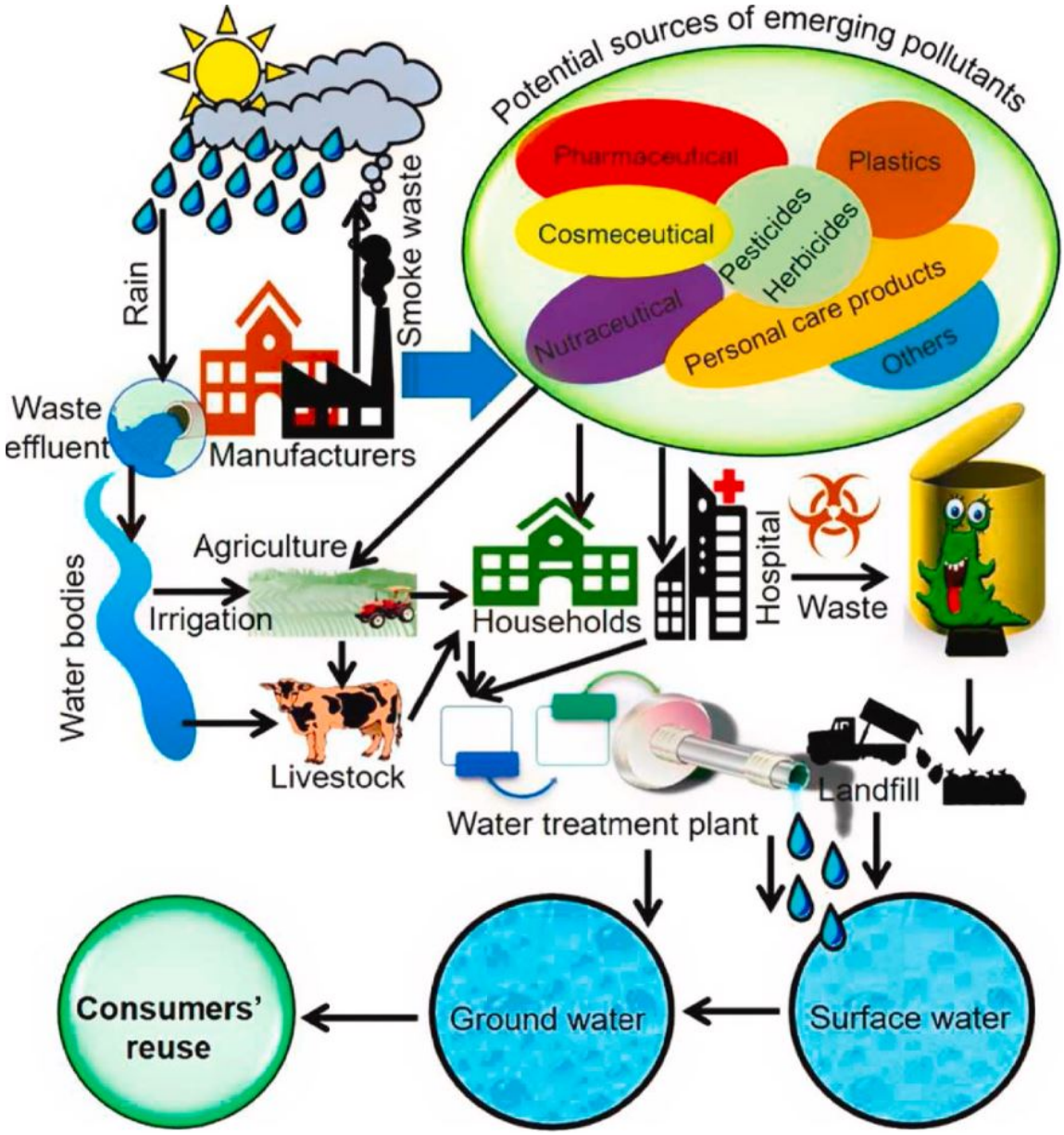

Figure 1.1: Life-cycle distribution of emerging (micro)-pollutants from sources to receptors viewpoint. [13]

open water bodies.

Plasma technology is introduced as a green method that is strong enough to degrade resistant pollutants in water. The flexibility of plasma technology makes it possible to be integrated to most water treatment facilities with different aspects. The unique feature of not adding any chemicals in water makes it more attractive than many competing methods. In addition, the power supply can be provided by renewable energies which reduces the environmental footprints.

1.1.2 Plasma technology

Plasma is the fourth state of matter[14]. It can be produced by subjecting gases such as air, argon and oxygen to high electric energy. The resultant ionized gas is a cocktail of highly reactive oxygen species (ROS) (O, O_3, OH, H_2O_2) and reactive nitrogen species (RNS) (NO, NO_2, NO_3)[15]. Plasma occurs both naturally (such as in solar winds resulting in Aroura Borealis and thunder bolts) and man-made. Huge potential difference causes electron excitation which in turn results in the dispersion of energy in different forms. There are some principal components in plasma systems:

- Charged particles (electrons, negative and positive ions)
- Excited atoms and molecules (vibrationaly and electronically)
- Active atoms and radicals
- UV photons

In order to have plasma, the gas needs to be just partially ionized. Both natural and artificial plasmas are quasi-neutral, which means that concentrations of positively charged particles (positive ions) and negatively charged particles (electrons and negative ions) are well balanced. The range of electron temperature falls in 1-20 eV (1 eV=11600 K) and electron densities (as the possibility of presence of electrons in infinitesimal element of space) are in the range of 10^6–$10^{18} cm^{-3}$. There are approaches

to classify plasma. One conventional method is to consider the temperature of the gas that is to be ionized. In this regard, plasma is categorized into thermal plasma and cold plasma (also known as non-thermal plasma or NTP). In order to have a sense of the temperature scales one must know there are mainly two kinds of temperature in this field. Electron temperature (T_e) which is usually in the range of 1 eV ($\sim$ 11600 K), and gas temperature (T_g) which is attributed to temperature of neutral gas molecules. In some references warm plasma is also added to previous groups as a third category [16, 17]. Based on this logic, in cold atmospheric plasma (CAP) electron temperature can go as high as 2 eV while the gas temperature which is the bulk of gas that we sense in the media remains in room conditions. This phenomenon can be achieved by producing a non-uniform electric field either by applying high voltage field on specific point locations (like sharp edges) or by applying a pulsating electric field which avoids gas temperature to reach high values. Whether we have a non-thermal or thermal plasma, the maximum temperature (T_e) is in the order of 1 eV which is 10 % of the total ionization energy required for ionization process. In other words, in NTP, electron density is smaller but those few electrons have higher temperatures. In contrast, in the case of warm and thermal plasma, T_e does not go so high but greater electron density causes the gas temperature to increase. It should also be noted that for NTP, pressure levels also remain in room conditions following the fact that temperature of gas molecules have not raised so much. Table 1.1 (taken from [16] with some changes) summarizes different types of plasma based on electron temperature, density and gas temperature. The reactive species in CAP (gas phase) can be directly applied to dry samples, or to samples in solution. CAP interacts with water to form additional reactive species, such as hydroxyl radicals, hydrogen peroxide, nitrous and nitric acids. Gas phase plasma can only have surface effects and the penetration of reactive species (O, O_3, and NO) is not considerable. On the other hand, in liquid phase, plasma species can interact with all surrounding components.

Based on the plasma-liquid interactions, plasma-liquid systems can be classified

Table 1.1: Typical features of three types of plasma[16]

	n_e (cm^-3)	T_e (eV)	T_g (K)	P (Pa)
Cold plasma	$\leq 10^{11}$	~ 2	~ 300	≤ 100
Warm plasma	$10^{11} - 10^{12}$	1-2	1500-3000	$\sim 10^5$
Thermal plasma	10^{13}	1-2	≥ 4000	$\sim 10^5$

into direct discharges in liquid and discharges in the gas phase over a liquid [18]. During direct plasma treatment, not only long-lived reactive species are persistently present during the treatment, but also short-lived radicals, atomic and molecular species, and electrons are transferred into the liquid.

1.1.3 Cold atmospheric plasma sources

There are also other classifications for cold plasma made in the literature based on other factors such as reactor type. More frequently systems used in water and decontamination purposes are dielectric barrier discharge (DBD)[19, 20], corona discharge [21–24], and gliding arc (GA)[25–27]. Generation principles of these configurations are described here.

Dielectric barrier discharge

As its name suggests, dielectric barrier discharge is when the current and charge transfer are limited by the dielectric barrier layer covering the electrode [28]. The insulating materials (glass, ceramics, silicon, quartz and polymers) can avoid conversion of plasma into a spark or an arc discharge. As a result, DBD is a safe configuration to generate CAP. DBDs can be generated by using alternate current (AC) (1-100 kV, 50 HZ – 1 MHZ) or pulsed voltage. Power source, the energy input, is associated with the intensity of plasma species, whereas gas type is related to the type of plasma species [28]. There are various DBD electrode arrangements that can be used to produce CAP [18, 28, 29], which are depicted in Fig 1.2. For example, the volume of DBD is

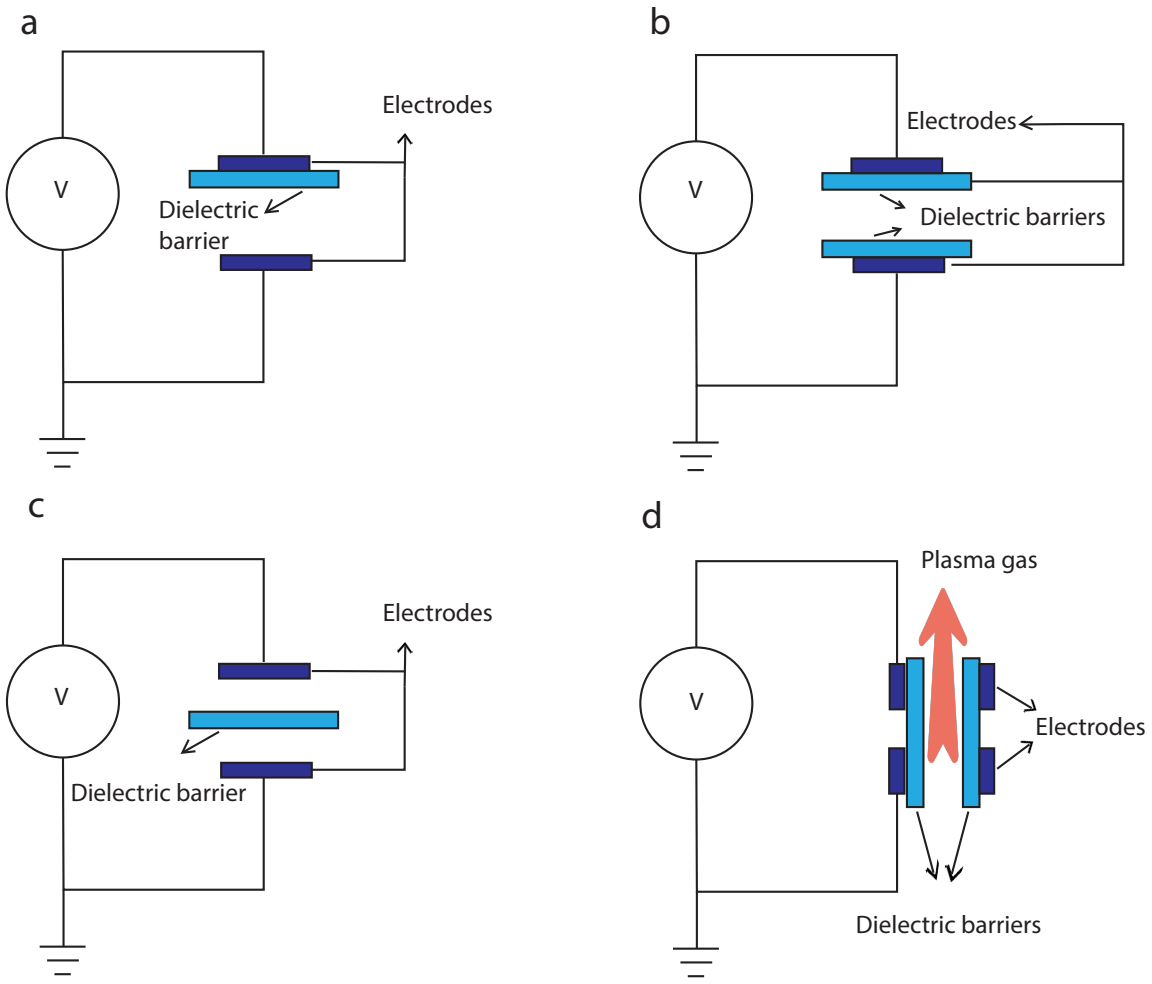

Figure 1.2: Typical configurations of dielectric barrier discharge adapted from [18, 29, 31]

comprised of two electrodes separated with a gap, and the insulating materials can be placed on one electrode or two electrodes (Fig 1.2a, b, and c). DBD is one of the most frequently used types of CAP due to its low cost and versatility. Application range from material science to agriculture and food industries [30].

Corona discharge

Corona discharge occurs when a high electric field is applied to a sharp edge or surface in atmospheric pressure. At that sharp point which is also called "corona", illumination of plasma commences and ionization of gas starts. Due to system configuration, corona discharge alone has been less studied and applied for different

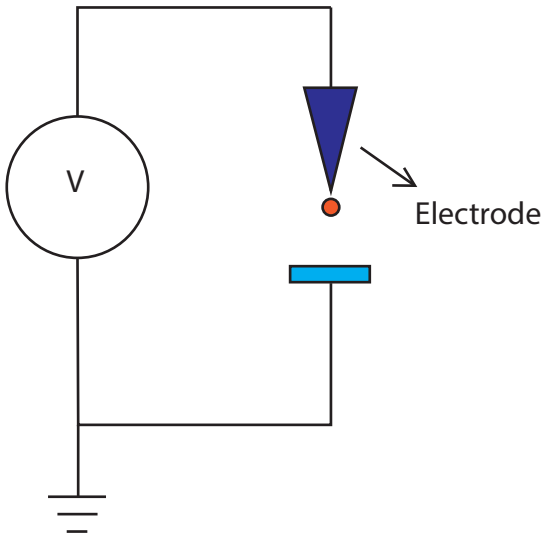

Figure 1.3: Schematic of corona discharge plasma configuration adapted from [18, 28, 31]

purposes. Banaschik et al. [32], have used pulsed corona discharge for degradation of pharmaceutical compounds. It has also been used for removal of textile dyes [33], and pesticides [34].

Continuous mixing of solution (wastewater) during corona discharge is essential for uniform distribution, effective mass transfer, and penetration of ROS species in batch reactors [35]. Wardenier et al. (2019) have reported that although, corona discharge represents good results but it cannot effectively be coupled with large wastewater systems in batch setup [36]. The reason is the short life time of reactive oxygen and nitrogen species (RONS) that are generated in gas phase. Besides, RONS generated may not be able to sufficiently penetrate to deep layers of water and thus may not be able to treat the bulk of water properly. A simplified schematic of corona discharge setup is sketched in 1.3.

Glow discharge

Glow discharge is a well-established and self-sustained plasma discharge that is widely used in analytical spectroscopy [37], textile industry [38], and seed germination [39]. In glow discharge mode, electron density is high and longer proximity where nitrogen

species are emitted can infuse more easily to samples and treat them more effectively. Elevating the operating pressure to higher than atmospheric levels can make the discharge unstable and convert the glow to a spark. Furthermore, operating glow discharge at atmospheric pressure levels require special configurations to obtain stable and uniform glow discharge at atmospheric pressure. For instance, the frequency of power supply should be higher than 1 kHz, dielectric barriers are needed, and the operating gas is best be helium [28, 40]. Thus, the operation of this mode is more difficult and more expensive despite its better performance for degradation.

Atmospheric pressure plasma jet

Atmospheric pressure plasma jet (APPJ) is a broad concept, which includes any plasma source with an open electrode and projection of plasma species into an open area [41]. In fact, in APPJ a stable array of plasma activated species can transfer to another media via a nozzle. As an example for its applications, thermal arc can be applied for etching and cutting in materials industry. For biomedical purposes, APPJ can be utilized for dental treatment, virus deactivation and decontamination of surfaces using different power supplies (AC, DC, RF, pulsed and microwave) and gases. APPJ has been used recently for food germination and microbial deactivation. Veerana et al. (2021) [42] have used non-thermal atmospheric pressure plasma jet to germinate α–amylase in potato dextrose broth (PDB). Normal maize starch was modified to a waxy maize starch by using APPJ [43]. The influence on the structure and physicochemical properties of both starches was demonstrated by treating a 5% starch suspension (w/w) with APPJ for times of 1 to 7 minutes. Nevertheless, APPJ, owing to its small dimensions is usually applied to small scales [44].

It should be mentioned that there are more different classes of plasma based on configuration and generation principles. However, the above-mentioned modes are more frequently used in the case of non-thermal plasma. Other modes and configurations involving warm and thermal plasma can be found in the literature [45–48].

1.1.4 Applications of cold plasma

During past decades, providing a reliable water resource for the growing world population is believed to be a serious challenge. Global warming and requirement to safely dispose wastewater (containing emerging contaminants) are two other compelling factors motivating scholars to think about novel water treatment approaches. Traditionally, biological oxidation, physical adsorption and chemical coagulation have been discussed intensively in the literature [49–53]. In some of the mentioned methods and in majority of conventional degradation processes, introducing new chemical agents and/or requirement to separate the products limits sustainable functionality. More robust techniques with minimum environmental footprints are desired to treat these trace and endocrine compounds.

Plasma is the fourth state of matter[14]. Gas molecules dissociate to other atoms and transfer energy upon contact and collision with other species including electrons, reactive species (radicals, peroxides, super oxides, hydroxyl radicals, singlet oxygen, alpha oxygen) and positive ions[54]. Based on gas and electron temperature, plasma is grouped into thermal, warm, and non-thermal (cold) subsets. Heat that is being sensed mainly comes from gas temperature which can go as high as 10000 K in thermal plasma[17]. Nonetheless, for cold plasma, electron temperature can reach the aforementioned values, while gas temperature and pressure remain at room conditions[16]. This fact has interested researchers to leverage non-thermal plasma for many applications including water treatment, food disinfection, CO_2 utilization, seed germination and etc. Plasma Activated Water (PAW) has been recently introduced as a method capable of being utilized in many applications. The principle in PAW is based on activating a gas media by high energy electric field to provide plasma.Providing a plasma activated environment and passing water through the system causes formation of PAW that can be used for decontamination [55–57], food germination [58–61], pollutant degradation [62–66], E-waste removal [67], and directly for antimicrobial

applications[68, 69]. Plasma can also be used for biomass conversion [70, 71], CO_2 utilization [16, 17], and surface modification. For instance, It was mentioned in [70] that gas discharge plasma can transfer renewable electric energy to chemical energy. This is accomplished by formation of highly reactive media which in turn can be used in agricultural waste valorization. The goal in many of the biomass conversion processes is to raise the energy in the waste and biomass with the aim of converting the raw materials to other more useful commodities or fuels. There are low and medium-temperature biomass conversion processes, including biomass pretreatment and delignification in order to help enzyme or acid-catalyzed hydrolysis to sugars and biomass liquefaction using plasma electrolysis. Besides, high and very high-temperature conversion processes, such as plasma-assisted pyrolysis and gasification to syngas are discussed. This includes plasma application to tar removal, combustion, and vitrification. A summary of plasma technology in biomass conversion is sketched in Figure 1.4. There are many reactions involved in plasma systems producing free radicals, ions and high energy species. Reactive oxygen and nitrogen species (RONS) comprise a great share of radicals generated with different life-times, including long-lived species. It is stated in [54, 72] that hydroxyl radicals (OH), nitrogen dioxide ($\bullet NO_2$), nitric oxide radicals and more durable species such as ozone (O_3), hydrogen peroxide (H_2O_2), nitrate (NO_3^-), and nitric oxide (NO) can be generated with respect to the gas atmosphere. As brought in [73] water molecules react with energetic electrons to form hydroxyl radicals. These hydroxyl groups can combine to form H_2O_2. Then H_2O_2 may react with UV light to yield OH radicals:

$$^*e^- + H_2O \mapsto \bullet H + \bullet OH + e^- \tag{1.1}$$

$$\bullet OH + \bullet OH \mapsto H_2O_2 \tag{1.2}$$

$$H_2O_2 + UV \mapsto \bullet OH + \bullet OH \tag{1.3}$$

Apart form producing many reactive species, NTP can emit UV and visible light, and generate shockwaves capable of inducing cavitation. Some works have investigated

NTP for water and wastewater treatments. Huang et al. [74], have used Dielectric Barrier Discharge (DBD) plasma to decompose methyl orange in water. It was shown that 99 % of dye molecules can be removed after 35 minutes. However, the volume of samples was only 25 mL and also the configuration is in a batch mode. Zhang et al.[75] have used DBD for degradation of norfloxacin in water. The volume was only 1 liter and different combination of O_2 and N_2 were tried. Different discharge schemes and reactor configurations are discussed in [76] and kinetics are analyzed, though in most cases, the discharge happens only at a superficial layer at the surface of liquid, inhibiting efficient collision between reactive species and pollutant molecules.

There are different approaches to put water in contact with plasma environment. Some scholars have tried generating plasma above water surface and then in contact with water [77, 78]. However, some works studied generating plasma in bubbles (Plasma Microbubbles PMBs) [62, 64]. Providing a mechanism to produce bubbles and then providing the plasma-activated air inside them is shown to result higher energy yields compared to GLDBD. In fact, Meropoulis and Aggelopoulos [79]have compared PMBs and GLDBD in their research. It is argued that generating plasma inside bubbles and then having them collapsed in the liquid environment can have a more powerful impact on degrading the pollutant species. In addition, there are more OH radicals in the PMBs compared with GLDBD and the energy yield dominate in the first case (82,1 g/kWh). Improved mass transport in the case of plasma microbubbles cause enhanced kinetics and better energy yields. In this study, hydrodynamic cavitation assists in producing plasma microbubbles. Having the plasma activated media embedded in microbubbles which are generated by hydrodynamic cavitation leverages faster mass transfer and thus more effective pollutant decontamination.

Plasma can also be applied for CO_2 conversion. As stated in [17] plasma is a complex mixture of highly reactive and excited species which is favorable in many applications. Plasma can be categorized to thermal, warm and cold depending on the temperature and pressure conditions. Thermal plasma is referred to the occasions

when the temperature is in the range of 4000 to 20000 K or the at high gas pressures. At temperatures as high as 2300 K the media cannot be effectively used for CO_2 conversion while it can be ideal for coating technology, fine powder synthesis, (extractive) metallurgy (e.g. welding, cutting) and the treatment of hazardous waste materials.

Electrons can be deemed as the initiators of highly reactive chemical mixture. This obvious key advantage of cold plasma: allowing gases as inert as CO_2 to be activated at room temperature by energetic electrons make the cold plasma an efficient process for conversion of CO_2. The second salient advantage of non-thermal plasma technology for CO_2 conversion is its flexibility or turnkey process. This can be immediately switched on or off with conversion and product yield stabilization times generally lower than 30 minutes. Besides, power consumption can be easily adjusted and scaled. Additional advantages of plasma conversion of CO_2 comparing with other emerging technologies include: low investment cost for the reactors (they do not rely on rare earth materials), and their simple scalability from watt to megawatt applications (as already demonstrated by the successful development of ozone generators [80].

Recent works have illustrated there is a transitional plasma type sharing properties of both thermal and cold plasma and is called warm plasma. Since the operating conditions are at the boundary levels, non equilibrium discharges are able to supply (re)active species, and also offer some controlled level of translational temperature. This translational temperature is still lower than electron temperatures but at the same time are much higher than room temperatures and can easily reach up to 2000-3000 K.

The way plasma is used is determined based on the intended application. Reactive species are first produced in gas phase. Then they can be transferred to the solid or liquid surface or stay in a gas phase mixture. In this thesis, we are mainly focused on systems in which plasma is applied to gas-liquid interface as this comprises the bulk

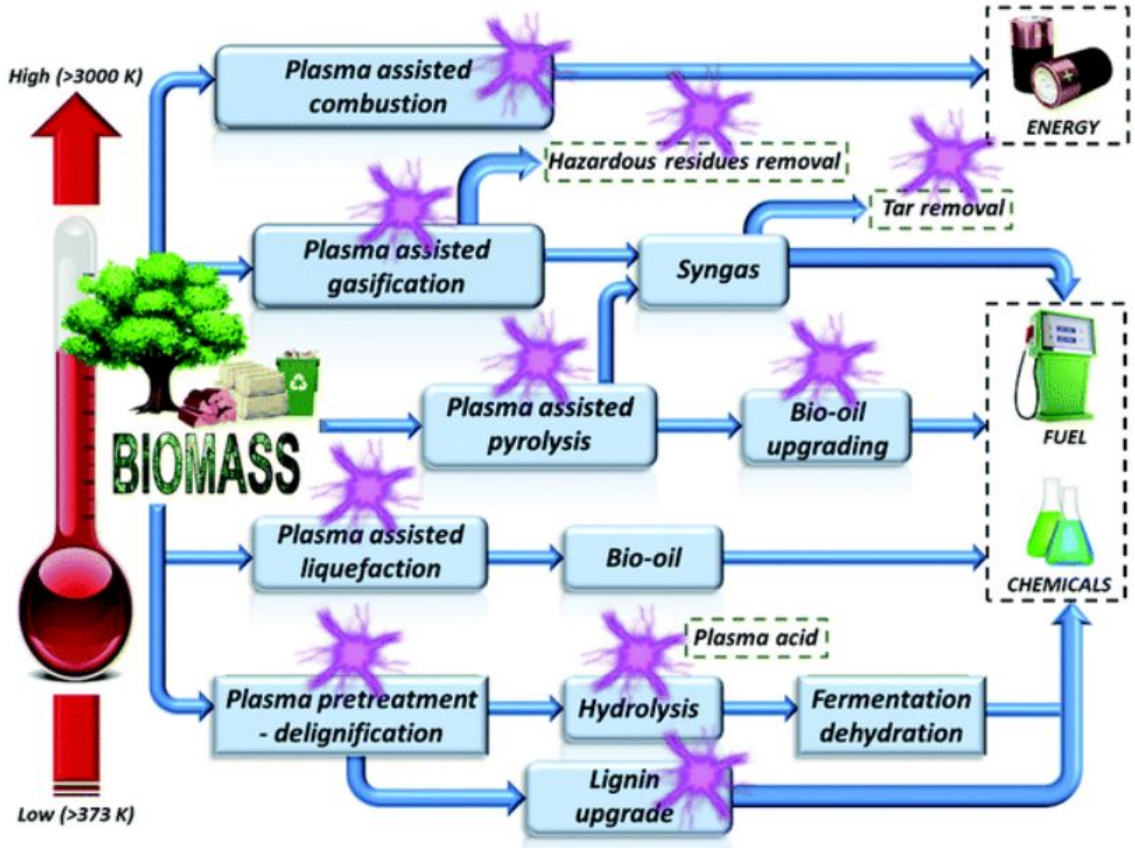

Figure 1.4: Plasma technology for biomass conversion to value-added products.The plasma cartoons represent the usage of plasma been reported. [70]

of projects in water and wastewater treatment with plasma technology.

1.1.5 Gas-liquid interface

One of the major hurdles in chemical industries is the problem of species transport from gas to liquid or vice versa. Attempts are done to enhance the transfer which in turn can intensify the process. By enhancing mass transfer, not only does the mass transfer rate of a device or system increase but energy consumption may be lowered and efficiency may rise. There are many ways to improve gas-liquid mass transfer such as increasing temperature, using nanoparticles and nanofluids [81], improving mixing by optimizing reactor design, and increasing surface area. The goal in all of these methods is to increase the contact time and contact area between gas and

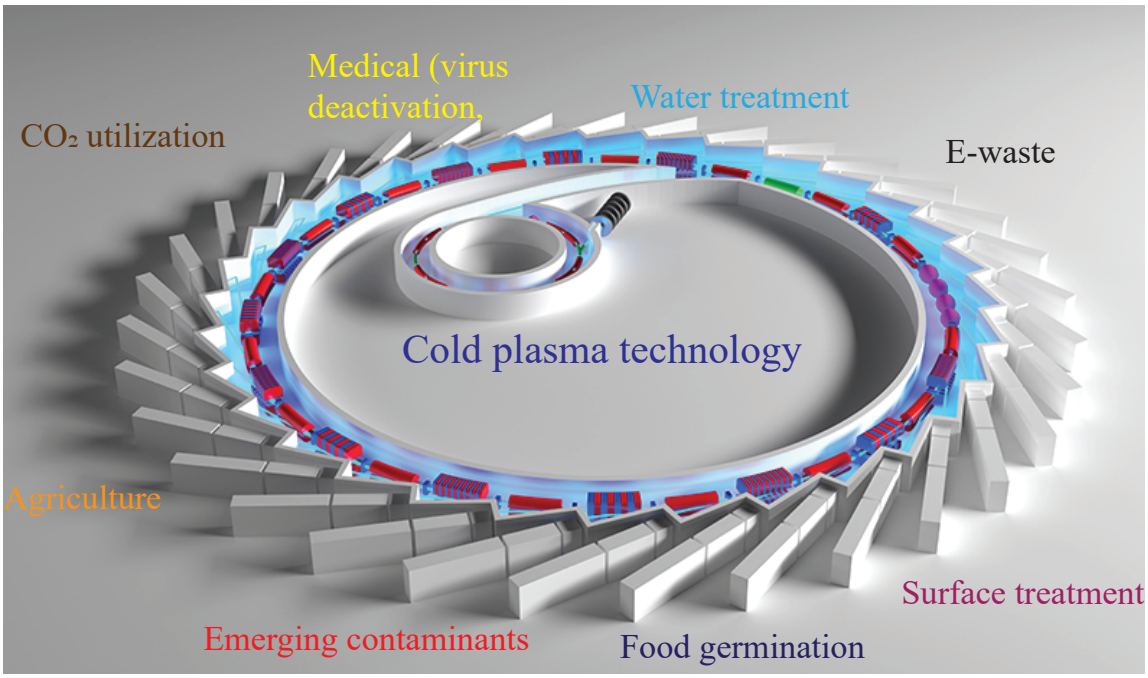

Figure 1.5: Diagram of applications of cold plasma technology in different industries

liquid phases. It is worthwhile to mention that same issue is faced in heat transfer where process engineers search for boosting heat transfer between the phases. One of the novel methods to achieve this target is to use microbubbles. Microbubbles with dimensions in the range of micrometer can yield considerable increase in surface area. Besides, there is no need to add a secondary chemical or particle to improve the mass transfer. The challenge for microbubbles is their generation and stability. Finding economical ways to produce bubbles and optimizing parameters such as pressure, temperature and viscosity to control their collapse can nominate this method as a clean and reliable approach for gas-liquid mass transfer. Liu et. al (2018) have reported that using microbubbles in combination with DBD plasma reactor can enhance the efficiency in degaradtion of aniline in water [82]. Hydroxyl radicals were mentioned to be the major reactive species contributing to degradation of recalcitrant chemicals and microbubbles collapsed under water surface increased production of hydroxyl radicals. More recently, Zhang et al (2021) [83] have tried microbubbles and non-thermal plasma for decomposition of perfluorooctanoic acid. Their research

was conducted in a needle–plate pulsed discharge reactor integrated with a water jet to which microbubbles with different carrier gases (air, N_2, and Ar) were introduced to enhance interfacial reactions. Although concentration of pollutants were high (30 mg/L), high energy requirements (up to 331.95 kWh/m^3) and small scale treatment shows the potential for further work in this field. There are different approaches to generate MBs such as using a gas diffuser, nano-bubble generator, using sonication methods or leveraging cavitation. In this research we are focused on MBs induced from hydrodynamic cavitation which is believed to give further advantages in degradation of pollutants owing to the generation mechanism i.e cavitation itself causes some reactive species to form.

1.1.6 Hydrodynamic cavitation

Hydrodynamic cavitation is one of the Advanced Oxidation Processes (AOPs) that can be used in conjunction with other methods to enhance the overall performance. Variation in pressure causes the liquid to reach below vapor pressure and form micro to nano-sized bubbles. Sudden collapse of bubbles results in transfer of internal gas along with release of massive point source energy. It can be used in a wide range of industries for different applications including wastewater treatment [84], chemical synthesis and food processing to mineral processing [85]. In mineral processing, it improves fine particle flotation efficiency. In flotation, there is density difference and the intended minerals which are hydrophobic agglomerate on top of the surface and can be collected. Flotation efficiency largely relies on the particle size. The recovery rate decreases significantly for particles smaller than 20 µm[85]. Therefore, hydrodynamic cavitation creates a practical approach for efficient fine particle flotation because of raising particle-bubble collision and attachment probability and at the same time decreasing chance of detachment. In summary, using cavitation for flotation has the following advantages: production of micron- and nano-sized vapor bubbles [86], which are effective in better particle aggregation and more effective collision of hydrophobic

particles with bubbles generated after cavitation. A schematic of the flotation column with the cavitation tube is depicted in Figure 1.6.

Few works have combined plasma with bubbles to degrade pollutants[65, 88]. Plasma treatment was enhanced by microbubbles in [65] to activate water for food decontamination and dye decolorization. Compared with systems without microbubbles, degradation rate constant was increased 5 times showing improvement in performance. The setup has the capability of self-injecting air into the chamber thus does not require forced injection of plasma. Another advantage of design is its applicability in a steady mode while allowing plasma-activated air to come in contact with flowing water. In spite of achieving high degradation levels, application was not scaled to larger volumes and the effect of initial concentration was not studied.

Performance of the cavitating Venturi tubes is hugely dependent on the geometry of the device. Factors such as the throat length, the throat diameter or the convergent and divergent angles play a crucial role. With the improvements in Computational Fluid Dynamics (CFD) and new cavitation models, our understanding of this phenomenon has increased. Bashir et al.[89] conducted CFD analyses of different Venturi tubes such as circular, slit, and elliptical Venturies. The throat diameter to throat length ratios were 1:0.5, 1:1, 1:2, and 1:3 and divergent angle (5.5,6.5, 7.5, and 8.5°). Margot et al.[90] tried various 3D turbulence models such as $k-\varepsilon$/low Re/hybrid, $k-\varepsilon$/high Re/standard, $k-\varepsilon$ Re-Normalisation Group (RNG)/standard, $k-\omega$ shear stress transport (SST) and standard/high and low Re/hybrid and standard to study the cavitation flow within a throttle channel at different operating conditions. The $k-\varepsilon$/low Re/hybrid showed better agreement with experimental data.

Some works have focused on studying the hydrodynamic cavitation in Venturi tubes. Shi et al.[87] have done experimental and numerical study on cavitation in Venturi tubes with different geometries. Each Venturi tube has a converging part and a diverging section. The converging angle was selected at 19 and 45°. It was shown that a 45°convergent angle enhances cavitation in comparison with 19°angle.

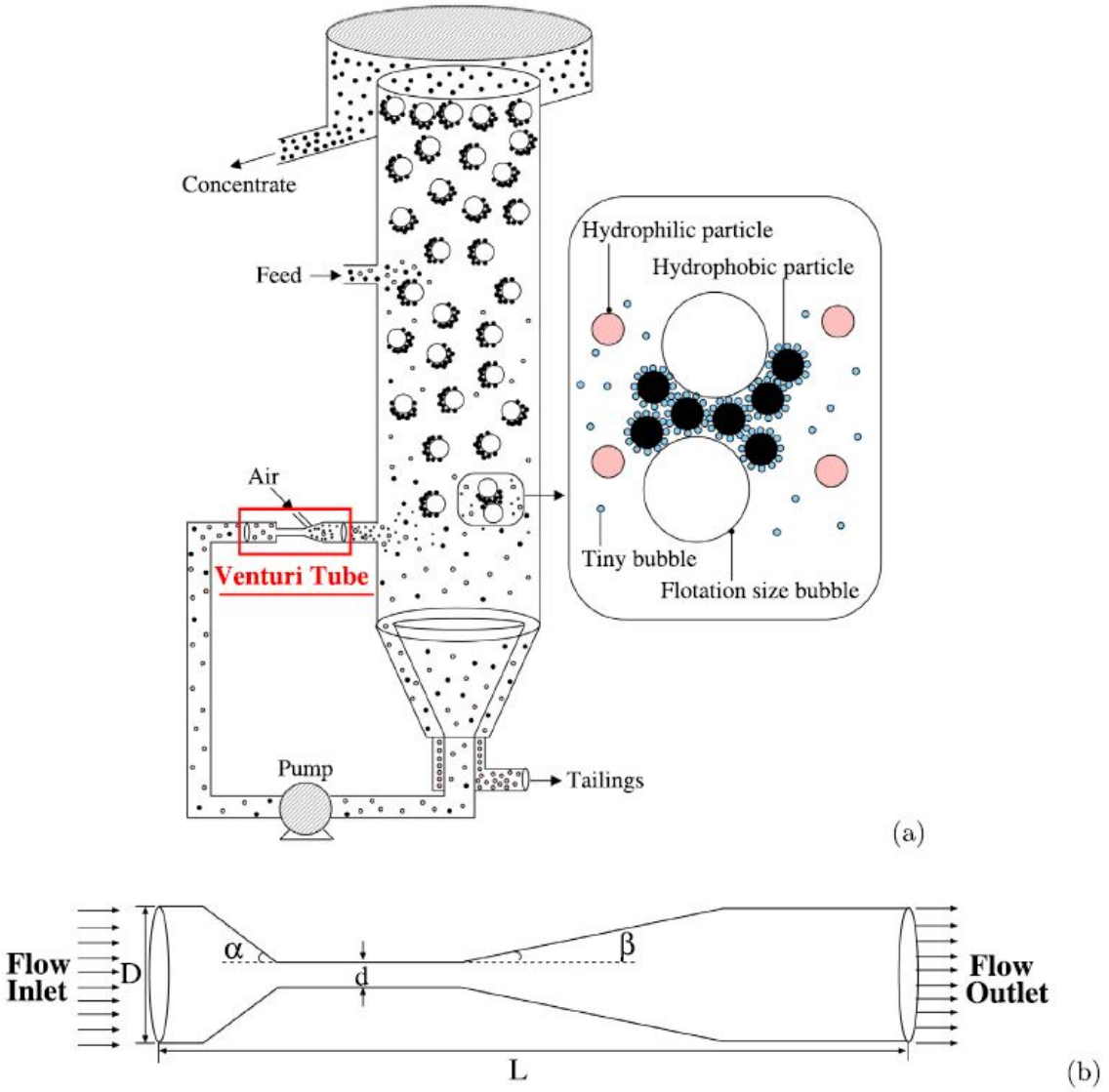

Figure 1.6: (a) Schematic view of flotation column used in mineral processing,(b) scheme of cavitation tube. [87]

The geometry was scaled up using CFD-based numerical simulation.

Dillon et al.[91] have performed experimental and CFD simulations at three water flow rates and three air flow rates. After validating the model with experimental data, it is used to study the effect of diverging angle and throat length/throat diameter ratio on produced microbubble size. It was revealed that increasing water flow rate and reducing the air flow rate produce smaller microbubbles. The prediction from the CFD results illustrated that throat length/throat diameter ratio and diffuser divergent angle have a small effect on bubble diameter distribution and average bubble diameter for the range of the throat water velocities used in the study.

1.2 Motivation

Previously, researchers have focused on studying the effect of plasma in combination with microbubbles. This study brings up a novel Venturi design that utilizes hydrodynamic cavitation along with cold plasma for water and waste water treatment. Few works have studied the synergetic effect of HC-cold plasma [65]. However, effect initial concentration of pollutants is not considered. Besides, by using different water flow rates in the flow system we can better study the effect of water flow rate in the system. Additionally, previous research works did not scale up the setup for larger applications. We have increased the sample column to 2, 10, and 20 L so as to analyze the behavior of the system at larger scales. In the literature, there are some numerical works that aimed to study the cavitation in Venturi tubes [65], but there is no validation for the models and this puts the results under question. Here, we have validated our model with the experimental results and a good agreement is shown. In turbulent flows like the one that is used in this setup, $k-\omega$ model can better capture flow behavior near walls. Therefore, this model is selected for CFD simulations. Mixture model was used for multiphase flow. It assumes that the velocities, temperature and densities of both the liquid phase and the vapor phase are the same at every position in the two-phase fluid field. Another advantage of using

mixture model is its compatibility with cavitation model that is used here.

Apart from studying the effect of initial concentration, three different types of pollutants are considered in order to show the applicability of the system for different water flows. Two antibiotics and a dye are selected to demonstrate the potential for degradation of potentially resistant agents.

1.3 Thesis Objectives

At the first step, this study aims to propose a novel modified Venturi design that can be used in combination with cold plasma technology for water treatment. The setup is prepared in a continuous system and the chemicals are treated in a parametric study. Studied factors include sample identity (chemistry), concentration, volume, and water flow rate. One of the key objectives was to investigate the effect of initial concentration of pollutants as it is a determining parameter in waste water treatment. In some applications, the concentration is so low that cause a challenge for the treatment facilities. Besides, working at the optimized conditions enables researchers to look for green and low cost methods.

CFD simulations are then carried out in the next chapter to demonstrate the applicability of the system for other volumes. Numerical studies allow better understanding of the cavitation phenomenon and its role in the system. Cavitation inception and effect of water flow rate is also studied. Different velocity, pressure and flow characteristics will be examined with the goal of optimizing the operating conditions and optimizing the system. As far as we know, it is the first time using mixture model to simulate the multi-phase flow in modified Venturi tubes and in combination with cold plasma.

1.4 Thesis Outline

In chapter 1, a comprehensive literature review of plasma systems is conducted and different plasma types are explained. Cold plasma is differentiated and focused more in details. There are many different methods and systems that utilize plasma. Some configurations used in the previous research works are illustrated. The application of plasma and more specifically cold plasma is described and its advantages are mentioned. Then concept of hydrodynamic cavitation are explained and its role in different industries is studied. Chapter 2 first summarizes the methodology and chemicals used in the experimental section and then the setup and parameters for the numerical study is explained. The parameters analyzed and formulas used in chapter 3 are described in detail in chapter 2. After that chapter 3 presents the microbubble-enhanced cold plasma activation for water decontamination. Degradation dynamics and energy yield in relation to pollutant concentration, total volume and flow rate of water is studied in this chapter. This is based on the published paper in the journal of Water Process Engineering. In chapter 4, the numerical simulations are performed to show a better understanding of the microbubbles interactions in the multi-phase system. Mixture model is used with $k - \omega$ model for the turbulence. Schnerr-Sauer model is utilized for cavitation in the chamber. Different flow conditions are simulated at different times and flow characteristics are sketched in contours and figures. Chapter 5 brings the conclusion of the thesis and then discusses the future works and the potential of the system to be used for other applications. Besides, parameters such as other chemical pollutants, other volumes, concentrations, and designs are discussed. Key findings and contributions of this work are summarized in chapter 5.

Chapter 2

Methods and procedure

2.1 Methods and procedures for chapter 3

2.1.1 Materials and chemicals

Methylene blue (MB) ($C_{16}H_{18}ClN_3S$), sulfathiazole (STZ) ($C_9H_9N_3O_2S_2$), and norfloxacin (NOR) ($C_{16}H_{18}FN_3O_3$) analytical standard $\geq$ 98 % were purchased from SigmaAldrich (see Fig 2.1). Pure water was obtained from water purification unit (Milli–Q, Merck, Germany), having electric conductivity of 18.2 μ $\Omega.cm^{-1}$ and natural pH of 6.23 at room temperature (25 °C) was measured. Samples were prepared by making stock solutions using pure water. For each chemical used, the respective amount of solid powder was dissolved in water and ultrasonicated to yield the final stock solution.

Concentrations chosen were 2, 5, 8, and 10 mg/L for 0.5 and 2 L volumes and 0.1, 0.5, and 2 mg/L for 10 and 20 L tests. Samples concentrations were quantitatively characterized using UV-visible spectrophotometry following Beer-Lambert's law. The Venturi tube used in this work was fabricated with a 3D printer (Form3 Low Force Stereolithography (LFS)). Preparation procedure is described in detail elsewhere [92]. In brief, the model was designed in SolidWorks, and exported to 3D printer for setting up supports and final layering. The converging angle (α) was 26°and the diverging angle (β) was designed to be 12 °. The diameter of the tube and the throat section were 9.7 mm and 3 mm, respectively. The throat length was 7.5 mm while the neck

diameter (denoted by e) was only 2 mm. A schematic of the model is shown in Fig 2.2.

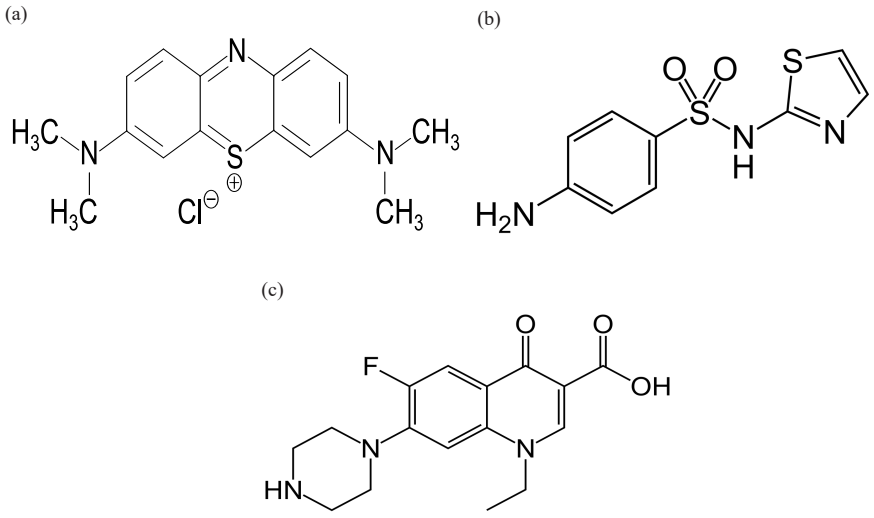

Figure 2.1: Molecular structures of three model compounds. (a) methylene blue (MB), (b) sulfathiazole (STZ), and (c) norfloxacin (NOR) [93–95].

2.1.2 Degradation pathways of pollutants

In the literature, various pathways are pointed out for these chemicals using High performance liquid chromatography-Mass spectrophotometry (HPLC-MS) or Surface enhanced Raman sepctroscopy (SERS) techniques. Possible degradation of MB is represented using LC-MS [96]. High energy ozone, electron and hydroxyl radicals are claimed to be main species responsible for production of intermediates. Presence of peak at molecular weight (m/z) of 284 proves the existence of MB. Demethylation of MB molecules results in generation of structures with m/z of 256, 270, and 228. Organic molecules with m/z values of 292 and 343 are attributed to the hydroxylation reaction. Dissociation of bonds in CH_3–$N(CH_3)C_6H_5$ and C_6H_5–S–C_6H_5 causes the formation of products with molecular weights of 273, 262, and 247[96]. Possible breakage of rings would then cause the formation of compounds with m/z of 170, 135, and 125. Final stage of degradation pathways comprises of mineralization to generation of CO_2, H_2O, SO_4^{2-}, and NO_3^-.

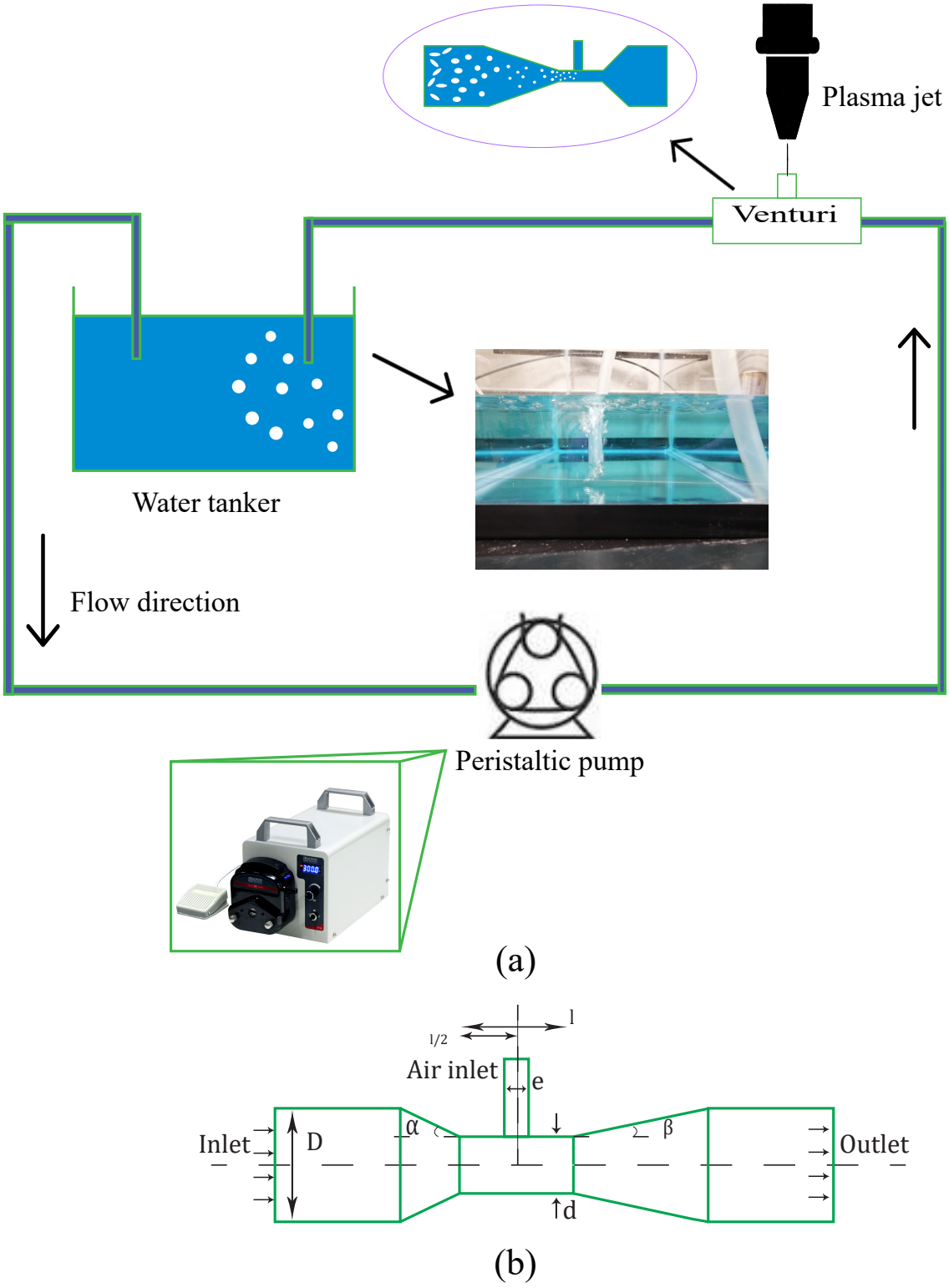

Figure 2.2: (a) Schematic of "Plasma-Venturi" treatment loop. Water is circulated with the pump. Plasma is generated and self sucked through Venturi neck and enters water tanker to close the loop.(b) Geometric model of the Venturi tube used in the system

Plasma treatment of sulfonamide antibiotics including STZ was studied was studied by Kim et al. [97]. Liquid chromatography - time of flight- mass spectrometry (LC-TOF-MS) technique was utilized to analyze intermediates. It is mentioned that ozone can contribute intensively to the degradation of these antibiotics especially when the generated ozone is dissolved in water. As shown in Figure A.2, 5 intermediates are introduced as possible degradation products of STZ. A3 ($C_9H_{11}N_3O_4S_2$ with m/z of 290.0264) results from hydroxylation of thiazole ring. Pathway B begins with hydroxylation of benzene ring and S-N bond in A2 can be broken to yield A1. Following path C, amine group is substituted by hydroxyl to produce A5 which can be oxidized further to A4 ($m/z = 256.0208$, $C_9H_9N_3O_2S_2$), subsequently. Breakage of S-N bond in A5 and A4 can also occur leading to generation of A1(2-amino thiazole, $m/z = 101.0174$, $C_3H_4N_2S$). Finally, more oxidation and mineralization will cause production of oxalate, acetate, and formate (see Figure A.1 Appendix A).

Treatment of NOR with oxygen plasma was studied and 5 degradation products were highlighted [98]. As shown in Figure A.3, at least three pathways can be considered for NOR. C - F bond of NOR breaks to form P1 with m/z=302. Then a substitution reaction on benzene ring starts to yield P5 ($m/z = 318$) due to hydroxyl radical attack [99]. Breakage of C - COOH bond in NOR results in formation of P4 ($m/z = 274$). Additionally, either C - OH bond of NOR or C - F and piperazine bonds are broken to form P3 with $m/z = 304$. Piperazine ring in NOR structure can also be broken to form P2 ($m/z = 279$)[100].

2.1.3 Methodology and experimental setup

The flow loop for cold plasma activation is sketched in Fig 2.2. The setup consisted of a peristaltic pump (WT600-4F, Longer, China), a plasma nozzle (BD-20AC, ETP, USA), a Venturi tube, and containers for liquids being treated. Flow rate is varied from 3 to 5 L/min. Activation time was 30 minutes in most conditions with the exception of sulfathiazole at 2 liter where the activation time was extended to 60

minutes in total. Samples were taken every 5 minutes in the first 20 minutes and every 10 minutes afterwards. Discharge power of the plasma activator was adjusted via the controller knob at the top of the device and was fixed at 40 W. Voltage was also fixed at 15 kV. Pump power was measured using BLUETTI EB70S Portable Power Station 800 W 716 Wh. The values were 26, 35, and 40 W for flow rates 3, 4, and 5 L/min, respectively. Concentrations were measured by UV-visible spectrophotometer model GENESYS 150. Concentrations were increased for more convenient detection with spectrophotometry device. For each activation condition, the experiments were repeated three times and the average values were reported in the plots and calculations.

Degradation Efficiency (DE) is calculated from the following equation:

$$DE = \frac{C_0 - C_i}{C_0} * 100 \tag{2.1}$$

where C_0 is the initial concentration and C_i is concentration at any time t. Degradation dynamics and energy yield (EY) can then be captured using set of below equations:

$$C_i = C_0.e^{-k.t} \tag{2.2}$$

$$EY = \frac{DE * V * C_0}{P * t} = \frac{Pollutant\ degraded}{Energy\ consumed} \tag{2.3}$$

Here, $k\,(min^{-1})$ is degradation rate constant and $EY\,(mg/J\ or\ m^3/kJ)$ is energy yield[101–103]. P (W) is the combined power of the plasma device and the pump and t is treatment time. V is the sample volume which in the case of small treatment is 500 ml and is further raised to 2, 10, and 20 L to treat water in larger volumes. Energy yield consists of volume, initial concentration, time, and efficiency. Therefore this term can be used to analyze the performance of the system. The larger EY conveys more samples can be treated per Joules of energy paid for.

Table 2.1: Solution and flow conditions used in this work

Compound	Initial Concentration (mg/L)	Volume (L)	Flow rate (L/min)
MB	2, 5, 8, 10	0.5	3, 4, 5
	2, 5, 8, 10	2	5
	0.1, 0.5, 2	10, 20	5
STZ	2, 5, 8, 10	0.5	3, 4, 5
	2, 5, 8, 10	2	5
NOR	2, 5, 8, 10	0.5	3, 4, 5
	2, 5, 8, 10	2	5
	0.1, 0.5, 2	10	5

2.2 Methods for Chapter 3, Numerical methodology

Experimental setup is described in detail in [104]. The experimental setup is composed of a peristaltic pump (WT600-4F, Longer, China), a plasma nozzle (BD-20AC, ETP, USA), a Venturi tube, pressure gauge (Digital Remote Transmission Pressure Gauge-Asmik), and containers for liquids being treated. Flow rate is varied from 3 to 5 L/min. Test conditions are brought in Table 2.5. Plasma nozzle is fixed at 15 kV via a rotating knob located at the top of the device and can provide a stable corona discharge. Venturi tube preparation procedure is explained in [92]. Model is designed in SolidWorks, and exported to 3D printer for setting up supports and final layerings. Converging angle (α) is 26°and diverging angle (β) is designed to be 12 °. Diameter of tube and throat section are 9.7 and 3 mm, respectively. Throat length is 7.5 mm while the neck diameter (denoted by e) is only 2 mm. X_1 and X_2 are 600 and 5 mm, respectively. A schematic of the model is shown in Fig 2.3.

Finite Volume Method (FVM) was used for solving transport equations via commercial CFD software package ANSYS ®Fluent 2020R2. For boundary conditions velocity and volume fraction are specified at water inlet and air inlet for all phases.

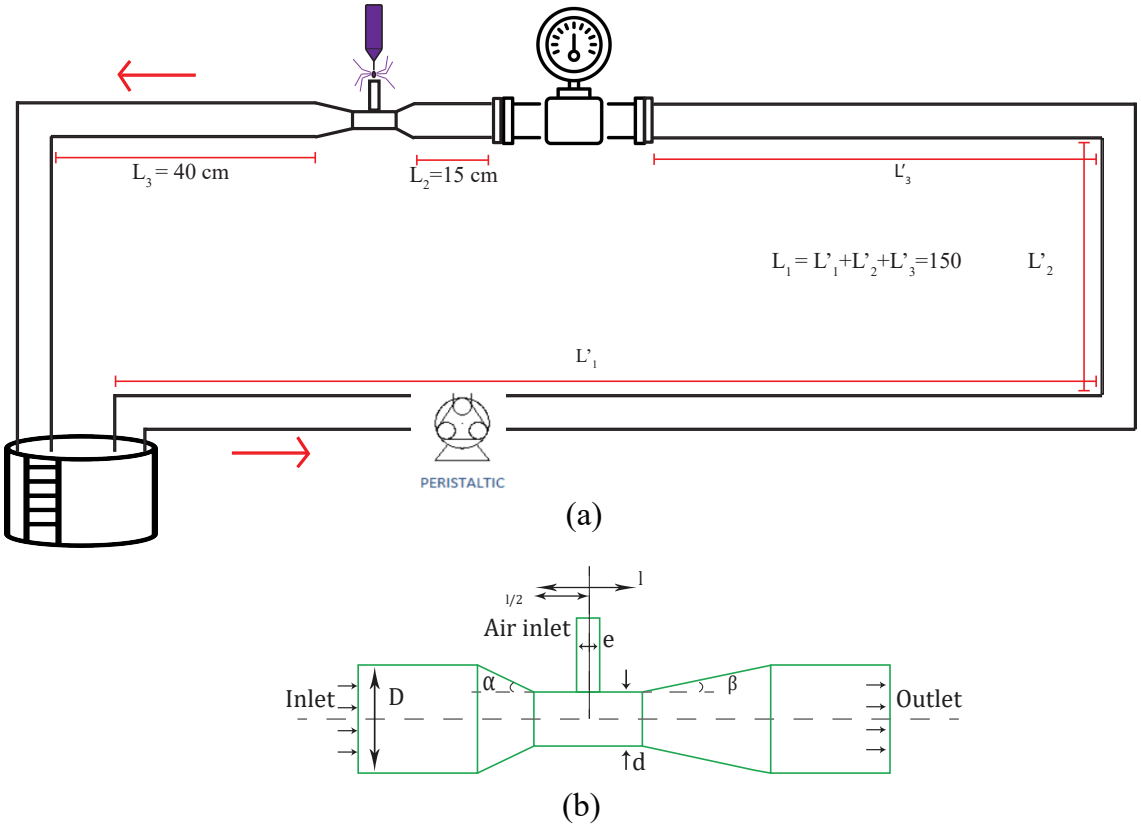

Figure 2.3: Schematic of (a) plasma setup including pressure sensor, Venturi tube, plasma jet and container, (b) Dimensions of the modified Venturi.

For walls, no-slip condition is selected and the outlet has the pressure outlet conditions at atmospheric pressure. Air velocity is specified at the air inlet (Please see Fig 2.3b) in the range 1.06 to 1.42 m/s according to experiments. Water inlet velocity was calculated from flow rate ranging in 3 to 7 L/min. Mixture model was used for multiphase flow. It assumes that the velocities, temperature and densities of both the liquid phase and the vapor phase are the same at every position in the two-phase fluid field. It is also compatible with cavitation model that is used here. The Schnerr-Sauer cavitation model [105] is used to model phase change from water to vapor. Assumptions used in this model are isothermal, incompressible, and zero-slip velocity between the liquid phase and vapor phase. Number of spherical bubbles per volume of liquid should be specified in multiphase model setup. As suggested in the literature [106, 107], it is taken as 10^{13} in this study. It should be noted that the effect of dissolved gas on cavitation is not considered in this model and vapor-induced cavitation is only highlighted [87]. For all cases, vapor saturation pressure is taken constant and is equal to 2338 Pa (at 20 °C).

For turbulence modeling, standard $k-\omega$ model is used which is a Reynolds-averaged Navier-Stokes (RANS) solver capable of solving two-phase turbulent flows [108]. Furthermore, $k-\omega$ model can interpret flow behavior near walls more accurately compared with $k-\epsilon$ model. The foundation is based on Boussinesq hypothesis and comprises of transport equations for the turbulent kinetic energy, TKE, and the specific dissipation rate, ω. Equations used to solve continuity, momentum, volume fraction, Schnerr and Sauer equations for cavitation, and turbulence model are summarized in Table 2.4. Simulation is conducted in a 3D geometry and meshing was carried out in ANSYS ICEM module. Solution parameters used in the mixture model are represented in Table 2.2. Pressure-velocity coupling was used to solve mass and momentum equations. Implicit discretization of pressure gradient terms is combined with coupling scheme to solve the mass and momentum conservation equations. The Quadratic Upwind Interpolation for Convection Kinematics (QUICK) scheme is used

Table 2.2: List of different models and schemes used in multiphase mixture model for modeling three–phase, water liquid-water vapor-air.

Model name	Parameter/scheme
Multiphase	Mixture
Volume fraction parameters	Implicit scheme
Viscous	RANS $k-\omega$ standard
Cavitation	Schnerr - Sauer [105]
Pressure-velocity coupling	Coupled scheme
Spatial discretization: gradient	Least squares cell based
Spatial discretization: pressure	PRESTO!
Spatial discretization: momentum	Second order upwind
Spatial discretization: volume fraction	QUICK [109]
Spatial discretization: turbulence	Second order upwind
Transient formulation	First order implicit

for discretization of convective terms present in volume fraction transport equation. For the convective terms in the momentum equation as well as the terms in RANS turbulence models, second order discretization scheme is used which is more accurate numerically compared with first order schemes[108]. Simulations are performed in transient mode with time step size of 1e-6 s with 20 iterations for each time step. Convergence criteria was set as 1e-4 for continuity, velocity and turbulence. Heat transfer is not included in simulations as the temperature difference is not considerable in the simulation time [65, 87].

For the analysis of the results, cavitation number (σ) is used which represents the potential of a flow to cavitate. Cavitation number (also known as Euler number) is inversely related to the cavitation potential of the flow [110]. In fact, this dimensionless number compares the pressure difference from the flow and the vapor pressure versus kinetic energy. With increase in pressure, velocity also increases but the rate of growth for kinetic energy is one order higher. In Equation 2.4, u_{th} is defined as the

Table 2.3: Physical properties of materials used in numerical model.

Material	Viscosity ($kg/m.s$)	Density (kg/m^3)
Water liquid	1e-3	998.2
Water vapor	1.34e-5	0.5542
Air	1.7894e-5	1.225

average velocity in the throat, and P_v is water vapor pressure. P is the downstream pressure [87] and ρ_l is the density of the liquid. Inlet Reynolds number is defined at water inlet based on Equation 2.5 where u_{in} is inlet velocity, d_{in} is inlet pipe diameter, and μ_l is the dynamic viscosity of the liquid. Numerical results from the transient model are averaged over time using data sampling to get the time-averaged variables and the mean values are retrieved and used in the result section.

$$\sigma = \frac{P - P_v}{\frac{1}{2}\rho_l u_{th}^2} \tag{2.4}$$

$$Re_{in} = \frac{\rho_l u_{in} d_{in}}{\mu_l} \tag{2.5}$$

Physical properties of liquid water, water vapor and air at 20°C is brought in Table 2.3 as in ANSYS Fluent data base.

Table 2.4: Equations embedded in mixture model available on ANSYS Fluent 2020 R2. Equations are used to solve the mixture model for the air-water vapor-water liquid system.

Continuity equation	$\frac{\partial \rho_m}{\partial t} + \bigtriangledown.(\rho_m \vec{v}_m) = 0$
	$\vec{v}_m = \frac{\sum_{k=1}^{n} \alpha_k \rho_k \vec{v}_k}{\rho_m}$
	$\rho_m = \sum_{k=1}^{n} \alpha_k \rho_k$
Momentum equation	$\frac{\partial}{\partial t}(\rho_m \vec{v}_m) + \bigtriangledown.(\rho_m \vec{v}_m \vec{v}_m) = - \bigtriangledown P + \bigtriangledown.[\mu_m(\bigtriangledown \vec{v}_m + \bigtriangledown \vec{v}_m^T)] + \rho_m \vec{g} + \vec{F} + \bigtriangledown.(\sum_{k=1}^{n} \alpha_k \rho_k \vec{v}_{dr,k} \vec{v}_{dr,k})$
	$\mu_m = \sum_{k=1}^{n} \alpha_k \mu_k$
Volume fraction equation for the vapor phase	$\frac{\partial}{\partial t}(\alpha_v \rho_v) + \bigtriangledown.(\alpha_v \rho_v \vec{v}_m) = R_e - R_c$
Schnerr and Sauer cavitation equations	$When\, P_v \geq P_\infty, R_e = \frac{\rho_v \rho_l}{\rho_m} \alpha_v (1 - \alpha_v) \frac{3}{R_B} (\frac{2}{3} \frac{P_v - P_\infty}{\rho_l})^{0.5}$
	$When\, P_v \leq P_\infty, R_{ec} = \frac{\rho_v \rho_l}{\rho_m} \alpha_v (1 - \alpha_v) \frac{3}{R_B} (\frac{2}{3} \frac{P_\infty - P_v}{\rho_l})^{0.5}$
	$\alpha_v = \frac{n \frac{4}{3} \pi R_B^3}{1 + n \frac{4}{3} \pi R_B^3}$
	$R_B = (\frac{\alpha_v}{1 - \alpha_v} \frac{3}{4 \pi n})^{\frac{1}{3}}$
	$n = 10^{13}$
Standard k-ω turbulence model	$\frac{\partial k}{\partial t} + u_j \frac{\partial k}{\partial x_j} = \tau_{ij} \frac{\partial u_i}{\partial x_j} - \beta_w^* k \omega + \frac{\partial}{\partial x_j}[(v + \sigma_w^* v_t) \frac{\partial \omega}{\partial x_j}]$
	$\frac{\partial \omega}{\partial t} + u_j \frac{\partial \omega}{\partial x_j} = \alpha_w \frac{\omega}{k} \tau_{ij} \frac{\partial u_i}{\partial x_j} - \beta_w \omega^2 + \frac{\partial}{\partial x_j}[(v + \sigma_w v_t) \frac{\partial \omega}{\partial x_j}]$
	$\alpha_w = \frac{5}{9}, \beta_w = \frac{3}{40}, \beta_w^* = \frac{9}{100}, \sigma_w = \sigma_w^* = \frac{1}{2}$
	$\tau_{ij} = 2 v_t S_{ij},\ S_{ij} = \frac{1}{2}(u_{i,j} + u_{j,i})$

Table 2.5: Solution and flow conditions used in this work

Compound	Initial Concentration (mg/L)	Volume (L)	Flow rate (L/min)
MB	2, 5, 8, 10	0.5	3, 4, 5
	2, 5, 8, 10	2	5
	0.1, 0.5, 2	10, 20	5
STZ	2, 5, 8, 10	0.5	3, 4, 5
	2, 5, 8, 10	2	5
NOR	2, 5, 8, 10	0.5	3, 4, 5
	2, 5, 8, 10	2	5
	0.1, 0.5, 2	10	5

Chapter 3

Microbubble-Enhanced Cold Plasma Activation for Water Decontamination: Degradation Dynamics and Energy Yield in Relation to Pollutant Concentration, Total Volume and Flow Rate of Water

Nima Shahsavari, Xuehua Zhang

Necessity to safely dispose effluents from industrial wastewater and also water shortage has motivated the search for novel techniques in water treatment. Cold plasma technology is a green, robust, and flexible approach that can sustainably address concerns about removal of pollutants in water. In this study, hydrodynamic cavitation (HC) in a venturi tube is combined with plasma activated water (PAW) in a continuous system to treat two common antibiotics (sulfathiazole and norfloxacin) and an azo dye (methylene blue). HC increases mass transfer of active species generated from cold plasma discharge from gas to liquid by formation and collapse of cavitation microbubbles. Effects of initial concentration, total volume of circulating water, and water flow rate are studied. Results show that operating at flow rate of 5 L/min and volume of 500 mL for 30 minutes, all three pollutants with initial concentration of 8

mg/L or lower can be degraded to more than 80 %. Energy yield and degradation kinetics of experiments are also elaborated. Thus, the setup ameliorates the hurdle of gas - liquid mass transfer. Finally, larger volume samples (2, 10, and 20 L) were treated to show the applicability of the method for more industrial scale levels. Lower concentrated samples degrade faster compared with more concentrated solutions. Besides, a direct relation is shown between water flow rate and degradation signifying the fact that at higher flow rates the amount of reactive species being able to enter the cavitation chamber are greater. The energy yield is estimated to be the highest as the higher initial concentration with short treatment time. Further studies can focus on optimization and extension of the current setup to other chemicals and other gas atmospheres.

3.1 Effect of initial concentration of contaminants in water

3.1.1 Degradation of methylene blue

Degradation dynamics of MB is presented in Fig. 3.1. As can be seen in this figure, samples with lower initial concentration degrade faster and easier compared with more concentrated samples. Fig. 3.1a shows the evolution of UV-visible spectra of samples at treatment time of 5 minutes for different concentrations. Reduction in the peak of intensity implies reduction of pollutant concentration. Fig. 3.1b shows the degradation efficiency (DE) calculated from 2.1 for MB at flow rate of 4 L/min. It is observed that lower concentrated samples are situated higher indicating more DE is achieved at a fixed time compared with highly concentrated samples. Considering 10 minute time interval, DE is 93.7 % for C_0=2 mg/L, and is 67.5, 65.6, and 62.2 for 5, 8, and 10 mg/L, respectively.

Raising concentration of MB causes a competition between reactive species to decompose the molecules present in the flow. As a result, degradation rate slows down.

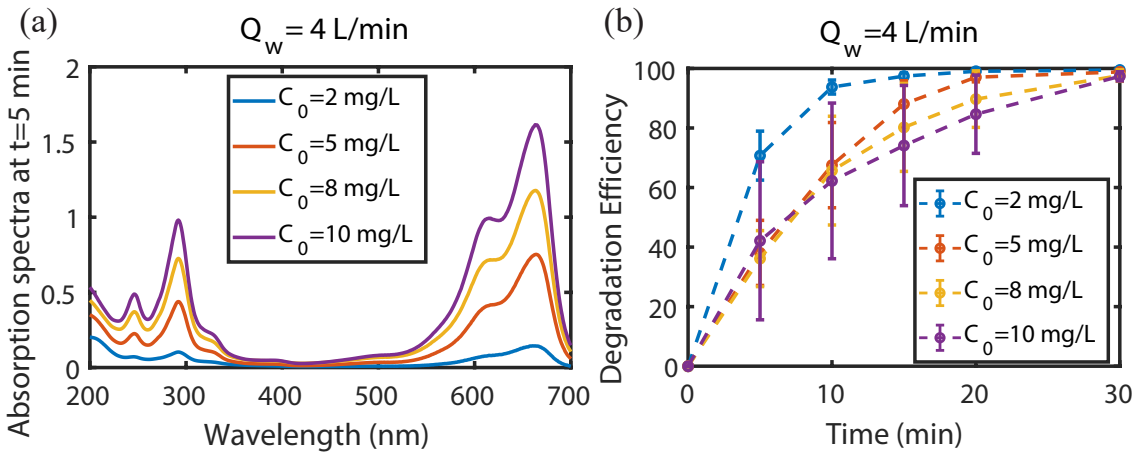

Figure 3.1: Effect of initial concentration on degradation of MB. a) absorption spectra at t=5 minutes, b) degradation efficiency vs time at four initial concentrations. Flow rate is 4 L/min and the total volume of solution is 500 ml.

However, extending the activation time results in nearly full degradation of samples even at rich concentrations [103]. In other words the total amount of pollutants in water can be degraded even starting at higher initial concentrations.

3.1.2 Degradation of sulfathiazole

Results from decomposition of sulfathiazole (STZ) at $Q_w = 4\,L/min$ are illustrated in Fig. 3.2 with the maximum absorption intensity at wavelength of 284 nm. As shown in Fig. 3.2b, samples at the lowest concentration C_0 of 2 mg/L have the highest DE, consistent with the degradation of MB. At treatment time of 10 minutes, the DE values decrease from 86.9 to 34.1 % for initial concentration from 2 to 10 mg/L, respectively.

STZ belongs to sulfonamide antibiotics, harder to degrade when compared with MB. This can also be implied by noting the same concentration (for instance 10 mg/L) treated in parallel activation conditions. DE of MB can reach to 90 % but of STZ can hardly reach 60% at same treatment time of 30 min.It should be pointed out that the biological effects of treated water needs to be verified further before real scale consumption.

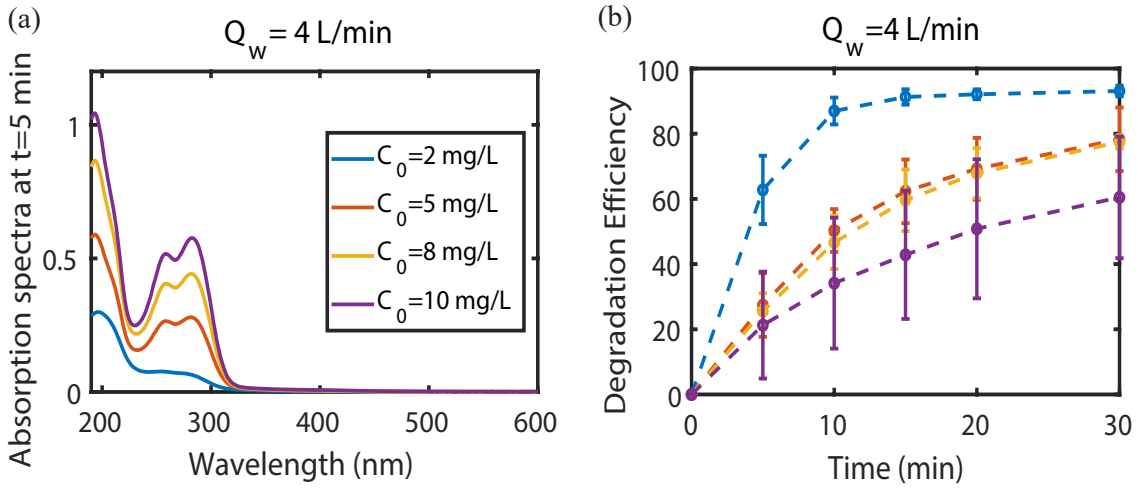

Figure 3.2: Effect of initial concentration on degradation of STZ. a) absorption spectra at t=5 minutes, b) degradation efficiency vs time at four initial concentrations. Flow rate is 4 L/min and the total volume of solution is 500 ml.

3.1.3 Degradation of norfloxacin

A few studies have focused on the effect of initial concentration on plasma treatment of norfloxacin. Zhang et al. [75] have reported that initial concentration has a reverse relation with degradation meaning that increment in concentration leads to decline in degradation. Our results are provided in Fig. 3.3. Absorption peak happens at about 274 nm and the DE and variation in absorption spectra at treatment time of 5 minutes are captured in this figure. After 10 minutes, DE decreases from 81.6 to 59.8. % as C_0 increases from 2 to 10 mg/L, respectively.

The dependence in DE with the increase in the concentration of norfloxacin is consistent with the report in literature [75]. DBD plasma activation with current of 1.8-2 (A) was performed to treat the solution in a centrifuge tube. DE at the initial concentration of 200 mg/L was 30 % after 1 minute of treatment while the respective value for initial concentration of 50 mg/L was three times greater.

Results from figures 3.1 to 3.3 indicate at fixed activation condition (voltage, flow rate, treatment time), the total number of reactive species generated by plasma may be the same. When the initial concentration is low, the reactive species are sufficient

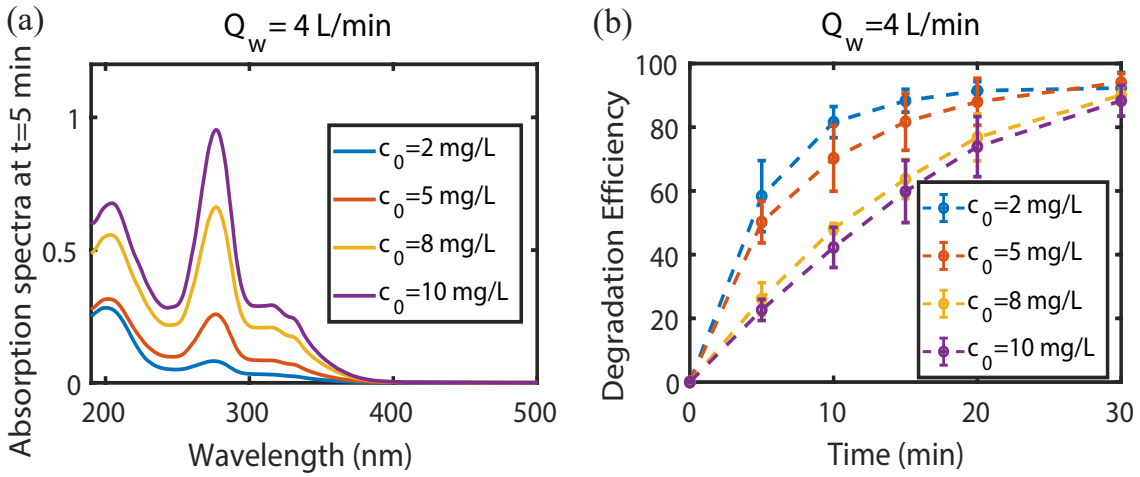

Figure 3.3: Effect of initial concentration on degradation of NOR. a) absorption spectra at t=5 minutes, b) degradation efficiency vs time at four initial concentrations. Flow rate is 4 L/min and the total volume of solution is 500 ml.

to degrade the compounds. It should also be noted that at high initial concentrations the total amount of pollutants that can be degraded is greater, despite of taking longer time to reach a target DE.

3.1.4 Degradation pathways of pollutants

In the literature, various pathways are pointed out for MB, STZ, and NOR using HPLC-MS (High Performance Liquid Chromatography-Mass Spetrophotometry)or SERS (Surface Enhanced Raman Sepctroscopy) techniques. In general, HPLC analysis is used to quantify the residual concentrations of the parent antibiotics molecules whereas UV-Vis spectroscopy investigates both the oxidation of parent molecules along with those with similar conjugate structures which absorb at near wavelengths [111]. Possible degradation of MB is represented using LC-MS [103]. High energy ozone, electron and hydroxyl radicals are claimed to be main species responsible for production of intermediates. Demethylation of MB molecules results in generation of structures with m/z of 256, 270, and 228. Organic molecules with m/z values of 292 and 343 are attributed to the hydroxylation reaction. Possible breakage of rings would then cause the formation of compounds with m/z of 170, 135, and 125. Fi-

nal stage of degradation pathways comprises of mineralization to generation of CO_2, H_2O, SO_4^{2-}, and NO_3^-.

Plasma treatment of sulfonamide antibiotics including STZ was studied by Kim et al. [97]. LC-TOF-MS (Liquid chromatography - time of flight- mass spectrometry) technique was utilized to analyze intermediates. It is mentioned that ozone can contribute intensively to the degradation of these antibiotics especially when the generated ozone is dissolved in water. As shown in Figure S2, 5 intermediates are considered as possible degradation products of STZ. A3 ($C_9H_{11}N_3O_4S_2$ with m/z of 290.0264) results from hydroxylation of thiazole ring. Pathway B begins with hydroxylation of benzene ring and S-N bond in A2 can be broken to yield A1. Following path C, amine group is substituted by hydroxyl to produce A5 which can be oxidized further to A4 ($m/z = 256.0208$, $C_9H_9N_3O_2S_2$), subsequently. Breakage of S-N bond in A5 and A4 can also occur leading to generation of A1(2-amino thiazole, $m/z = 101.0174$, $C_3H_4N_2S$). Finally, more oxidation and mineralization will cause production of oxalate, acetate, and formate (see Figure S1 in Supporting Information).

Treatment of NOR with oxygen plasma was studied and 5 degradation products were highlighted [98]. As shown in Figure S3, at least three pathways can be considered for NOR. C - F bond of NOR breaks to form P1 with m/z=302. Then a substitution reaction on benzene ring starts to yield P5 ($m/z = 318$) due to hydroxyl radical attack [112]. Breakage of C - COOH bond in NOR results in formation of P4 ($m/z = 274$). Additionally, either C - OH bond of NOR or C - F and piperazine bonds are broken to form P3 with $m/z = 304$. Piperazine ring in NOR structure can also be broken to form P2 ($m/z = 279$)[113].In our previous work [65], it is shown that during treatment, pH of water that is initially pure drops to as low as 4. After 30-minute treatment, acidity does not increase much further. As for temperature, it is illustrated that temperature of water does not rise to more than 32°C after 30 minutes of treatment. Additionally, temperature increase only happens in some lo-

cations, not for the whole volume of water. Besides the setup is in a loop hence heat transfer occurs rapidly helping cooling off the water.

3.2 Effect of water flow rate on degradation

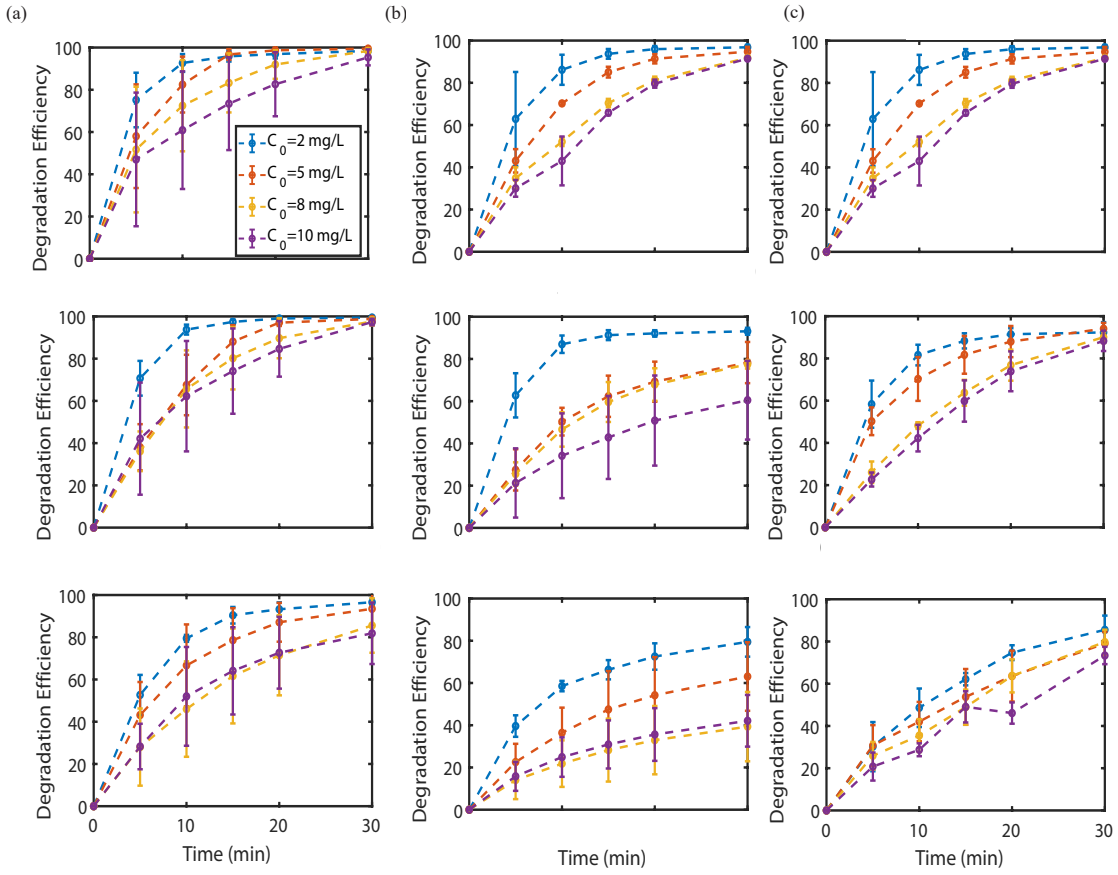

Figure 3.4: Degradation of (a) MB (b) STZ, and (c) NOR at 5 L/min (top), 4 L/min (middle), and 3 L/min (bottom) starting with different concentrations. Same colors in curves represent same initial concentrations from 2 to 10 mg/L. Q_w refers to water flow rate and sample volume is 500 mL.

Fig. 3.4 shows the effect of the flow rate for MB. Moving from 3 L/min to higher flow rates, we can see a shift in degradation efficiency levels, indicating more pollutants are getting degraded with increment in flow rate. This effect is also indirectly shown in the literature [103]. In their setup, air was injected at different rates to the system, different from our setup where air flow is controlled with flow rate of water.

Considering STZ degradation, a low flow rate shows poorer DE as provided in

Fig. 3.4a. At treatment time of 10 minute and for $C_0 = 5\,mg/L$, DE is only 36 %. The respective value at $Q_w = 4\,L/min$ is 50 % and at $Q_w = 5\,L/min$ is 63 %. this clearly conveys the significant effect from flow rate on degradation of compounds in our microbubble-enhanced plasma activation processes.

The effect for norfloxacin is provided in Fig. 3.4. DE values starting with $C_0 = 2\,mg/L$ at $Q_w = 3\,L/min$ is 48 %. Raising the flow to 4 and 5 L/min yields 81 and 86 % degradation. Another point that can be taken from this figure is the sharper slope of degradation in the case of higher flow rates indicating faster removal of pollutants. Also, the difference from $C_0 = 8$ and $C_0 = 10mg/L$ is not notable at different flow rates. One of the main challenges in chemical industries is the problem of mass transfer between gas and liquid phases. Here hydrodynamic cavitation can help with decontamination in the following ways. First, cavitation lowers the barrier of mass transfer between gas and liquid phase resulting in better transfer. Second, at higher flow rates, the volume of plasma air that can be injected from Venturi neck is higher. Consequently, the amount of reactive RONS and other free radicals can be controlled by adjusting water flow rate. Furthermore, it should also be noted that cavitation itself causes generation of highly energetic molecules such as ozone and OH radicals. Hydrodynamic cavitation is utilized in many different industries leveraging the formation and collapse of bubbles. It is simply based on variation in pressure field. At points where the local pressure drops below vapor pressure, micro to nano-sized cavitation bubbles are formed. Then at some points downstream where the pressure reverts to higher magnitudes, abrupt collapse of bubble clouds cumulatively can produce huge point energy. In water treatment, hydrodynamic cavitation has been used in conjunction with advanced oxidization processes to treat micro pollutants in waste streams and free bodies of water [84, 91, 114]. On the basis of formation and growth of bubbles, cavitation can be classified into hydrodynamic cavitation, vaporous cavitation, gaseous cavitation, and vibrational (also known as

Table 3.1: Different plasma systems used for dye removal

Volume (ml)	C_0 (mg/L)	Plasma Configuration	Electrical specifications	Plasma gas	Pollutant	Degradation and treatment duration	Ref
17000	10	Venturi tube + Corona	30 kV, 41.4 W	air	Methyl orange	95 %, 240 min	[65]
100	10	Pulsed corona	40 kV, 0.6 W	air	Methyl orange	90 %, 15 min	[118]
100	10	Pulsed corona discharge	40 kV, 0.6 W	air	Methyl orange	99 %, 25 min	[118]
450	10	Surface discharge	22 kV, 50 Hz	air	Methyl orange	90 %, 15 min	[119]
100	50-75-100-150-200	DBD with air flow from a diffuser	6-8 kV, 30-50 mA	air	Methylene blue	90 % after 30 min	[103]
50	100	DBD plasma with double chamber	6 kV, 18 W	air oxygen	Methylene blue	85.3 % after 100 min 99.98%, 20 min	[102]
20	13.25	Pulsed corona	40 kV	air oxygen	Methylene blue	100 % after 120 min 100 %, 25 min	[120]
170	1 5 10 15	DBD in solution	450 V, 6 A	-	Rhodamine B	100%, 180 min 100%, 210 min 100%, 270 min 100%, 330 min	[121]

acoustic) cavitation[84]. More works on hydrodynamic cavitation can be found in the literature[115–117].

In the current study, hydrodynamic cavitation can assist in plasma treatment due to the fact that it can provide bubbles with greater surface area which in turn leads to better mass transfer from gas to liquid phase. In other words, plasma is the main influential factor and hydrodynamic cavitation can enhance the transfer of reactive agents from gas phase to liquid media. Active species in air are self-injected due to low pressure caused by sudden constriction in flow. Keeping the Venturi geometry constant and increasing the water flow rate results in higher pressure drop inside the throat section of Venturi tube. As a result, more activated air can be injected to the tube.

3.3 Treatment of a large volume of water and potential for scale-up

Application of plasma treatment in most of the previous works is limited to small volume solutions. As outlined in table 3.1, few works have been dedicated to treat large volumes of dyes or other pollutants with plasma. Set-up used in this study can work in continuous conditions rather than a batch process and does not require plasma gas to be entered by force. Self suction of air through the neck and flow system facilitate expanding the method to larger scales. Fig. 3.5 (a) and (b) represents treating of 2 liters MB with 4 initial concentrations. Due to long treatment times

and power considerations, and to better study the effect of parameters at large scales, 0.1, 0.5, and 2 mg/L were chosen as initial concentration levels for volumes of 10 and 20 L. As can be seen in Fig. 3.5b, 62, 89, and 96 % of samples with C_0 of 8, 5, and 2 mg/L could be degraded after 30 minutes. Even in the case of most concentrated pollutant (C_0=10 mg/L) DE of 38 % could be attained after 30 minutes. In these experiments, volumetric flow rate was fixed at 5 L/min and treatment time was tailored experimentally with regard to the compound being tested. It should be pointed out that the same trend between C_0 and DE in small samples also applies here (i.e DE is higher in leaner solutions).

In order to identify and verify the applicability of system for large volume solutions, we performed experiments with 10 and 20 liters of MB solution treated in a same approach as discussed in methodology section. From DE vs treatment curves, provided in Figure 3.5, it can be perceived that the system is capable of treating higher volumes of MB.

Figures 3.5 middle and bottom are associated with results after 30 minutes of treating MB respectively for 10 and 20 liters. At initial concentration of 2 mg/L and after 15 minutes, DE value is 75.40 % for $V = 2\,L$. When the volume is increased to 10 liters, DE gets to 50.76 % and further raising the volume to 20 L gives in the DE value of 33.77 %. This means that even at fixed flow rate, we still can degrade the pollutants at 10 times greater volumes. For 10 liter samples starting with 0.5 ppm of pollutant, we can end up with 93 % of DE after 30 minutes. And doubling the volume to 20 L with $C_0 = 0.5\,mg/L$ we still can reach 67 % degradation after 30 minutes. In the case of 0.1 mg/L samples, above 91 % DE can be obtained after treatment both in 10 and 20 liters tests. Fig. 3.6 shows solutions ($C_0 = 0.1\,mg/L$) before and after treatment. Decoloration is completed for this dye compound using plasma-microbubble scheme. To the best of our knowledge, it is the first time applying plasma treatment of dye waste at these scales.

Experiments are extended to other compounds at different volumes. As plotted

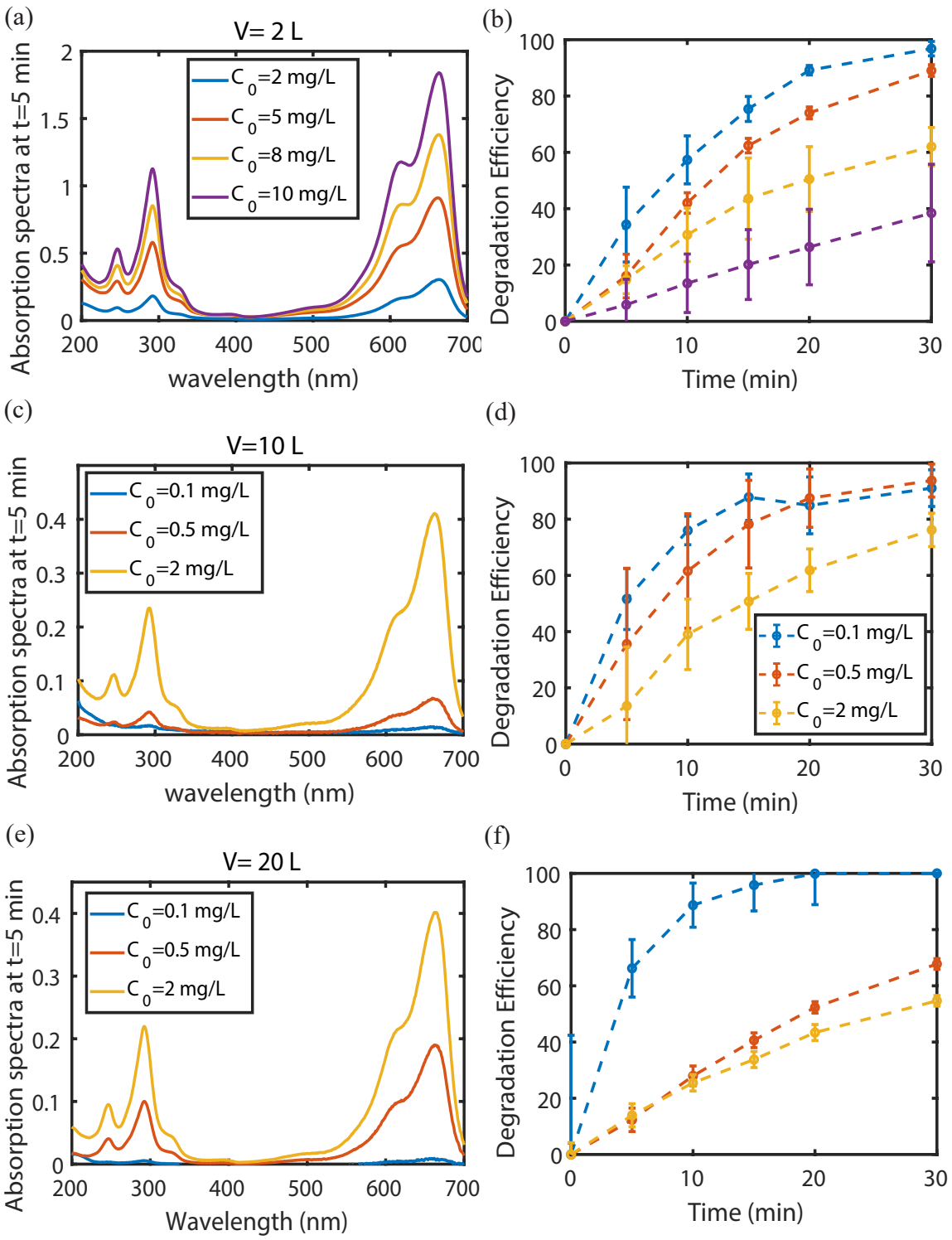

Figure 3.5: (a) UV absorption spectra at time=5 minutes of activation for MB. (b) Degradation efficiency versus activation time. Volume of samples is 2 L. flow rate (Q_w) is 5 L/min and initial concentrations are 2, 5, 8, and 10 mg/L. (c) and (e) UV absorption spectra at time=5 minutes of activation for MB. Initial concentrations are 0.1, 0.5, and 2 mg/L. (d) and (f) Degradation efficiency versus activation time. Volume of samples is 10 and 20 L. Flow rate (Q_w) is 5 L/min.

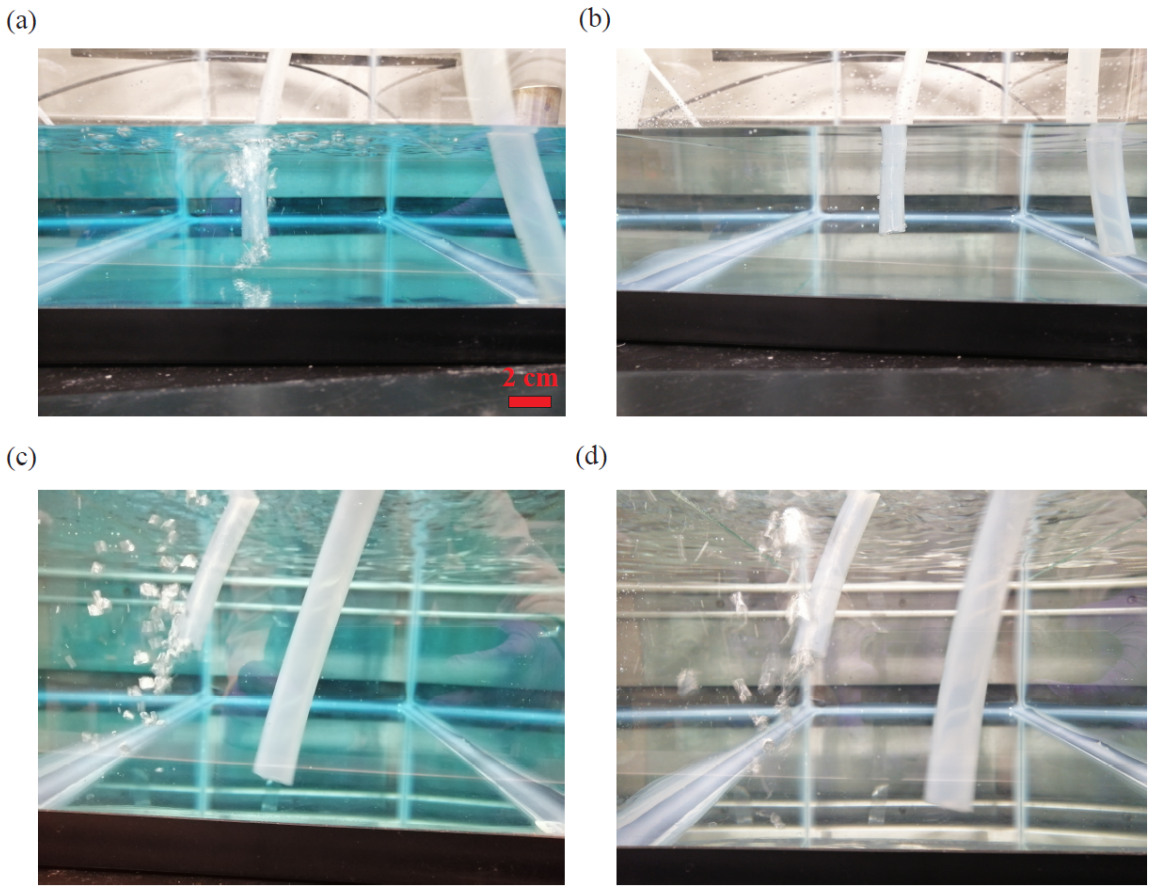

Figure 3.6: MB container with $C_0 = 0.1\,mg/L$ (a) 10 L at start of activation. (b) after 30 minutes of plasma treatment (c) before treatment V=20 L, and (d) after 30 minutes of treatment

in Fig. 3.7, STZ solutions were decomposed during 60 minutes of activation. For initial concentration of 2 mg/L more than 85 % of pollutants can be degraded after 1 hour but more time is needed to decompose samples with higher concentrations at this volume. The reason can be attributed to presence of endocrine benzene and sulfonamide groups at structure of STZ. Either more reactive species or more contact time is needed to fully degrade the samples. It is noteworthy to mention that DE values for lower initial concentrations are higher compared with more concentrated samples.

Tests with volumes of 2 and 10 liter with NOR is done and results are available at Figures 3.7 top and middle. Peak of absorption occurs at 274 nm[75]. NOR can be effectively degraded to more than half in 30 minutes. Increasing the volume to 10 liters, 0.1 mg/L samples are degraded to 90 % and DE values are 86 and 76 % respectively for two higher initial concentrations.

3.4 Kinetic study and energy yield analysis

In this part, the kinetics and energy consumption of the system is analyzed. Results for DE values are calculated based on Equation 2.1. For each experimental condition, the degradation rate constant can be calculated by fitting a pseudo-first order reaction rate on the data at $V = 500\,ml$. Then, these values are plotted against C_0 at each flow rate and results are presented in Fig. 3.8.

For a fixed initial concentration, degradation constant K value is often greater at high levels of flow rate. As can be observed in Fig. 3.8a, rate constants for MB follow a descending pattern with increase in C_0. Values of K start from 0.011 $1/min$ at $C_0 = 5\,mg/L$ and $Q_w = 3\,L/min$ and increase to 0.121 $1/min$ for $Q_w = 4\,L/min$ and finally to 0.180 $1/min$ at same concentration and for flow rate of 5 L/min. With respect to STZ at $C_0 = 8\,mg/L$ (see Fig. 3.8 b) the rate constants start from 0.017 $1/min$ for $Q_w = 3\,L/min$ and increase to 0.056 and 0.067 $1/min$ for two higher flow rates. The descending pattern between K and the initial concentration applies at all

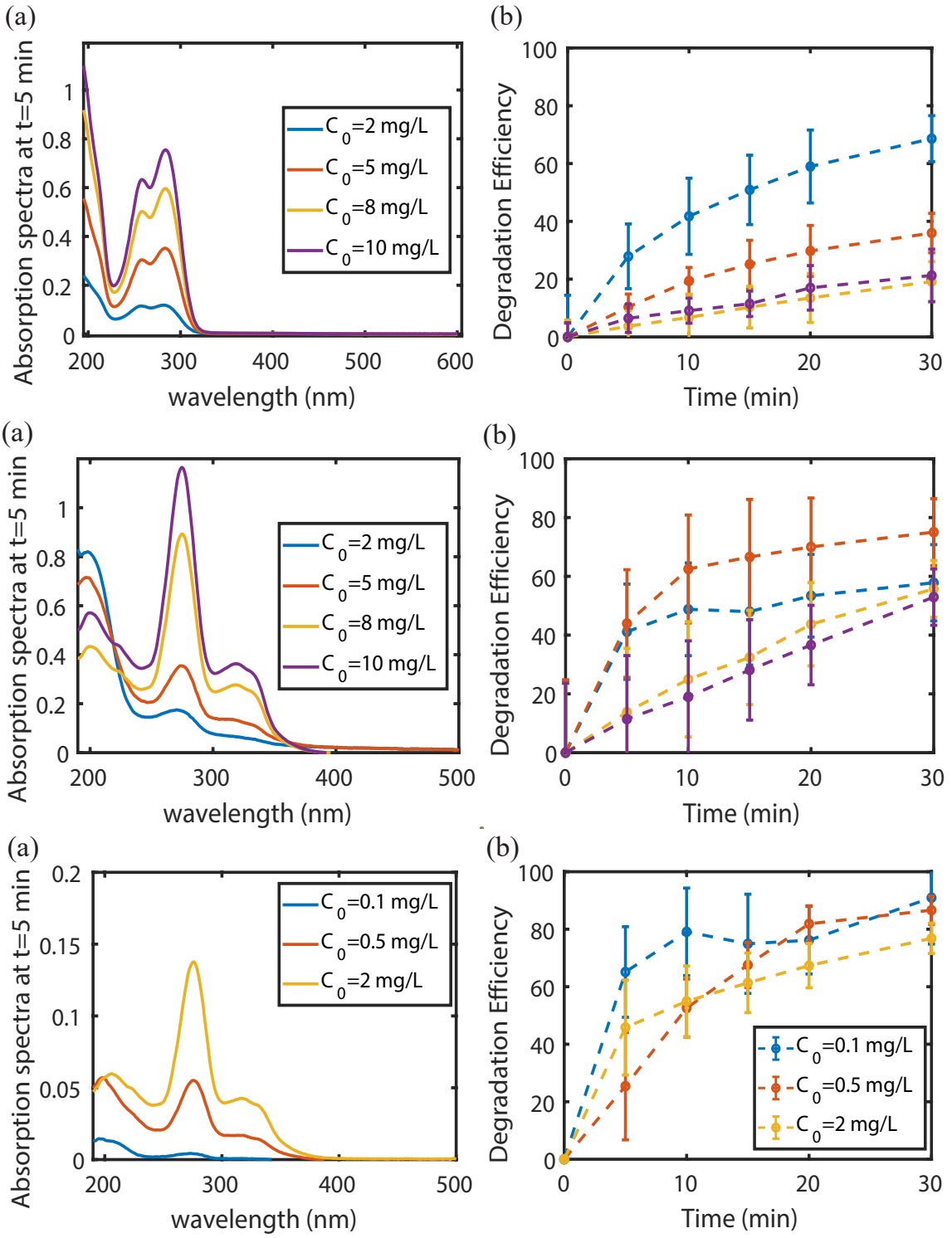

Figure 3.7: (a) UV absorption spectra at time = 5 minutes of activation for STZ. (b) Degradation efficiency versus activation time. Volume of samples is 2 L. Flow rate (Q_w) is 5 L/min and initial concentrations are 2, 5, 8, and 10 mg/L. (a) UV absorption spectra at time = 5 minutes of activation for NOR. (b) Degradation efficiency versus activation time. Volume of samples is 2 L. flow rate (Q_w) is 5 L/min and initial concentrations are 2, 5, 8, and 10 mg/L. (a) UV absorption spectra at time = 5 minutes of activation for NOR. (b) Degradation efficiency versus activation time. Volume of samples is 10 L. flow rate (Q_w) is 5 L/min and initial concentrations are 0.1, 0.5, and 2 mg/L

flow rates. For norfloxacin (see Fig. 3.8 c), the rate constants are 0.038, 0.063, and 0.072 $1/min$ for $C_0 = 10\,mg/L$ at Q_w from 3 to 5 L/min.

Following the initial concentration series, rate constant for MB at $Q_w = 3\,L/min$ and $C_0 = 5$ is 0.076. The respective value for same flow rate is 0.1502, 0.051, and 0.04 for $C_0 = 2, 8, and 10\,mg/L$. In the case of STZ, at fixed Q_w of 3 L/min, rate constants are 0.051, 0.026, 0.011, and 0.014 $1/min$ for C_0 of 2 to 10 mg/L. Finally, for NOR and at specific flow rate of 3 L/min, K = 0.077, 0.057, 0.054, and 0.043 $1/min$ for initial concentrations of 2, 5, 8, and 10 mg/L.

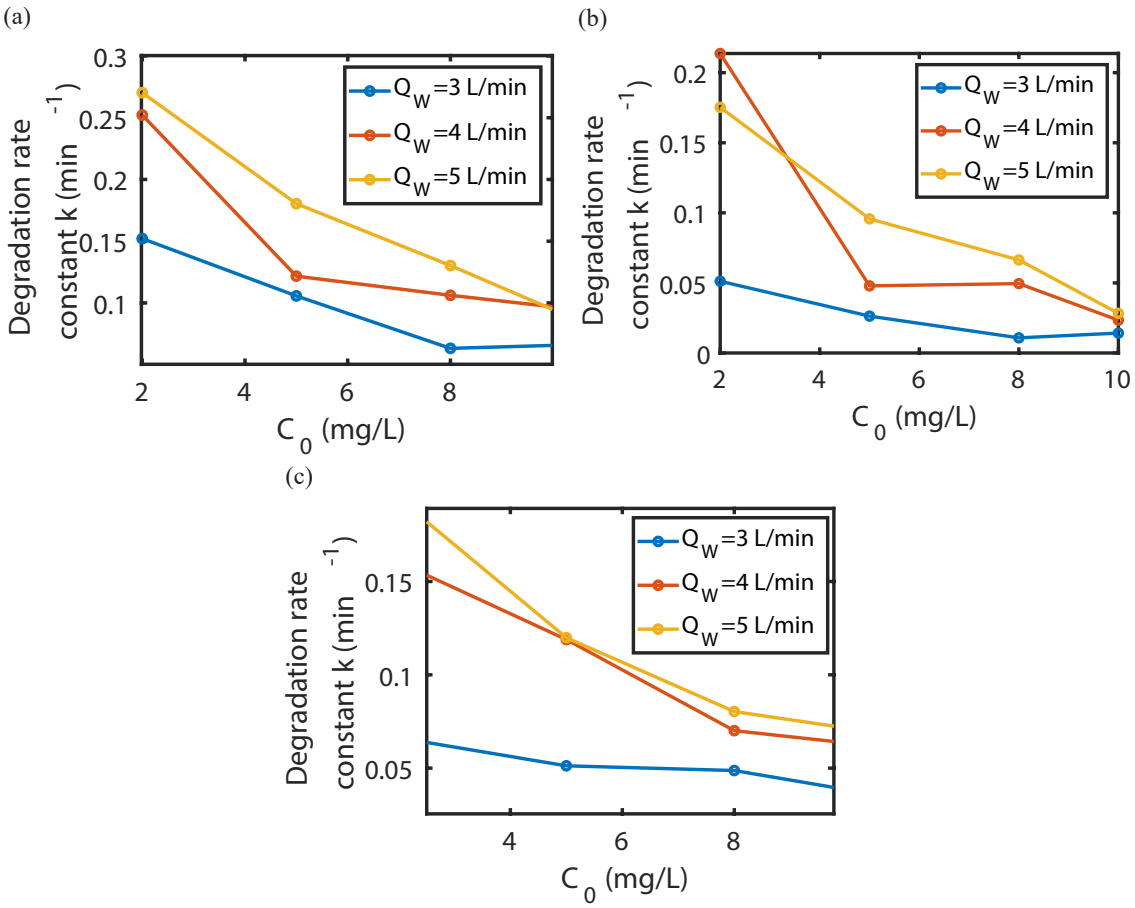

Figure 3.8: Degradation rate constant k for (a) MB, (b) STZ, and (c) NOR at different flow rates plotted as a function of C_0. Initial concentrations vary from 2 to 10 mg/L and volume of samples is 500 mL

In order to further analyze the energy used to decompose each pollutant, energy yield [102] is defined and calculated based on Equation 2.3.Energy Yield (EY) shows

mass of solution being degraded per unit of energy consumed. Plotting EY curve against time for each one of the compounds at various initial concentrations results in Figure 3.9.

As can be seen in Fig. 3.9, energy yield tends to decrease with increase in treatment time. This is because the amount of energy being consumed increases as time elapses. In other words, energy yield conveys the amount of pollutants that can be decomposed per Joules of energy. What's more, in most of conditions, at a fixed flow rate, energy yield increases at higher initial concentrations. For instance, EY for MB at $Q_w = 3\,L/min$, $t = 5\,min$, and $C_0 = 10\,mg/L$ is only 6.93 mg/kJ. In contrast the respective value for $C_0 = 2\,mg/L$ is 2.58 mg/kJ. Similar trend is observed in the case of STZ and NOR. As presented in Fig. 3.9b,e, and h, the gap between various initial concentrations are larger for STZ and NOR compared with other pollutant.

However, this difference is gradually reduced at higher flow rates since DE values are improved at greater flow rates (Fig. 3.9e and Fig 3.9h). Comparing results for NOR at flow rate of 3 L/min (see Fig. 3.9c) at treatment time of 10 min, EY values are 3.52, 3.48, 2.58, and 1.19 mg/kJ for $C_0 = 10, 8, 5$, and $2\,mg/L$, respectively. At same conditions results are 3.05, 2.14, 2.23, and 1.43 L/kJ for STZ. Furthermore, the respective values for MB are 6.37, 4.51, 4.09, and 1.95 mg/kJ. It be inferred from above mentioned comparison that MB is showing to be degraded more easily followed by NOR, and STZ. This is also elaborated in the results of degradation at higher volumes (V=2 L). However, increasing the plasma voltage and increasing residence time can help decontaminating STZ even at higher volumes and concentrations.

Results of EY for three compounds at higher flow rates are shown in Figure 3.9 (d-i). In general, there is improvement in EY in most cases because of the augmentation in hydrodynamic effect. For instance, EY for MB at t=10 min and $C_0 = 5\,mg/L$ ranges from 3.81 to 4.30 mg/kJ for Q_w ranging from 3 to 5 L/min. For STZ, considering treatment time of 10 minutes and C_0 of 5 mg/L, the energy yield varies from 2.23 to 3.32 mg/kJ with flow changing from 3 to 5 L/min. The change in EY for

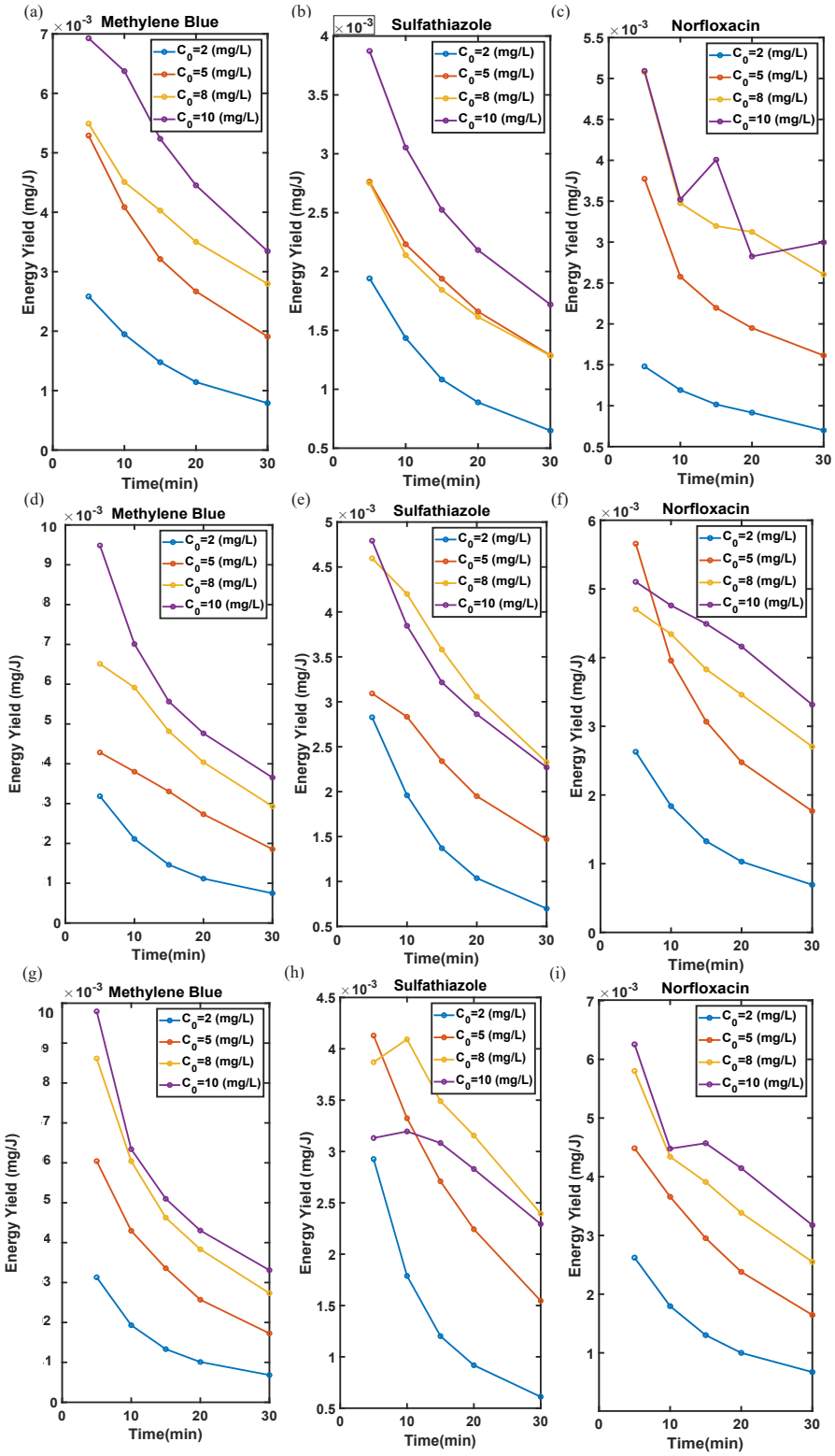

Figure 3.9: Energy yield EY plotted as a function of treatment time for (a-c) MB, STZ, and NOR at $Q_w = 3\,L/min$. (d-f) MB, STZ, and NOR at $Q_w = 4\,L/min$. (g-i) MB, STZ, and NOR at $Q_w = 5\,L/min$. Initial concentrations are 2,5,8, and 10 mg/L.

norfloxacin is smaller ranging from 2.58 to 3.95 mg/kJ when looking at $C_0 = 5\,mg/L$ at $t = 10\,min$. This is confirmed when looking at the DE values at stated conditions. The same trend is also reported in the literature[102] where the yield is defined as the quantity of pollutant removed (g) per discharge power ($kW.h$). Increase in treatment time results in consumption of more energy and despite of increase in DE, the overall energy yield drops.

3.5 Conclusion

A setup design that integrates a cavitation tube and plasma discharge in air is used for microbubble-enhanced cold plasma activation to remove various pollutants in water at low concentrations. This novel setup design enables scale up and treatment of a large volume of water. The model compounds methylene blue, sulfathiazole, and norfloxacin are degraded in a small (500 ml) and larger volumes (2,10, and 20 L) with lower initial concentrations degrade faster than their more concentrated counterparts. The reason may be attributed to the fact that at any fixed plasma discharge, there is a certain amount of reactive species capable of removing pollutant molecules. Therefore, RONS and other free radicals cannot effectively react and degrade molecules. Increasing water flow rate can enhance the degradation performance by means of improving hydrodynamic cavitation and self-suction of more reactive species into the flow. Degradation efficiency of methylene blue reaches more than 70 % with three initial concentration levels ($C_0 = 0.1, 0.5$, and $2\,mg/L$) for 10 and 20 liters. Among three compounds tested, sulfathiazole is degraded less from same treatment time in larger volumes. Energy yield (EY) is a measure for the compound degraded by per unit of energy consumed. This study demonstrates the potential of microbubble-enhanced cold plasma activation as a sustainable approach for water and wastewater treatment in a flow system.

Chapter 4

Numerical simulation of cold plasma system for degradation of pollutants in water

With the growth in world population and increase in demand for a reliable water source, the search for a green water resource is ongoing. There are certain features when thinking to a premium water resource such as being recyclable, having lowest possible environmental footprints, and being cheap and accessible to communities. Non thermal plasma technology is a clean energy able to treat wastewater.

Hydrodynamic Cavitation (HC) is considered as an Advanced Oxidation Process (AOP) which can be coupled with other treatment methods to enhance the overall performance. The key factor is the variation in pressure that causes the formation of microbubbles and in turn with their collapse, the polutants get degraded. Combining cold plasma with hydrodynamic cavitation can be a novel green method that can be nominated as a reliable water source.

In this study, Computational Fluid Dynamic (CFD) simulations are performed to study the interactions in a three phase system. Cavitation effect is elaborated in detail along with the impact from air as the plasma activated gas. Effect of different water flow rates on generation and expansion of cavitating bubbly flow is studied and results are validated versus experiments that were conducted in the first chapter. Transient simulations are performed in ANSYS Fluent 2020R2 commercial CFD

software. Reynolds Averaged Navier-Stokes (RANS) models are utilized to capture turbulence phenomena and mixture model is considered for multiphase flow. Post processing of results are performed in CFD-Post to better understand the dynamics and physical behavior of the system.

4.1 Grid independence

In order to ensure the independence from grid refinements on numerical results, grid independence study is done using three meshes. Hexahedral structured grids are generated in ICEM meshing which is embedded in ANSYS ®CFD package using blocking and O-grid methods. Grid 1 is the most coarse grid with 1406000 elements, grid 2 consists of 1839000 elements, and grid 3 comprises of 2293000 elements. A schematic of grid 2 is shown in Fig 4.1.

The purpose in grid independence analysis is to ascertain the effect from refinement of calculation grid is minimal in results. Therefore, refining the mesh from grid 1 (the most poor grid) to grid 3 (the finest grid) should not cause considerable change in the flow behavior. As shown in Fig 4.1 d and e, pressure at center-line passing through the pipe is taken as the flow variable. As can be observed in Fig 4.1 e, refining the grid from grid 2 to grid 3 does not improve the results considerably. Thus, to maintain good accuracy and moderate computational cost simultaneously, all the simulations are performed using the fine grid. Other researchers have also used the same approach to perform mesh independence analysis [122, 123]

4.2 Model validation

To validate the results obtained from the numerical model, experimental data are used and compared with numerical model. As elucidated in Fig 4.2, there is good agreement between the simulation results and the experimental results. Both data sets are time-averaged pressure at the inlet of the Venturi tube and the experiments

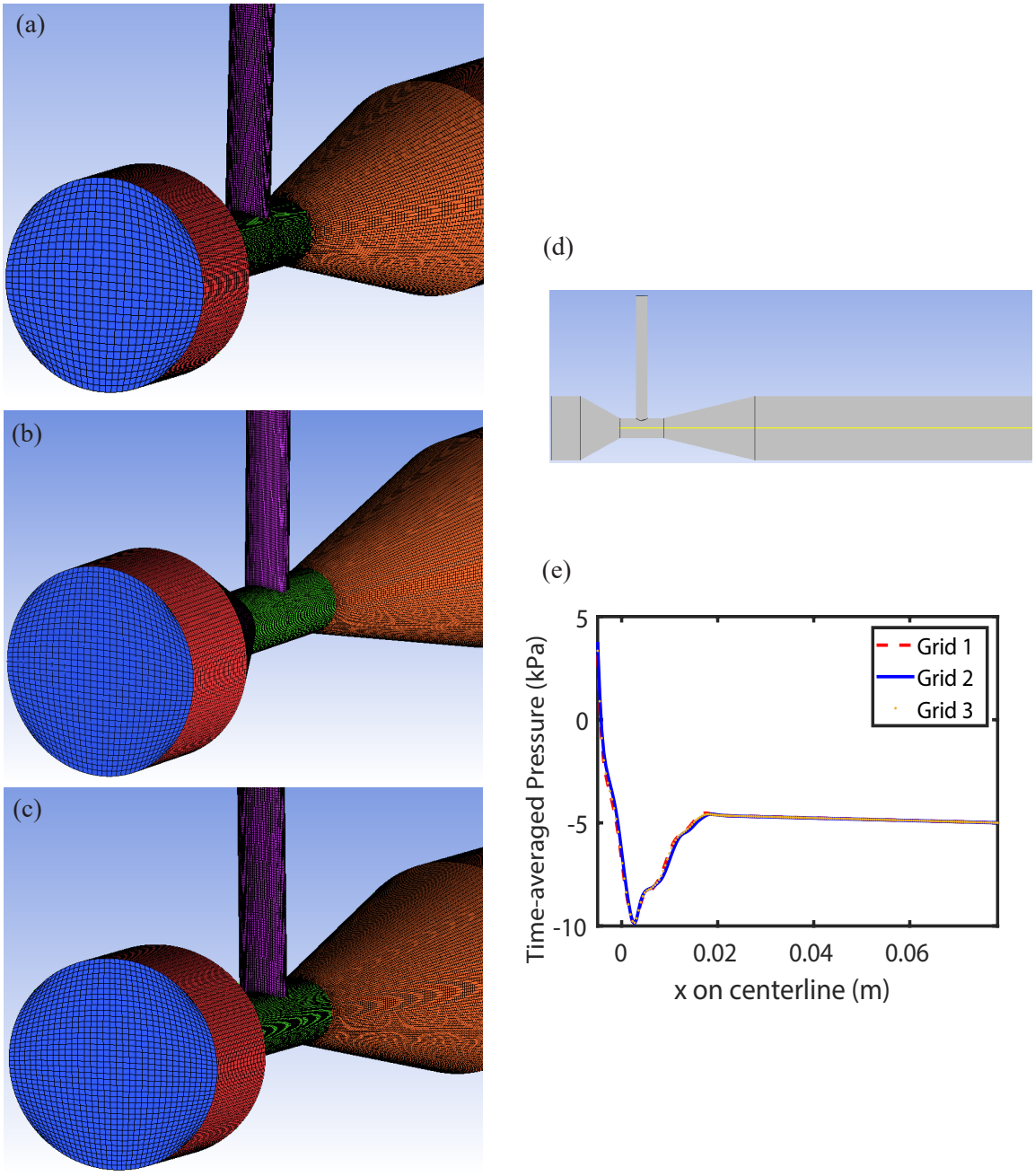

Figure 4.1: Schematic of grids used in mesh independence study (a) grid 1 (b) grid 2 (c) grid 3. (d) center-line where the flow variable is plotted. (e) time-averaged pressure plotted in the center-line for three grids.

are measured with water flow rates varying from 3 to 6 L/min with increment of 0.5 L/min. The trend as reported in the literature [87, 123] tends to increase with the increase in water flow rate. Maximum relative error of numerical results is 6.37 % calculated based on Equation 4.1 where F represents the pressure at Venturi inlet. Standard deviation from the experimental results can also be calculated according to Equation 4.2 [87] with the value of 2.64 %. σ_{est} is the standard deviation, and N is number of data points.

$$Err_{rel} = \frac{|F_{exp} - F_{numerical}|}{F_{exp}} \times 100 \tag{4.1}$$

$$\sigma_{est}\% = \sqrt{\frac{\sum(F_{exp} - F_{numerical})^2}{N}} \times 100 \tag{4.2}$$

4.2.1 Cavitation inception

In cavitating flows, the start of the transition from liquid to vapor is known as cavitation inception. As elaborated in Fig 4.3 (a), Re at inlet is plotted as a function of cavitation number. cavitation number is inversely related to the potential of a flow to cavitate [110], thus lower values represent higher Re numbers a well as higher inlet water flow rates. As can be observed in 4.3 (a) there is a variation in the trend before and after a critical σ number where can be taken as the inception of cavitation. It should be mentioned that unlike systems with only water, here presence of air plasma ameliorates the sudden change in the trend of $Re - \sigma$ [124]. Based on the numerical results, at flow rate of 4.5 L/min which corresponds to $Re_{in} = 9.8e3$, volume fraction of vapor begins to raise sharply (see Fig 4.3 (b)). Vapor volume fraction is calculated considering the time-averaged values over the whole fluid domain. Similar trend is also reported in the literature [87, 110, 123]. Relationship between pressure drop across the Venturi and the Re at inlet is shown in 4.3 (c). There is an ascending pattern with increase in flow velocity which causes higher pressure drop when the

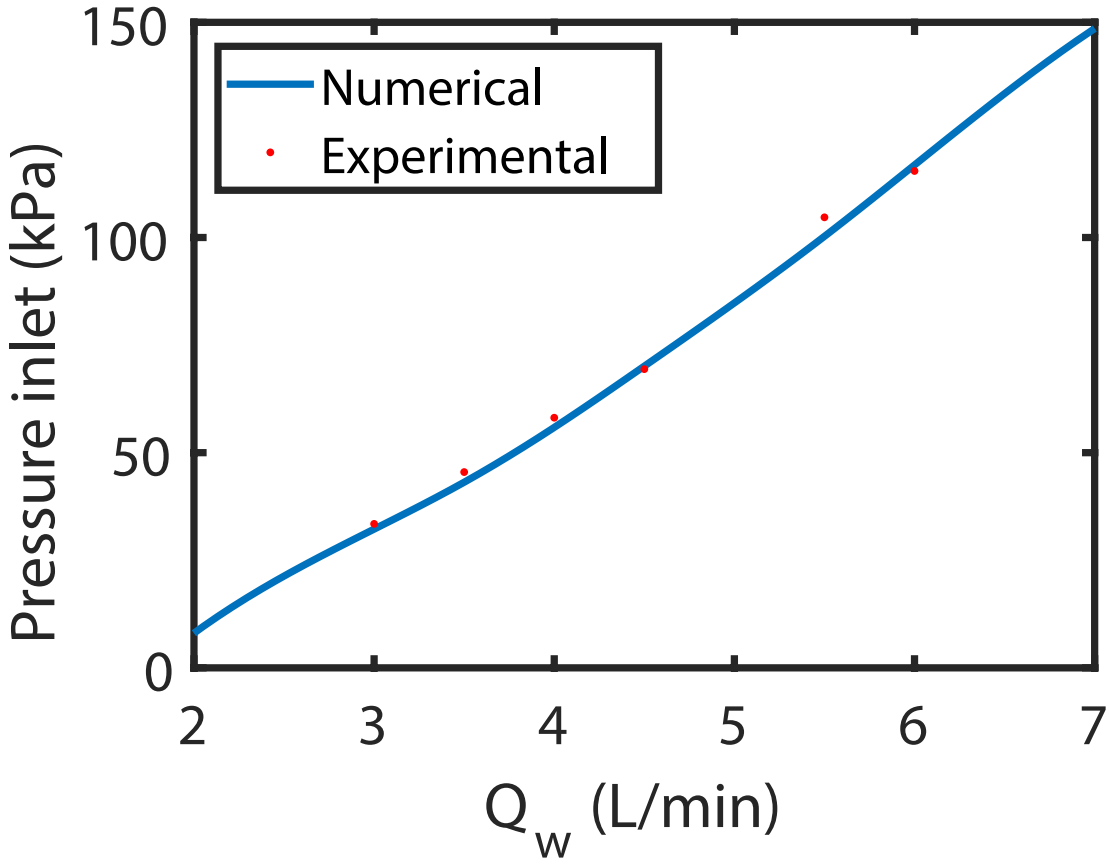

Figure 4.2: Validation: Experimental and CFD results of average pressure at the inlet of the Venturi tube

flow passes through the constriction region [87, 110]. In other words, higher velocities cause higher pressure drop thus making local pressure drop to lower than vapor pressure. As a result more water can cavitate. This is also in agreement with the results in 4.3 (d). As can be observed in this figure, volume fraction of vapor and air are plotted with respect to cavitation number. Around σ value of 1.76, vapor volume fraction starts to grow more rapidly which signifies more water is vaporizing after this flowrate. On the other hand, noting the volume fraction of air in the same diagram (see Fig 4.3 d) it can be inferred that air volume reduces with increment in vapor present in fluid domain.

4.3 Simulation results

4.3.1 Air self-suction

In this section effect of water flow rate on self injection of plasma air is discussed. In conventional Venturi tubes passage of flow from a constriction causes variation in pressure field. This sheds light on the idea to change the design to leverage the pressure drop inside the throat of tube. In current design, reduction of pressure to sub-ambient levels causes air (which is activated with plasma discharge) to flow spontaneously inside the throat. As shown in Fig 4.4, air volume rendering is shown in three cases for times= 0.1, 6, and 10 ms. Starting from flow rate of 3 L/min the amount of air that is being injected grows. In all cases, from left to right more air can be entrained into the chamber with elapse of time. Air plasma that gets trapped in the Venturi then can release the reactive species to degrade the pollutant molecules. Comparing Flow rates (4.4 (A) to (C)) higher water flows can cause more intensive air flow rate. It should also be mentioned that increasing water flow rate also adds to operation costs. Therefore, there is a balance between operating at higher voltages or longer times (plasma generator factor) or increasing the water flow rate (pump factor). Based on the experiments conducted here, maintaining the flow level at 5

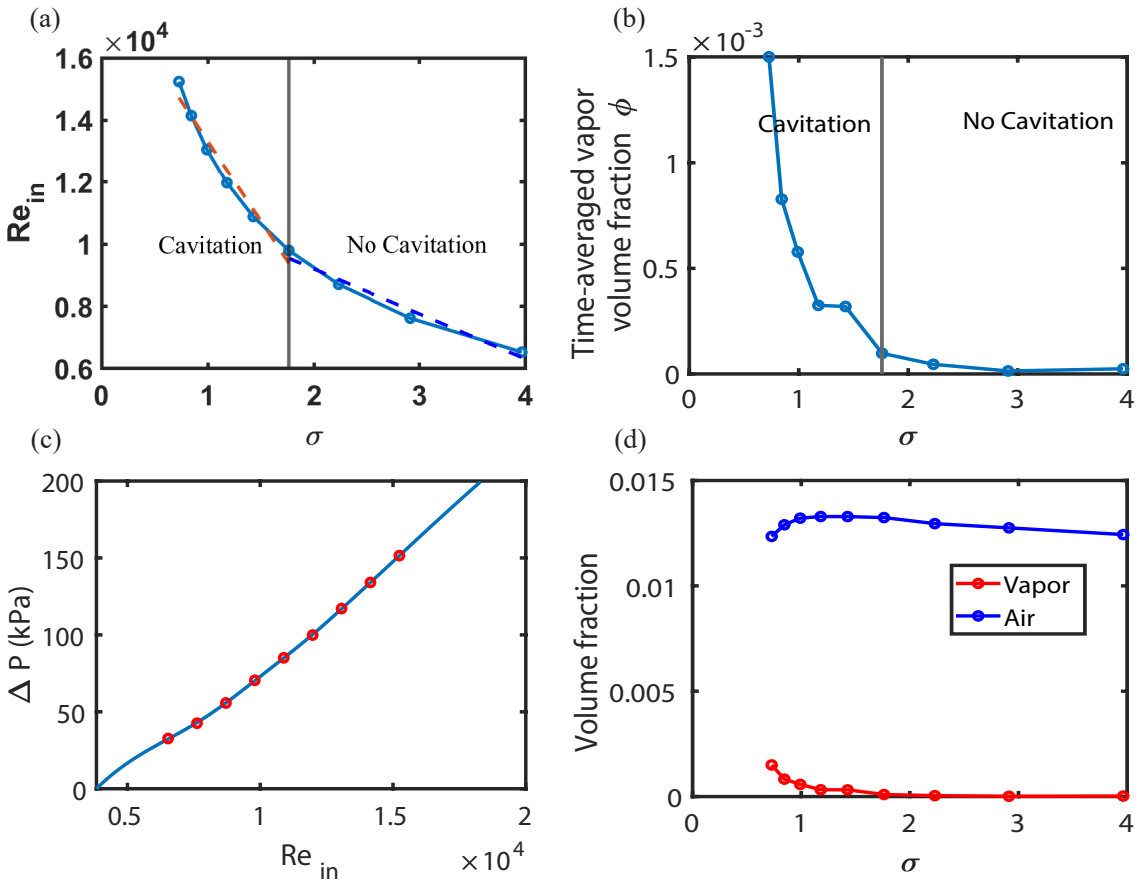

Figure 4.3: (a) Re at inlet plotted as a function of cavitation number (σ). There is a change in the trend at $\sigma = 1.76$ corresponding to flow rate of 4.5 L/min which represents the cavitation inception [123]. (b) Time-averaged volume fraction of vapor as a function of cavitation number. There is a sudden increase in the amount of vapor in the system for σ values lower than 1.76 which separates the region to cavitation and no cavitation conditions.(c) pressure drop plotted versus inlet Re number. Increase in flow rate causes greater pressure drop. (d) volume fraction of air and vapor as a function of cavitation number. Lower cavitation numbers is equivalent to higher Re and higher vapor fraction.

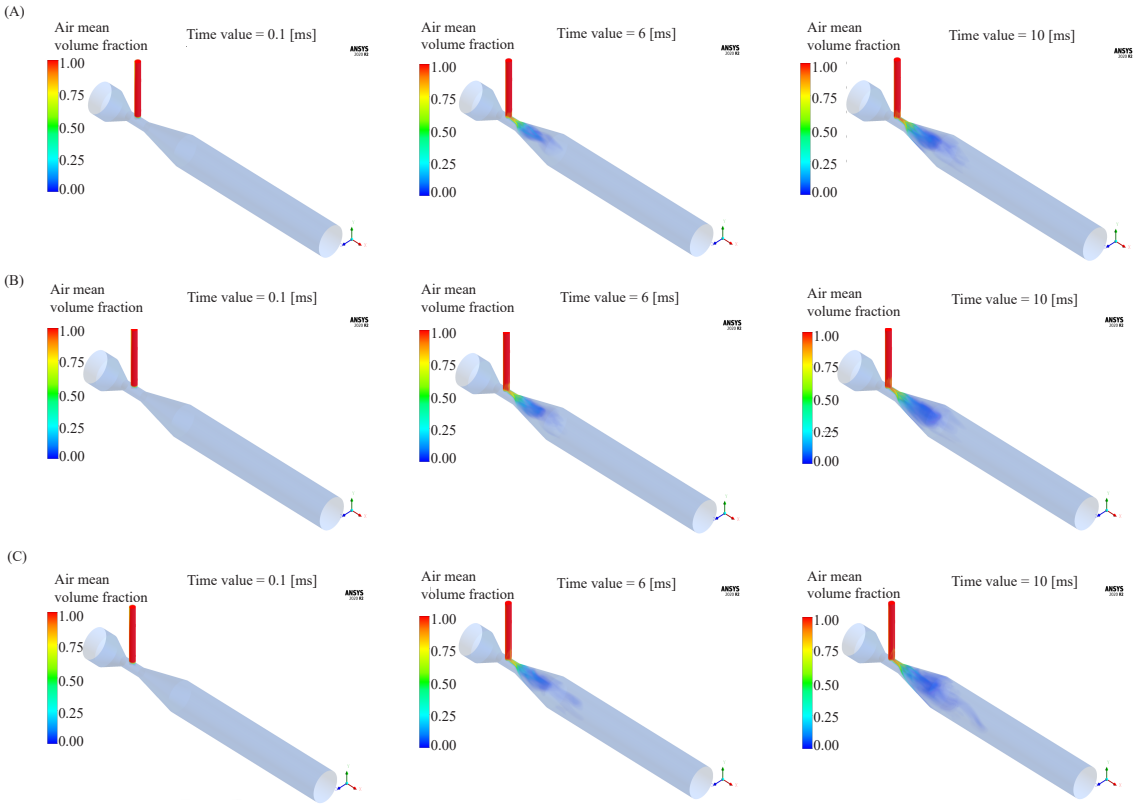

Figure 4.4: Air mean volume fraction for water flow rates of (A) 3, 4, and 5 L/min. Columns from left to right are for $t = 0.1$, 6, and 10 ms. Air volume fraction is shown as volume rendering from post processing of CFD simulations

L/min with plasma discharge at 15 kV can be capable of decontaminating a wide range of pollutants.

One of the novelties of this design is the better mixing of the plasma and pollutant molecules. As sketched in Figure 4.5 air plasma can better mix and agitate in higher flow rates. Fig 4.5 (A) to (C) show the turbulence kinetic energy (TKE) in the fluid domain. TKE is the mean kinetic energy per unit mass associated with eddies in turbulent flow [125]. It is defined according to Eq 4.3 where u', v', and w' are the difference between average and instantaneous velocity components in turbulent regime.

$$TKE = 1/2((\overline{u'})^2 + (\overline{v'})^2 + (\overline{w'})^2) \tag{4.3}$$

What is demanded for this application is to have the maximum vortexes and high

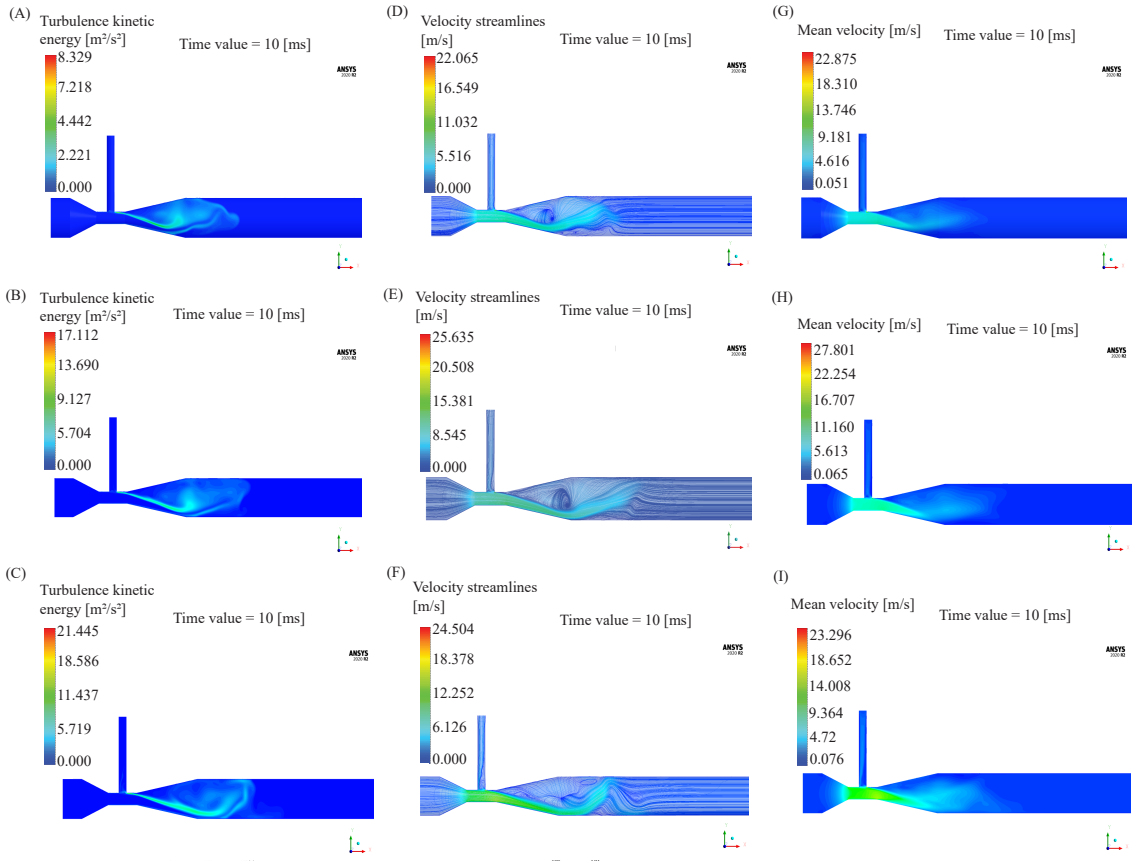

Figure 4.5: turbulent and velocity contours at $t = 10\,(ms)$. (A) to (C): TKE for $Q_w = 3\,to\,5\,L/min$. (D) to (F): velocity streamline for same flow rates implying the formation of vortices after divergent section. (G) to (I) Mean velocity contour for Q_w from 3 to $5\,L/min$

agitation. As shown in the streamline contour for three cases after 10 ms of flow time (see Fig. 4.5 (D) to (F)), the constriction in the flow field causes the formation of vortices and this enhances the mixing process. Secondary flows perpendicular to the main flow streams yield more proper mixing. Intensity of turbulent features are higher for flow rate of 5 L/min as shown in the same figure and implied by TKE values. In other words, eddies movement are more impressive and these fluctuations can transfer the reactive oxygen and nitrogen species faster. After flow get passed from the divergent section it slides towards the bottom of the pipe since gravity body force is activated. Vortex shedding continues to develop in the rest of the pipe until effects of constriction gradually fades and pressure field reverts back to atmospheric levels. Besides, the velocity contours for same conditions show that flow can achieve higher turbulence and velocity levels at the flow rate of 5 L/min compared with lower flow rates (see Fig. 4.5 (G) to (I)). Impact of air injection inside the Venturi tube is also elaborated in [65] where volume of fluid (VoF) model is used to simulate the multi phase flow. However, here, the effect of cavitation is also investigated using mixture model for multi phase flow containing liquid water, air, and vapor.

4.3.2 Effect of cavitation and vaporization

Cavitation is one of the advanced oxidation processes used recently in a wide range of configurations for water treatment [84]. Either hydrodynamic cavitation (in which vaporization occurs over a larger active zone) or acoustic cavitation (where the cavitation happens in smaller area but with higher intensity) [126] can be used in conjunction with other advanced oxidation processes to enhance the overall performance. This involves Fenton reaction, UV radiation, ozonation, and other AOPs [114, 127–129]. As the flow faces a constriction on its path, velocity raises. This phenomena can be better interpreted considering the continuity of flow. As the velocity increases the pressure gets reduced according to Bernoulli equation along any streamline (Eq 4.4). In the equation, P, v, and ρ stand for pressure, velocity and density of the

fluid. Reaching values lower than vapor pressure results in the formation of cavitation bubbles inside the flow which can then collapse downstream where pressure returns to higher values. Cumulative collapse of microbubbles in this manner can generate considerable energy inside the fluid and this helps in degradation of endocrine pollutants.

$$P + \frac{1}{2}\rho v^2 + \rho g h = c \tag{4.4}$$

Time-averaged of vapor volume fraction is presented for different flow rates at various time instances. Noting Fig. 4.6 vapor starts to form in the throat section just after the neck where the plasma air is introduced to the main flow. Then the shearing forces stretch the vapor over a wider range. As depicted in Fig4.6 vapor slowly begins to detach to smaller bubbles downstream and finally completely disappears at the outlet. Breakdown of the bubbles to micro bubbles is also beneficial in mass transfer due to the availability of higher surface area. Additionally, higher values for vapor volume fraction at higher flow rates confirm the fact that operating at increased velocities results in generation of more vapor bubbles which can assist in decomposition of pollutant species. It should be mentioned that here, there is a contribution from air plasma bubbles mixing in the main fluid and there are cavitation bubbles which are fewer compared with the volume occupied by air.

In order to delve more into the cavitation mechanism, Fig. 4.7 shows the mean vapor volume fraction as well as mean absolute pressure contours for flow rate of $5\,L/min$ at the beginning and at $t = 10\,(ms)$. As brought in (C) and (D) the vapor starts to form in zones with minimum pressure. To be more specific near the exit of the throat region and when the flow starts to expand in the divergent section of pipe. It should also be pointed out that pressure in the convergent section of pipe reaches higher than atmospheric levels, thus changing the geometrical parameters alter the pressure field.

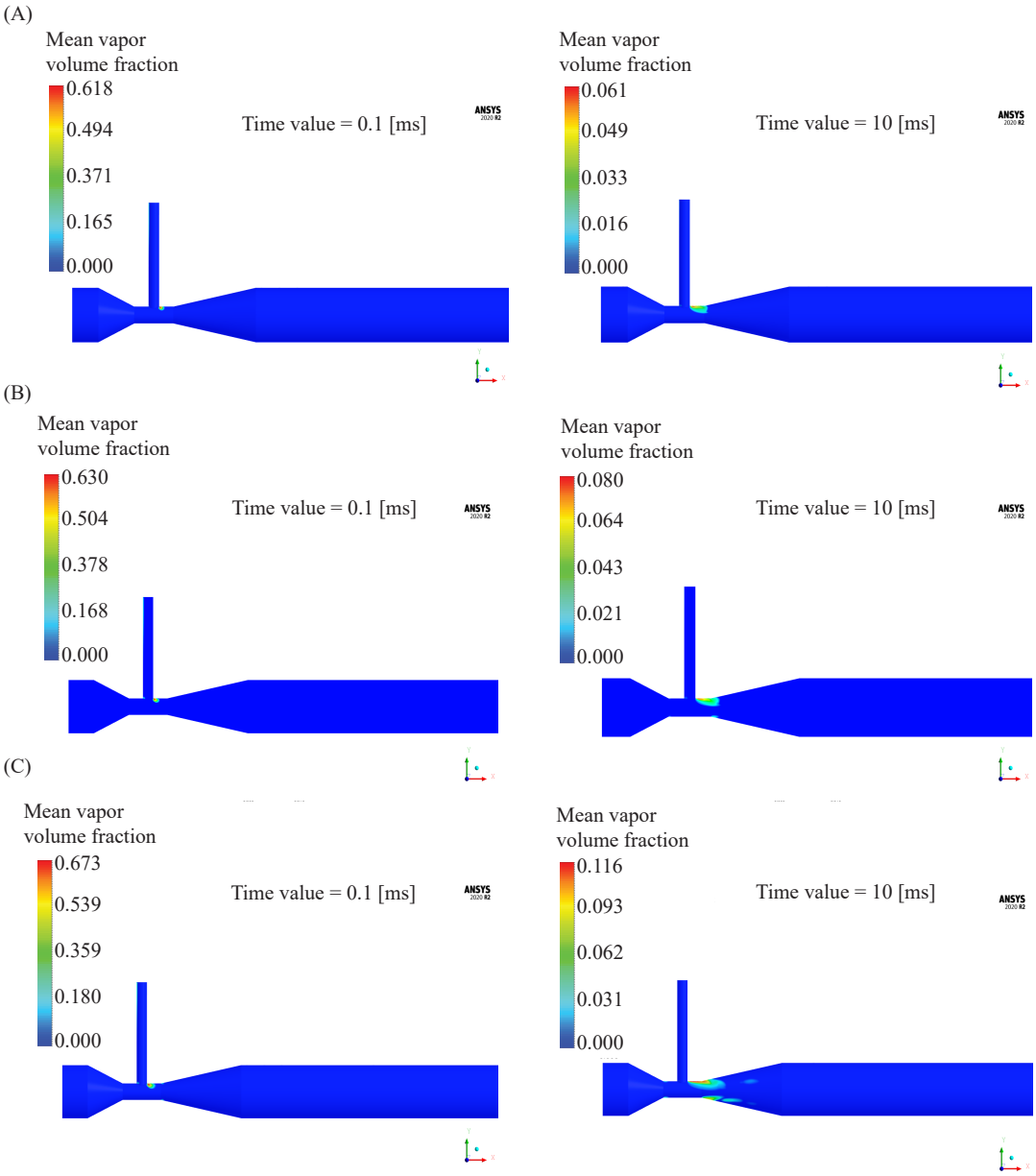

Figure 4.6: Mean volume fraction of vapor (A)-(C) respectively for $Q_w = 3, 4$ and $5\,L/min$ depicted at the beginning and after 10 ms of flow time.

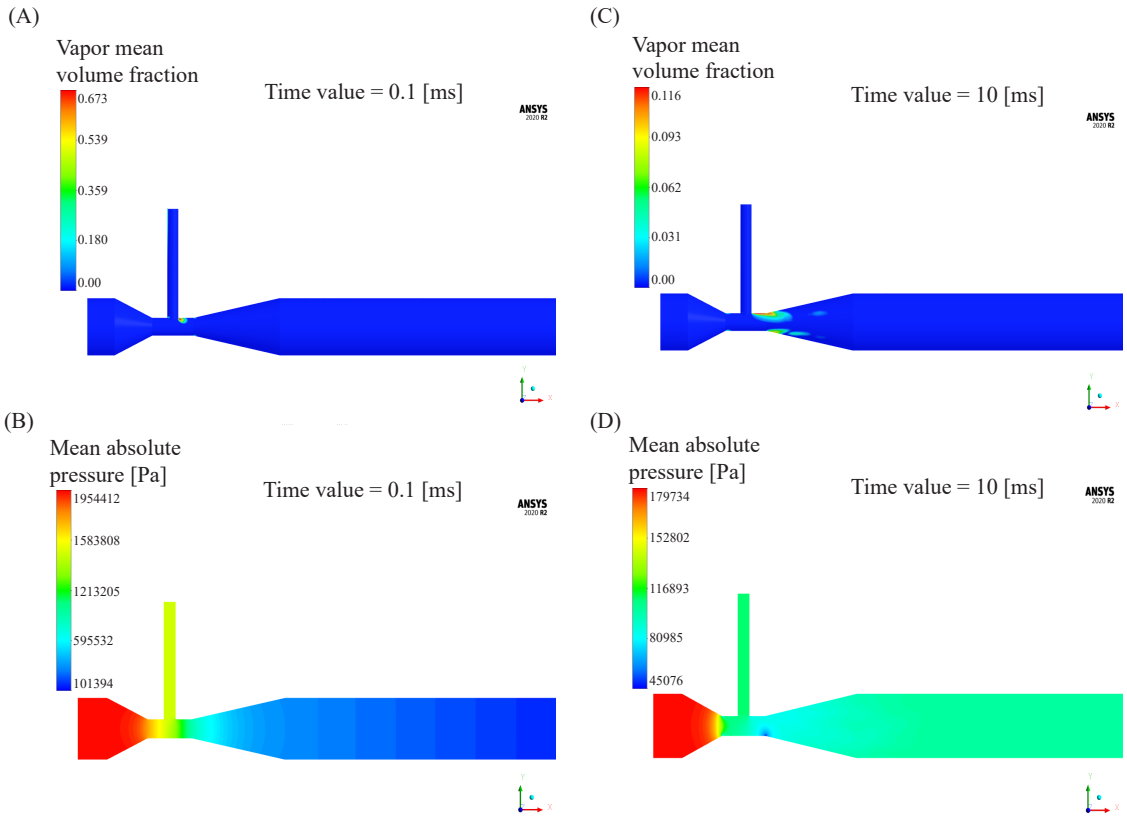

Figure 4.7: Mean air volume fraction and mean absolute pressure (A) and (B) at $t = 0.1\,(ms)$ and (C) and (D) at $t = 10\,(ms)$

4.3.3 Analysis of hydrodynamic cavitation

In the current study, the mixture contains water liquid as the main component, water vapor (relating to cavitation), and air (as the plasma component). The modified design of the Venturi paves the path for simultaneously leveraging the air bubbles and vapor bubbles. In other words, reduction in local pressure field not only results in self-suction of the air into the media, but also causes the formation of vapor micro bubbles which collapse downstream and act as a disrupting agent in decontamination. However, numerical results show that after some points, increasing the water flow rate does not add to the amount of air that can enter the tube. In fact, at higher flow rates, where the cavitation begins, the composition of the total gases present in the media shifts towards more vapor fraction. This means vapor bubbles populate the tube more and former air bubbles give their place to newly formed cavitation bubbles. Figure 4.8 demonstrates this fact by plotting time-averages volume of total gases present in the fluid domain. At low Re numbers majority of the composition comes from the air plasma. Increasing the water flow rate causes more intense cavitation, thus air volume gradually is substituted with water vapor. It should also be mentioned that still at greater Re values, air makes up a higher portion of the mixture. For instance, at $Re = 1306284$ corresponding to $Q_w = 6\,(L/min)$ air accounts for 75 (μL) of the total gas volume. This value reduces to about 70 at flow rate of $7\,(L/min)$. On the other hand, vapor constitutes 3.29 $(\mu\, L)$ at $Q_w = 6(L/min)$ and increases to 8.55 at flow rate of 7 (L/min). Results are in agreement with Fig 4.3 (d) where the volume fraction of air and vapor are plotted as a function of σ values. Cavitation inception can also be deduced from this figure where there is a high raise in volume of vapor in the fluid media.

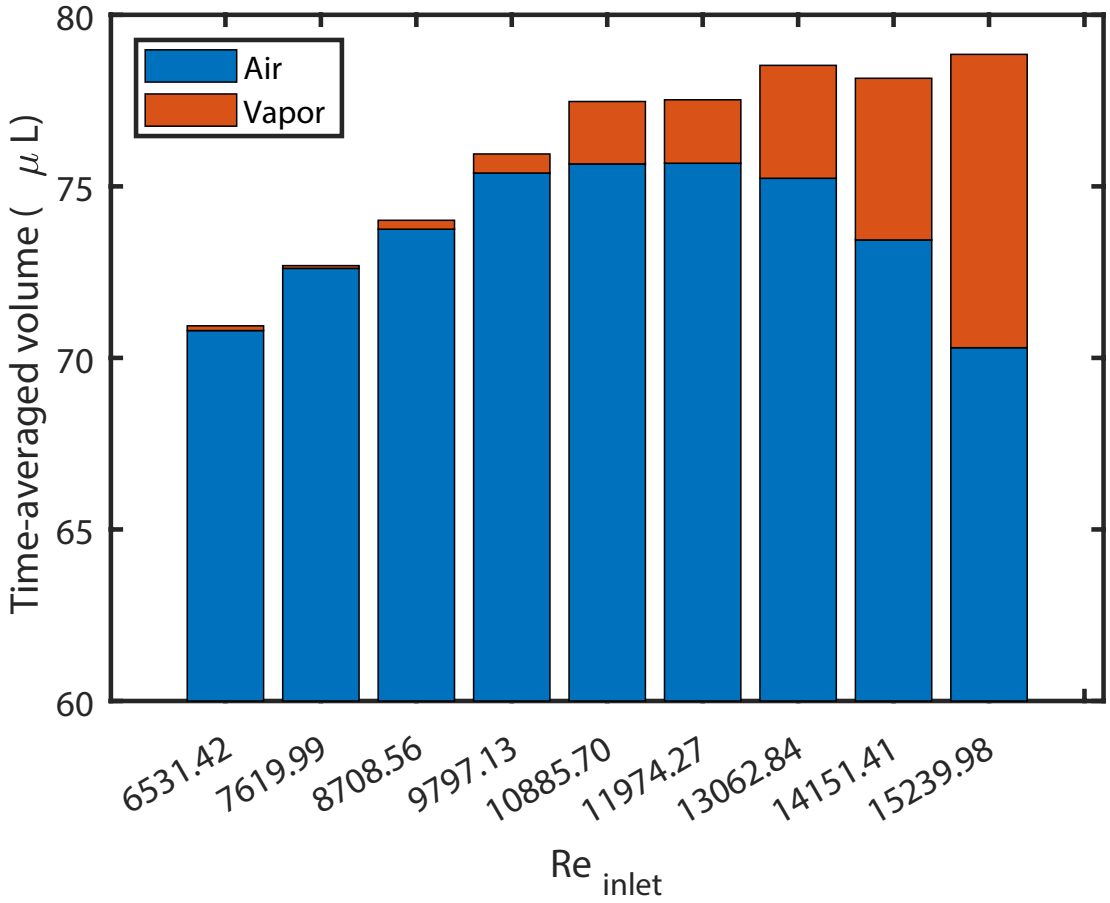

Figure 4.8: Averaged volume of gases in the fluid domain with respect to Re. Orange bars represent the vapor volume and blue bars stand for air volume

4.4 Conclusion

In this study, a novel design of Venturi tube is modeled using computational fluid dynamics to leverage cold plasma treatment combined with hydrodynamic cavitation for water treatment. The mixture model for multi phase could capture flow characteristics and results are in agreement with experiments previously done in our research group. It is demonstrated that the self suction of the modified Venturi causes air plasma to easily enter the fluid domain. Besides, the convergent-divergent nozzle in the loop triggers a pressure drop in flow domain resulting in the cavitation. Therefore, better mass transfer can be achieved downstream by collapse of vapor micro bubbles as well as the breakdown of the plasma air bubbles. Numerical results also show at higher flow rates the composition of gases present in the fluid domain shift towards more vapor bubbles. Utilizing hydrodynamic cavitation along cold plasma treatment can select this method to be used for water and wastewater as a state-of-art AOP. Since there are no extraneous chemicals used in this method, it can be considered a green technology and there is the possibility to use sustainable energy sources to power the plasma generator.

Chapter 5

Conclusions, Recommendations, & Future Work

5.1 Conclusions

In chapter 3, it was found that non thermal plasma can be used in combination with hydrodynamic cavitation to represent a novel green and sustainable water treatment technology. Microbubbles generated after the cavitation effect carry the highly reactive species (RONs) produced because of plasma generation. Then collapse of these micro-sized bubbles transfer the species and radicals to the water environment and degrade the pollutants present in water. This system has some unique advantages compared with other AOPs including removing the gas-liquid transfer hurdle and not producing any chemical agent. Besides, the operation is in a loop which enables the high degradation results. In this research, a range of pollutants in mili-Q water were tried. Two antibiotics and a dye were tested with a reasonable performance. Factors such as initial concentration of pollutants, volume of the samples and water flow rate were varied and their effect on degradation results were studied. Higher flow rates cause better degradation and this is related to the stronger hydrodynamic cavitation at higher flow rates. More concentrated samples tend to degrade more slowly since the reactive species start in a competition to degrade the core pollutant molecules. Treatment of larger volumes was also done successfully.

In chapter 4, a simulation study was performed in order to better understand the

mechanism supporting the hydrodynamic cavitation. The CFD modeling was done in ANSYS software and three flow rates were tested. The mixture model was selected to simulate the multi-phase flow and Schnerr-Sauer model was used for the cavitation. Flow characteristics such as pressure, velocity, and turbulent quantities (Turbulence kinetic energy) were measured and presented to give a better comparison between test conditions. It was concluded that higher flow rates can cause a higher pressure drop in the Venturi tube causing generation of more microbubbles which in turn helps with transferring the reactive species more effectively.

The findings from this research can be used in water treatment facilities and also providing a green and novel solution for the water shortage globally. It is the first time the modified Venturi tube used in the system is modeled and this can be helpful for optimizing the system and scaling it up for other industrial purposes. Besides, the powerful cold plasma combined with cavitation can be applied for a range of pollutants that are hard to degrade. While most of the plasma work is done in a water environment and in a batch mode, this research uses a continuous flow avoiding direct contact with the liquid phase which considerably increases the lifetime of the device and cuts down the costs.

5.2 Future Work

Cold plasma is considered a new technology which has gained a lot of attention in the last decade. The exceptional features provided by this technology and its applicability in many industries makes huge research devoted in this field necessary. Here we have summarized the future work and recommendations.

1. One possible research method involves the identification of chemicals that remain in the treated water. Although RONs formed after plasma activation have minuscule lifetimes, it is still strongly advised to put considerable effort on detecting all chemicals that might exist in water. This fact becomes more

significant if the treated water is to be used for drinking purposes.

2. Another approach is to scale up the set up to even more volumes. The unique characteristics of cold plasma makes the potential for searching for the capability to scale up the system for treating even higher capacities. Obviously, a tremendous feasibility study is required and the environmental aspects and regulations should also be considered.

3. Recently the problem of emerging contaminants have become a major challenge in societies. Advancements in biotechnology, medical industries, and new fertilizers used in farming sector has led to introduction of new contaminants. These emerging contaminants are resistant to traditional remediation methods and require more effective strategies. Non-thermal plasma combined with hydrodynamic cavitation is flexible enough to be implemented in the treatment facilities and is strong to address the endocrine contaminants. Examples of wastes that can be investigates are biohazards and microplastics.

4. The plasma generator can also be modified. Plasma device plays a crucial role in the treatment. Analyzing the available plasma generators, their energy requirements, and their performance can hand in a more optimized plasma device. It is advantageous to use renewable energy sources such as solar or wind energy to power the system. As a result, the whole setup can be called a green and sustainable treatment scheme.

Bibliography

[1] K. Guo, Z. Wu, C. Chen, and J. Fang, "Uv/chlorine process: An efficient advanced oxidation process with multiple radicals and functions in water treatment," *Accounts of Chemical Research*, vol. 55, no. 3, pp. 286–297, 2022.

[2] S. W. Sharshir *et al.*, "New hydrogel materials for improving solar water evaporation, desalination and wastewater treatment: A review," *Desalination*, vol. 491, p. 114 564, 2020.

[3] K. Q. Jabbar, A. A. Barzinjy, and S. M. Hamad, "Iron oxide nanoparticles: Preparation methods, functions, adsorption and coagulation/flocculation in wastewater treatment," *Environmental Nanotechnology, Monitoring & Management*, vol. 17, p. 100 661, 2022.

[4] C. Wei, F. Zhang, Y. Hu, C. Feng, and H. Wu, "Ozonation in water treatment: The generation, basic properties of ozone and its practical application," *Reviews in Chemical Engineering*, vol. 33, no. 1, pp. 49–89, 2017.

[5] B Legube and N. K. V. Leitner, "Catalytic ozonation: A promising advanced oxidation technology for water treatment," *Catalysis today*, vol. 53, no. 1, pp. 61–72, 1999.

[6] S. N. Malik, P. C. Ghosh, A. N. Vaidya, and S. N. Mudliar, "Hybrid ozonation process for industrial wastewater treatment: Principles and applications: A review," *Journal of Water Process Engineering*, vol. 35, p. 101 193, 2020.

[7] D. Zhu and Q. Zhou, "Action and mechanism of semiconductor photocatalysis on degradation of organic pollutants in water treatment: A review," *Environmental Nanotechnology, Monitoring & Management*, vol. 12, p. 100 255, 2019.

[8] C Mejia-Morales, D. Cortés-Hernández, F Hernández-Aldana, R. Peña-Moreno, and N Bonilla y Fernández, "Broadband characterization method for photochemical systems used in hospital wastewater treatment," *Journal of Water Chemistry and Technology*, vol. 41, pp. 228–235, 2019.

[9] J. Gomes, A. Matos, M. Gmurek, R. M. Quinta-Ferreira, and R. C. Martins, "Ozone and photocatalytic processes for pathogens removal from water: A review," *Catalysts*, vol. 9, no. 1, p. 46, 2019.

[10] Y. Zhuang *et al.*, "Inactivation of antibiotic resistance genes in municipal wastewater by chlorination, ultraviolet, and ozonation disinfection," *Environmental Science and Pollution Research*, vol. 22, pp. 7037–7044, 2015.

[11] Y. Zhao *et al.*, "Hydrated electron based photochemical processes for water treatment," *Water Research*, p. 119 212, 2022.

[12] Y. Sukhatskiy, M Shepida, M Sozanskyi, Z Znak, and P. R. Gogate, "Periodate-based advanced oxidation processes for wastewater treatment: A review," *Separation and Purification Technology*, vol. 304, p. 122 305, 2023.

[13] S. Khan, M. Naushad, M. Govarthanan, J. Iqbal, and S. M. Alfadul, "Emerging contaminants of high concern for the environment: Current trends and future research," *Environmental Research*, vol. 207, p. 112 609, 2022.

[14] A. Fridman, *Plasma chemistry*. Cambridge university press, 2008.

[15] Y. Gorbanev, A. Privat-Maldonado, and A. Bogaerts, *Analysis of short-lived reactive species in plasma–air–water systems: The dos and the do nots*, 2018.

[16] Y. Yin, T. Yang, Z. Li, E. Devid, D. Auerbach, and A. W. Kleyn, "CO2conversion by plasma: how to get efficient CO2conversion and high energy efficiency," *Physical Chemistry Chemical Physics*, vol. 23, no. 13, pp. 7974–7987, 2021, ISSN: 14639076. DOI: 10.1039/d0cp05275b.

[17] R. Snoeckx and A. Bogaerts, "Plasma technology-a novel solution for CO2 conversion?" *Chemical Society Reviews*, vol. 46, no. 19, pp. 5805–5863, 2017, ISSN: 14604744. DOI: 10.1039/c6cs00066e. [Online]. Available: http://dx.doi.org/10.1039/C6CS00066E.

[18] P. Bruggeman *et al.*, "Plasma–liquid interactions: A review and roadmap," *Plasma sources science and technology*, vol. 25, no. 5, p. 053 002, 2016.

[19] C. Aggelopoulos, S. Meropoulis, M. Hatzisymeon, Z. Lada, and G. Rassias, "Degradation of antibiotic enrofloxacin in water by gas-liquid nsp-dbd plasma: Parametric analysis, effect of h2o2 and cao2 additives and exploration of degradation mechanisms," *Chemical Engineering Journal*, vol. 398, p. 125 622, 2020, ISSN: 1385-8947. DOI: https://doi.org/10.1016/j.cej.2020.125622. [Online]. Available: https://www.sciencedirect.com/science/article/pii/S1385894720317502.

[20] C. Sarangapani *et al.*, "Degradation kinetics of cold plasma-treated antibiotics and their antimicrobial activity," *Scientific reports*, vol. 9, no. 1, pp. 1–15, 2019.

[21] M. El Shaer *et al.*, "Antibiotics Degradation and Bacteria Inactivation in Water by Cold Atmospheric Plasma Discharges Above and Below Water Surface," *Plasma Chemistry and Plasma Processing*, vol. 40, no. 4, pp. 971–983, 2020, ISSN: 1572-8986. DOI: 10.1007/s11090-020-10076-0. [Online]. Available: https://doi.org/10.1007/s11090-020-10076-0.

[22] H. Guo *et al.*, "Pulsed discharge plasma assisted with graphene-WO3 nanocomposites for synergistic degradation of antibiotic enrofloxacin in water," *Chemical Engineering Journal*, vol. 372, no. January, pp. 226–240, 2019, ISSN: 13858947. DOI: 10.1016/j.cej.2019.04.119.

[23] C. Wang, G. Qu, T. Wang, F. Deng, and D. Liang, "Removal of tetracycline antibiotics from wastewater by pulsed corona discharge plasma coupled with natural soil particles," *Chemical Engineering Journal*, vol. 346, pp. 159–170, 2018, ISSN: 1385-8947. DOI: https://doi.org/10.1016/j.cej.2018.03.149. [Online]. Available: https://www.sciencedirect.com/science/article/pii/S1385894718305072.

[24] A. Sokolov, M. Kråkström, P. Eklund, L. Kronberg, and M. Louhi-Kultanen, "Abatement of amoxicillin and doxycycline in binary and ternary aqueous solutions by gas-phase pulsed corona discharge oxidation," *Chemical Engineering Journal*, vol. 334, pp. 673–681, 2018, ISSN: 1385-8947. DOI: https://doi.org/10.1016/j.cej.2017.10.071. [Online]. Available: https://www.sciencedirect.com/science/article/pii/S1385894717317862.

[25] J.-L. Brisset *et al.*, "Chemical reactivity of discharges and temporal post-discharges in plasma treatment of aqueous media: Examples of gliding discharge treated solutions," *Industrial & Engineering Chemistry Research*, vol. 47, no. 16, pp. 5761–5781, 2008.

[26] L. Yang *et al.*, "Mechanism of amoxicillin degradation in water treated by atmospheric-pressure air microplasma," *IEEE Transactions on Plasma Science*, vol. 48, no. 4, pp. 953–960, 2020.

[27] E. Acayanka, J.-B. Tarkwa, and S. Laminsi, "Evaluation of energy balance in a batch and circulating non-thermal plasma reactors during organic pollutant oxidation in aqueous solution," *Plasma Chemistry and Plasma Processing*, vol. 39, no. 1, pp. 75–87, 2019.

[28] X. Lu *et al.*, "Plasma electrolytic oxidation coatings with particle additions–a review," *Surface and Coatings Technology*, vol. 307, pp. 1165–1182, 2016.

[29] M. Magureanu, F. Bilea, C. Bradu, and D. Hong, "A review on non-thermal plasma treatment of water contaminated with antibiotics," *Journal of Hazardous Materials*, vol. 417, no. February, 2021, ISSN: 18733336. DOI: 10.1016/j.jhazmat.2021.125481.

[30] B. Subedi, K. Balakrishna, D. I. Joshua, and K. Kannan, "Mass loading and removal of pharmaceuticals and personal care products including psychoactives, antihypertensives, and antibiotics in two sewage treatment plants in southern india," *Chemosphere*, vol. 167, pp. 429–437, 2017.

[31] H. Tolouie, M. A. Mohammadifar, H. Ghomi, and M. Hashemi, "Cold atmospheric plasma manipulation of proteins in food systems," *Critical reviews in food science and nutrition*, vol. 58, no. 15, pp. 2583–2597, 2018.

[32] R. Banaschik *et al.*, "Degradation of pharmaceutical residues in water by pulsed corona discharges—investigation of reaction mechanism," in *2015 IEEE International Conference on Plasma Sciences (ICOPS)*, IEEE, 2015, pp. 1–1.

[33] N. Koutahzadeh, M. R. Esfahani, and P. E. Arce, "Sequential use of uv/h2o2—(psf/tio2/mwcı mixed matrix membranes for dye removal in water purification: Membrane permeation, fouling, rejection, and decolorization," *Environmental Engineering Science*, vol. 33, no. 6, pp. 430–440, 2016.

[34] J. Zhang, D. Liu, W. Bian, and X. Chen, "Degradation of 2, 4-dichorophenol by pulsed high voltage discharge in water," *Desalination*, vol. 304, pp. 49–56, 2012.

[35] F. Holzer and B. R. Locke, "Influence of high voltage needle electrode material on hydrogen peroxide formation and electrode erosion in a hybrid gas–liquid series electrical discharge reactor," *Plasma Chemistry and Plasma Processing*, vol. 28, no. 1, pp. 1–13, 2008.

[36] N. Wardenier, Z. Liu, A. Nikiforov, S. W. Van Hulle, and C. Leys, "Micropollutant elimination by o3, uv and plasma-based aops: An evaluation of treatment and energy costs," *Chemosphere*, vol. 234, pp. 715–724, 2019.

[37] R. K. Marcus and J. A. Broekaert, *Glow discharge plasmas in analytical spectroscopy*. Wiley Online Library, 2003.

[38] K. Samanta, M. Jassal, and A. K. Agrawal, "Atmospheric pressure glow discharge plasma and its applications in textile," 2006.

[39] M Braşoveanu, M Nemţanu, C Surdu-Bob, G Karaca, and I Erper, "Effect of glow discharge plasma on germination and fungal load of some cereal seeds," *Romanian Reports in Physics*, vol. 67, no. 2, pp. 617–624, 2015.

[40] S. Okazaki, M. Kogoma, M. Uehara, and Y. Kimura, "Appearance of stable glow discharge in air, argon, oxygen and nitrogen at atmospheric pressure using a 50 hz source," *Journal of Physics D: Applied Physics*, vol. 26, no. 5, p. 889, 1993.

[41] J Winter, R Brandenburg, and K. Weltmann, "Atmospheric pressure plasma jets: An overview of devices and new directions," *Plasma Sources Science and Technology*, vol. 24, no. 6, p. 064 001, 2015.

[42] M. Veerana, E. H. Choi, and G. Park, "Influence of non-thermal atmospheric pressure plasma jet on extracellular activity of α-amylase in aspergillus oryzae," *Applied Sciences (Switzerland)*, vol. 11, no. 2, pp. 1–14, 2021, ISSN: 20763417. DOI: 10.3390/app11020691.

[43] Y. Zhou, Y. Yan, M. Shi, and Y. Liu, "Effect of an atmospheric pressure plasma jet on the structure and physicochemical properties ofwaxy and normal maize starch," *Polymers*, vol. 11, no. 1, 2019, ISSN: 20734360. DOI: 10.3390/polym11010008.

[44] Y.-H. Jiang, J.-H. Cheng, and D.-W. Sun, "Effects of plasma chemistry on the interfacial performance of protein and polysaccharide in emulsion," *Trends in Food Science & Technology*, vol. 98, pp. 129–139, 2020.

[45] E Gomez, D. A. Rani, C. Cheeseman, D Deegan, M Wise, and A. Boccaccini, "Thermal plasma technology for the treatment of wastes: A critical review," *Journal of hazardous materials*, vol. 161, no. 2-3, pp. 614–626, 2009.

[46] R. Pristavita, J.-L. Meunier, and D. Berk, "Carbon nano-flakes produced by an inductively coupled thermal plasma system for catalyst applications," *Plasma Chemistry and Plasma Processing*, vol. 31, no. 2, pp. 393–403, 2011.

[47] B. Ashford and X. Tu, "Non-thermal plasma technology for the conversion of CO2," *Current Opinion in Green and Sustainable Chemistry*, vol. 3, pp. 45–49, 2017, ISSN: 24522236. DOI: 10.1016/j.cogsc.2016.12.001. [Online]. Available: http://dx.doi.org/10.1016/j.cogsc.2016.12.001.

[48] O Fukumasa, H Abe, and R Itatani, "Anomalous effect of weak collisions on the nonlinear interaction in a small-cold-beam, warm-plasma system," *Physical review letters*, vol. 40, no. 6, p. 393, 1978.

[49] H.-L. Liu and Y.-R. Chiou, "Optimal decolorization efficiency of reactive red 239 by uv/tio2 photocatalytic process coupled with response surface methodology," *Chemical Engineering Journal*, vol. 112, no. 1, pp. 173–179, 2005, ISSN: 1385-8947. DOI: https://doi.org/10.1016/j.cej.2005.07.012. [Online]. Available: https://www.sciencedirect.com/science/article/pii/S1385894705002470.

[50] D. D. Asouhidou, K. S. Triantafyllidis, N. K. Lazaridis, K. A. Matis, S.-S. Kim, and T. J. Pinnavaia, "Sorption of reactive dyes from aqueous solutions by ordered hexagonal and disordered mesoporous carbons," *Microporous and Mesoporous Materials*, vol. 117, no. 1, pp. 257–267, 2009, ISSN: 1387-1811. DOI: https://doi.org/10.1016/j.micromeso.2008.06.034. [Online]. Available: https://www.sciencedirect.com/science/article/pii/S1387181108003235.

[51] E. Alver and A. Metin, "Anionic dye removal from aqueous solutions using modified zeolite: Adsorption kinetics and isotherm studies," *Chemical Engineering Journal*, vol. 200-202, pp. 59–67, 2012, ISSN: 1385-8947. DOI: https://doi.org/10.1016/j.cej.2012.06.038. [Online]. Available: https://www.sciencedirect.com/science/article/pii/S1385894712007590.

[52] J. P. Scott and D. F. Ollis, "Integration of chemical and biological oxidation processes for water treatment: Ii. recent illustrations and experiences," *Journal of Advanced Oxidation Technologies*, vol. 2, no. 3, pp. 374–381, 1997.

[53] S. A. Mohammadi, H. Najafi, S. Zolgharnian, S. Sharifian, and N. Asasian-Kolur, "Wastewater treatment process by biological oxidation methods: A crucial review," *Science of The Total Environment*, p. 157 026, 2022.

[54] R. C. Sanito, S. J. You, and Y. F. Wang, "Degradation of contaminants in plasma technology: An overview," *Journal of Hazardous Materials*, vol. 424, no. PA, p. 127 390, 2022, ISSN: 18733336. DOI: 10.1016/j.jhazmat.2021.127390. [Online]. Available: https://doi.org/10.1016/j.jhazmat.2021.127390.

[55] A. Sakudo, Y. Yagyu, and T. Onodera, "Disinfection and sterilization using plasma technology: Fundamentals and future perspectives for biological applications," *International journal of molecular sciences*, vol. 20, no. 20, p. 5216, 2019.

[56] B. A. Niemira, "Cold plasma decontamination of foods," *Annual review of food science and technology*, vol. 3, pp. 125–142, 2012.

[57] S. Güçeri, A. Fridman, K. Gibson, and C. Haas, *Plasma Assisted Decontamination of Biological and Chemical Agents*. Jan. 2008, ISBN: 978-1-4020-8440-9. DOI: 10.1007/978-1-4020-8439-3_14.

[58] X. Zhang *et al.*, "Atmospheric cold plasma jet for plant disease treatment," *Applied Physics Letters*, vol. 104, no. 4, p. 043 702, 2014.

[59] R. Thirumdas *et al.*, "Plasma activated water (paw): Chemistry, physicochemical properties, applications in food and agriculture," *Trends in food science & technology*, vol. 77, pp. 21–31, 2018.

[60] Y. Gao, K. Francis, and X. Zhang, "Review on formation of cold plasma activated water (paw) and the applications in food and agriculture," *Food Research International*, p. 111 246, 2022.

[61] S. H. Ji *et al.*, "Assessment of the effects of nitrogen plasma and plasma-generated nitric oxide on early development of coriandum sativum," *Plasma Processes and Polymers*, vol. 12, no. 10, pp. 1164–1173, 2015.

[62] T. Zhang *et al.*, "Degradation of cefixime antibiotic in water by atmospheric plasma bubbles: Performance, degradation pathways and toxicity evaluation," *Chemical Engineering Journal*, vol. 421, p. 127 730, 2021, ISSN: 1385-8947. DOI: https://doi.org/10.1016/j.cej.2020.127730. [Online]. Available: https://www.sciencedirect.com/science/article/pii/S1385894720338511.

[63] R. Zhou *et al.*, "Underwater microplasma bubbles for efficient and simultaneous degradation of mixed dye pollutants," *Science of The Total Environment*, vol. 750, p. 142 295, 2021, ISSN: 0048-9697. DOI: https://doi.org/10.1016/j.scitotenv.2020.142295. [Online]. Available: https://www.sciencedirect.com/science/article/pii/S0048969720358241.

[64] R. Zhou *et al.*, "Plasmacatalytic bubbles using ceo2 for organic pollutant degradation," *Chemical Engineering Journal*, vol. 403, p. 126 413, 2021, ISSN: 1385-8947. DOI: https://doi.org/10.1016/j.cej.2020.126413. [Online]. Available: https://www.sciencedirect.com/science/article/pii/S1385894720325419.

[65] Y. Gao, M. Li, C. Sun, and X. Zhang, "Microbubble-enhanced water activation by cold plasma," *Chemical Engineering Journal*, vol. 446, no. P4, p. 137 318, 2022, ISSN: 13858947. DOI: 10.1016/j.cej.2022.137318. [Online]. Available: https://doi.org/10.1016/j.cej.2022.137318.

[66] R. C. Sanito, Y.-W. Chen, S.-J. You, H.-H. Yang, Y.-K. Hsieh, and Y.-F. Wang, "Hydrogen and methane production from styrofoam waste using an atmospheric-pressure microwave plasma reactor," *Aerosol and Air Quality Research*, vol. 20, no. 10, pp. 2226–2238, 2020. DOI: 10.4209/aaqr.2020.05.0252. [Online]. Available: https://doi.org/10.4209%2Faaqr.2020.05.0252.

[67] R. C. Sanito, S.-J. You, and Y.-F. Wang, "Application of plasma technology for treating e-waste: A review," *Journal of environmental management*, vol. 288, p. 112 380, 2021.

[68] I. Adamovich *et al.*, "The 2017 plasma roadmap: Low temperature plasma science and technology," *Journal of Physics D: Applied Physics*, vol. 50, no. 32, p. 323 001, 2017.

[69] C. Sarangapani, A. Patange, P. Bourke, K. Keener, and P. Cullen, "Recent advances in the application of cold plasma technology in foods," *Annual review of food science and technology*, vol. 9, pp. 609–629, 2018.

[70] P. Dimitrakellis, E. Delikonstantis, G. Stefanidis, and D. Vlachos, "Plasma technology for lignocellulosic biomass conversion toward an electrified biorefinery," *Green Chemistry*, 2022.

[71] A. Tamošiūnas, P. Valatkevičius, V. Valinčius, and R. Levinskas, "Biomass conversion to hydrogen-rich synthesis fuels using water steam plasma," *Comptes Rendus Chimie*, vol. 19, no. 4, pp. 433–440, 2016.

[72] P. Lukes, B. R. Locke, and J. L. Brisset, "Aqueous-Phase Chemistry of Electrical Discharge Plasma in Water and in Gas-Liquid Environments," *Plasma Chemistry and Catalysis in Gases and Liquids*, no. Chapter 6, pp. 243–308, 2012. DOI: 10.1002/9783527649525.ch7.

[73] L Chandana, P. M. K. Reddy, and C. Subrahmanyam, "Atmospheric pressure non-thermal plasma jet for the degradation of methylene blue in aqueous medium," *Chemical Engineering Journal*, vol. 282, pp. 116–122, 2015.

[74] F. Huang, L. Chen, H. Wang, T. Feng, and Z. Yan, "Degradation of methyl orange by atmospheric DBD plasma: Analysis of the degradation effects and degradation path," *Journal of Electrostatics*, vol. 70, no. 1, pp. 43–47, 2012, ISSN: 03043886. DOI: 10.1016/j.elstat.2011.10.001. [Online]. Available: http://dx.doi.org/10.1016/j.elstat.2011.10.001.

[75] Q. Zhang, H. Zhang, Q. Zhang, and Q. Huang, "Degradation of norfloxacin in aqueous solution by atmospheric-pressure non-thermal plasma: Mechanism and degradation pathways," *Chemosphere*, vol. 210, pp. 433–439, 2018, ISSN: 18791298. DOI: 10.1016/j.chemosphere.2018.07.035. [Online]. Available: https://doi.org/10.1016/j.chemosphere.2018.07.035.

[76] G. R. Stratton, C. L. Bellona, F. Dai, T. M. Holsen, and S. M. Thagard, "Plasma-based water treatment: Conception and application of a new general principle for reactor design," *Chemical Engineering Journal*, vol. 273, pp. 543–550, 2015.

[77] H. Krause, B. Schweiger, J. Schuhmacher, S. Scholl, and U. Steinfeld, "Chemosphere Degradation of the endocrine disrupting chemicals (EDCs) carbamazepine , clofibric acid , and iopromide by corona discharge over water," *Chemosphere*, vol. 75, no. 2, pp. 163–168, 2009, ISSN: 0045-6535. DOI: 10.1016/j.chemosphere.2008.12.020. [Online]. Available: http://dx.doi.org/10.1016/j.chemosphere.2008.12.020.

[78] M. Magureanu, C. Bradu, D. Piroi, N. B. Mandache, and V. Parvulescu, "Pulsed corona discharge for degradation of methylene blue in water," *Plasma Chemistry and Plasma Processing*, vol. 33, no. 1, pp. 51–64, 2013, ISSN: 02724324. DOI: 10.1007/s11090-012-9422-8.

[79] S. Meropoulis and C. A. Aggelopoulos, "Plasma microbubbles vs gas-liquid DBD energized by low-frequency high voltage nanopulses for pollutants degradation in water: Destruction mechanisms, composition of plasma-activated water and energy assessment," *Journal of Environmental Chemical Engineering*, vol. 11, no. 3, p. 109 855, 2023, ISSN: 22133437. DOI: 10.1016/j.jece.2023.109855. [Online]. Available: https://doi.org/10.1016/j.jece.2023.109855.

[80] U. Kogelschatz, "Dielectric-barrier discharges: Their history, discharge physics, and industrial applications," *Plasma chemistry and plasma processing*, vol. 23, pp. 1–46, 2003.

[81] J.-Z. Jiang, S. Zhang, X.-L. Fu, L. Liu, and B.-M. Sun, "Review of gas–liquid mass transfer enhancement by nanoparticles from macro to microscopic," *Heat and Mass Transfer*, vol. 55, no. 8, pp. 2061–2072, 2019.

[82] Y. Liu *et al.*, "Degradation of aniline in aqueous solution using non-thermal plasma generated in microbubbles," *Chemical Engineering Journal*, vol. 345, pp. 679–687, 2018.

[83] H. Zhang *et al.*, "Enhancing interface reactions by introducing microbubbles into a plasma treatment process for efficient decomposition of pfoa," *Environmental Science & Technology*, vol. 55, no. 23, pp. 16 067–16 077, 2021.

[84] M. Gągol, A. Przyjazny, and G. Boczkaj, "Wastewater treatment by means of advanced oxidation processes based on cavitation – A review," *Chemical Engineering Journal*, vol. 338, pp. 599–627, 2018, ISSN: 13858947. DOI: 10.1016/j.cej.2018.01.049. [Online]. Available: https://doi.org/10.1016/j.cej.2018.01.049.

[85] Z. Zhou, Z. Xu, J. Finch, H Hu, and S. Rao, "Role of hydrodynamic cavitation in fine particle flotation," *International Journal of Mineral Processing*, vol. 51, no. 1-4, pp. 139–149, 1997.

[86] H Oliveira, A Azevedo, and J Rubio, "Nanobubbles generation in a high-rate hydrodynamic cavitation tube," *Minerals Engineering*, vol. 116, pp. 32–34, 2018.

[87] H. Shi, M. Li, P. Nikrityuk, and Q. Liu, "Experimental and numerical study of cavitation flows in venturi tubes: From cfd to an empirical model," *Chemical Engineering Science*, vol. 207, pp. 672–687, 2019.

[88] H. Zhang *et al.*, "Enhancing Interface Reactions by Introducing Microbubbles into a Plasma Treatment Process for Efficient Decomposition of PFOA," *Environmental Science & Technology*, vol. 55, no. 23, pp. 16 067–16 077, 2021, ISSN: 0013-936X. DOI: 10.1021/acs.est.1c01724. [Online]. Available: https://doi.org/10.1021/acs.est.1c01724.

[89] T. A. Bashir, A. G. Soni, A. V. Mahulkar, and A. B. Pandit, "The cfd driven optimisation of a modified venturi for cavitational activity," *The Canadian Journal of Chemical Engineering*, vol. 89, no. 6, pp. 1366–1375, 2011.

[90] X. Margot, S Hoyas, A Gil, and S. Patouna, "Numerical modelling of cavitation: Validation and parametric studies," *Engineering Applications of Computational Fluid Mechanics*, vol. 6, no. 1, pp. 15–24, 2012.

[91] D. A. Wilson, K. Pun, P. B. Ganesan, and F. Hamad, "Geometrical optimization of a venturi-type microbubble generator using cfd simulation and experimental measurements," *Designs*, vol. 5, no. 1, pp. 1–18, 2021, ISSN: 24119660. DOI: 10.3390/designs5010004.

[92] Y. Gao, A. M. Dashliborun, J. Z. Zhou, and X. Zhang, "Formation and stability of cavitation microbubbles in process water from the oilsands industry," *Industrial and Engineering Chemistry Research*, vol. 60, no. 7, pp. 3198–3209, 2021, ISSN: 15205045. DOI: 10.1021/acs.iecr.0c04795.

[93] F. Moubarak, R. Atmani, M. Elkouali, M. Talbi, Y. Gondaf, and N. Amardo, "Adsorption of Methylene Blue in Solution on Activated Carbon Based of Banana Peels Residue.," *International Journal of Scientific and Engineering Research*, vol. 9, no. 10, pp. 617–622, 2018.

[94] S. Zor, "Sulfathiazole as potential corrosion inhibitor for copper in 0.1 M NaCl," *Protection of Metals and Physical Chemistry of Surfaces*, vol. 50, no. 4, pp. 530–537, 2014, ISSN: 2070206X. DOI: 10.1134/S2070205114040200.

[95] M. A. Khan *et al.*, "Norfloxacin loaded lipid polymer hybrid nanoparticles for oral administration: Fabrication, characterization, in silico modelling and toxicity evaluation," *Pharmaceutics*, vol. 13, no. 10, 2021, ISSN: 19994923. DOI: 10.3390/pharmaceutics13101632.

[96] L. Wu *et al.*, "Degradation of methylene blue via dielectric barrier discharge plasma treatment," *Water (Switzerland)*, vol. 11, no. 9, 2019, ISSN: 20734441. DOI: 10.3390/w11091818.

[97] K. S. Kim, S. K. Kam, and Y. S. Mok, "Elucidation of the degradation pathways of sulfonamide antibiotics in a dielectric barrier discharge plasma system," *Chemical Engineering Journal*, vol. 271, pp. 31–42, 2015, ISSN: 13858947. DOI: 10.1016/j.cej.2015.02.073. [Online]. Available: http://dx.doi.org/10.1016/j.cej.2015.02.073.

[98] Q. Huang, C. Fang, M. Muhammad, and G. Yao, "Assessment of norfloxacin degradation induced by plasma-produced ozone using surface-enhanced Raman spectroscopy," *Chemosphere*, vol. 238, p. 124 618, 2020, ISSN: 18791298. DOI: 10.1016/j.chemosphere.2019.124618. [Online]. Available: https://doi.org/10.1016/j.chemosphere.2019.124618.

[99] G. Wang, D. Zhao, F. Kou, Q. Ouyang, J. Chen, and Z. Fang, "Removal of norfloxacin by surface fenton system (mnfe2o4/h2o2): Kinetics, mechanism and degradation pathway," *Chemical Engineering Journal*, vol. 351, pp. 747–755, 2018, ISSN: 1385-8947. DOI: https://doi.org/10.1016/j.cej.2018.06.033. [Online]. Available: https://www.sciencedirect.com/science/article/pii/S1385894718310714.

[100] W. Ling, W. Ben, K. Xu, Y. Zhang, M. Yang, and Z. Qiang, "Ozonation of norfloxacin and levofloxacin in water: Specific reaction rate constants and defluorination reaction," *Chemosphere*, vol. 195, pp. 252–259, 2018, ISSN: 0045-6535. DOI: https://doi.org/10.1016/j.chemosphere.2017.12.079. [Online]. Available: https://www.sciencedirect.com/science/article/pii/S0045653517320490.

[101] B. Wang, B. Dong, M. Xu, C. Chi, and C. Wang, "Degradation of methylene blue using double-chamber dielectric barrier discharge reactor under different carrier gases," *Chemical Engineering Science*, vol. 168, pp. 90–100, 2017, ISSN: 00092509. DOI: 10.1016/j.ces.2017.04.027. [Online]. Available: http://dx.doi.org/10.1016/j.ces.2017.04.027.

[102] C. Wang, G. Qu, T. Wang, F. Deng, and D. Liang, "Removal of tetracycline antibiotics from wastewater by pulsed corona discharge plasma coupled with natural soil particles," *Chemical Engineering Journal*, vol. 346, no. December 2017, pp. 159–170, 2018, ISSN: 13858947. DOI: 10.1016/j.cej.2018.03.149. [Online]. Available: https://doi.org/10.1016/j.cej.2018.03.149.

[103] L. Wu *et al.*, "Degradation of methylene blue via dielectric barrier discharge plasma treatment," *Water*, vol. 11, no. 9, p. 1818, 2019.

[104] N. Shahsavari and X. Zhang, "Microbubble-enhanced cold plasma activation for water decontamination: Degradation dynamics and energy yield in relation to pollutant concentration, total volume and flow rate of water," *Journal of Water Process Engineering*, vol. 55, p. 104 169, 2023.

[105] G. H. Schnerr and J. Sauer, "Physical and numerical modeling of unsteady cavitation dynamics," in *Fourth international conference on multiphase flow*, ICMF New Orleans New Orleans, LO, USA, vol. 1, 2001.

[106] W. Li, H. Pu, Q. Liu, G. Chen, and S. Zhang, "Ansys-based dynamic analysis of high-speed motorized spindle," in *2009 International Conference on Computer Engineering and Technology*, IEEE, vol. 2, 2009, pp. 336–340.

[107] A.-h. LIU, Q. YANG, and J.-p. WU, "A practical ansys 3-d numerical simulation method for in-situ stress field," *Journal of Geomechanics*, vol. 19, no. 2, pp. 133–142, 2013.

[108] Ansys, "Ansys fluent theory guide," *Ansys Inc., USA*, vol. 15317, pp. 724–746, 2011.

[109] B. P. Leonard, "A stable and accurate convective modelling procedure based on quadratic upstream interpolation," *Computer methods in applied mechanics and engineering*, vol. 19, no. 1, pp. 59–98, 1979.

[110] M. Li, A. Bussonnière, M. Bronson, Z. Xu, and Q. Liu, "Study of Venturi tube geometry on the hydrodynamic cavitation for the generation of microbubbles," *Minerals Engineering*, vol. 132, no. September 2018, pp. 268–274, 2019, ISSN: 08926875. DOI: 10.1016/j.mineng.2018.11.001. [Online]. Available: https://doi.org/10.1016/j.mineng.2018.11.001.

[111] S Meropoulis, S Giannoulia, S Skandalis, G Rassias, and C. Aggelopoulos, "Key-study on plasma-induced degradation of cephalosporins in water: Process optimization, assessment of degradation mechanisms and residual toxicity," *Separation and Purification Technology*, vol. 298, p. 121 639, 2022.

[112] G. Wang, D. Zhao, F. Kou, Q. Ouyang, J. Chen, and Z. Fang, "Removal of norfloxacin by surface fenton system ($MnFe_2O_4/H_2O_2$): Kinetics, mechanism and degradation pathway," *Chemical Engineering Journal*, vol. 351, pp. 747–755, 2018.

[113] W. Ling, W. Ben, K. Xu, Y. Zhang, M. Yang, and Z. Qiang, "Ozonation of norfloxacin and levofloxacin in water: Specific reaction rate constants and defluorination reaction," *Chemosphere*, vol. 195, pp. 252–259, 2018.

[114] M. Li, A. Bussonnière, M. Bronson, Z. Xu, and Q. Liu, "Study of Venturi tube geometry on the hydrodynamic cavitation for the generation of microbubbles," *Minerals Engineering*, vol. 132, no. April 2018, pp. 268–274, 2019, ISSN: 08926875. DOI: 10.1016/j.mineng.2018.11.001. [Online]. Available: https://doi.org/10.1016/j.mineng.2018.11.001.

[115] B. Wang *et al.*, "Hydrodynamic cavitation and its application in water treatment combined with ozonation: A review," *Journal of Industrial and Engineering Chemistry*, vol. 114, pp. 33–51, 2022, ISSN: 1226-086X. DOI: https://doi.org/10.1016/j.jiec.2022.07.031. [Online]. Available: https://www.sciencedirect.com/science/article/pii/S1226086X22003938.

[116] S. M. A. Movahed, L. Calgaro, and A. Marcomini, "Trends and characteristics of employing cavitation technology for water and wastewater treatment with a focus on hydrodynamic and ultrasonic cavitation over the past two decades: A Scientometric analysis," *Science of The Total Environment*, p. 159 802, 2022, ISSN: 0048-9697. DOI: https://doi.org/10.1016/j.scitotenv.2022.159802. [Online]. Available: https://www.sciencedirect.com/science/article/pii/S0048969722069029.

[117] A. G. Chakinala, P. R. Gogate, A. E. Burgess, and D. H. Bremner, "Treatment of industrial wastewater effluents using hydrodynamic cavitation and the advanced fenton process," *Ultrasonics Sonochemistry*, vol. 15, no. 1, pp. 49–54, 2008, ISSN: 1350-4177. DOI: https://doi.org/10.1016/j.ultsonch.2007.01.003. [Online]. Available: https://www.sciencedirect.com/science/article/pii/S1350417707000089.

[118] L. R. Grabowski, E. M. Van Veldhuizen, A. J. Pemen, and W. R. Rutgers, "Breakdown of methylene blue and methyl orange by pulsed corona discharge," *Plasma Sources Science and Technology*, vol. 16, no. 2, pp. 226–232, 2007, ISSN: 09630252. DOI: 10.1088/0963-0252/16/2/003.

[119] B. Sun, N. N. Aye, Z. Gao, D. Lv, X. Zhu, and M. Sato, "Characteristics of gas-liquid pulsed discharge plasma reactor and dye decoloration e ffi ciency," *Journal of Environmental Sciences*, vol. 24, no. 5, pp. 840–845, 2012, ISSN: 1001-0742. DOI: 10.1016/S1001-0742(11)60837-1. [Online]. Available: http://dx.doi.org/10.1016/S1001-0742(11)60837-1.

[120] M. A. Malik, Ubaid-Ur-Rehman, A. Ghaffar, and K. Ahmed, "Synergistic effect of pulsed corona discharges and ozonation on decolourization of methylene blue in water," *Plasma Sources Science and Technology*, vol. 11, no. 3, pp. 236–240, 2002, ISSN: 09630252. DOI: 10.1088/0963-0252/11/3/302.

[121] G. Panomsuwan, T. Morishita, J. Kang, R. Rujiravanit, T. Ueno, and N. Saito, "Degradation of synthetic dye in water by solution plasma process," *Journal of the Korean Society of Marine Engineering*, vol. 40, pp. 888–893, Dec. 2016. DOI: 10.5916/jkosme.2016.40.10.888.

[122] M. Bal and B. C. Meikap, "Prediction of hydrodynamic characteristics of a venturi scrubber by using cfd simulation," *south african journal of chemical engineering*, vol. 24, no. 1, pp. 222–231, 2017.

[123] J. Jablonská, M. Mahdal, and M. Kozubková, "Spectral analysis of pressure, noise and vibration velocity measurement in cavitation," *Measurement Science Review*, vol. 17, no. 6, p. 250, 2017.

[124] H. Shi, M. Li, P. Nikrityuk, and Q. Liu, "Experimental and numerical study of cavitation flows in venturi tubes: From CFD to an empirical model," *Chemical Engineering Science*, vol. 207, pp. 672–687, 2019, ISSN: 00092509. DOI: 10.1016/j.ces.2019.07.004. [Online]. Available: https://doi.org/10.1016/j.ces.2019.07.004.

[125] S. B. Pope and S. B. Pope, *Turbulent flows*. Cambridge university press, 2000.

[126] P. R. Gogate and G. S. Bhosale, "Comparison of effectiveness of acoustic and hydrodynamic cavitation in combined treatment schemes for degradation of dye wastewaters," *Chemical Engineering and Processing: Process Intensification*, vol. 71, pp. 59–69, 2013.

[127] S. Tian, Y. Tu, D. Chen, X Chen, and Y Xiong, "Degradation of acid orange ii at neutral ph using fe2 (moo4) 3 as a heterogeneous fenton-like catalyst," *Chemical Engineering Journal*, vol. 169, no. 1-3, pp. 31–37, 2011.

[128] A. G. Chakinala, P. R. Gogate, A. E. Burgess, and D. H. Bremner, "Industrial wastewater treatment using hydrodynamic cavitation and heterogeneous advanced fenton processing," *Chemical Engineering Journal*, vol. 152, no. 2-3, pp. 498–502, 2009.

[129] T. Kurbus, A. M. Le Marechal, and D. B. Voncina, "Comparison of h2o2/uv, h2o2/o3 and h2o2/fe2+ processes for the decolorisation of vinylsulphone reactive dyes," *Dyes and Pigments*, vol. 58, no. 3, pp. 245–252, 2003.

Appendix A: Supplementary information

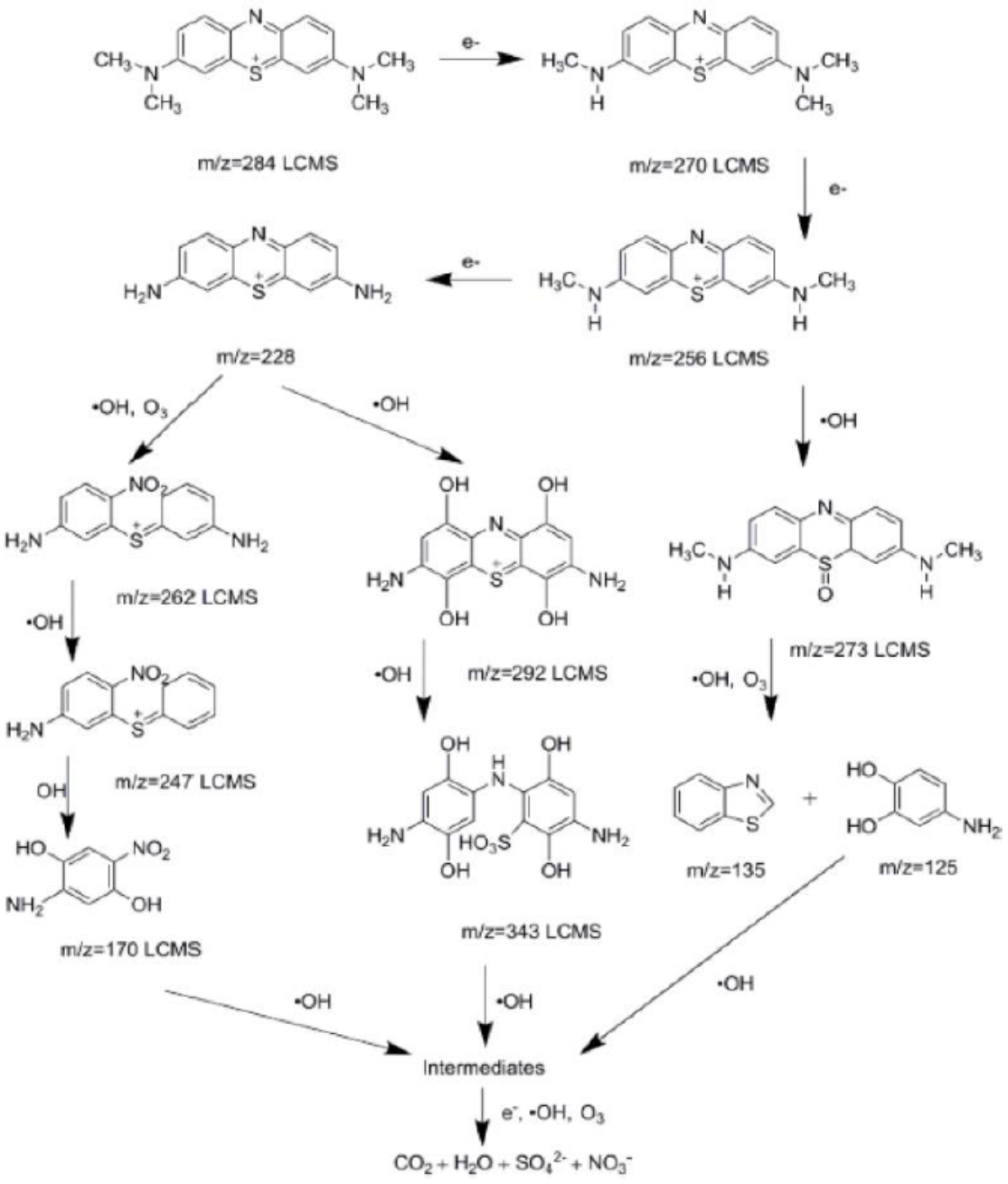

Figure A.1: Possible degradation pathway of MB. m/z represents the molecular weight of the intermediates identified by liquid Chromatography Mass Sepctrometry (LCMS)[96].

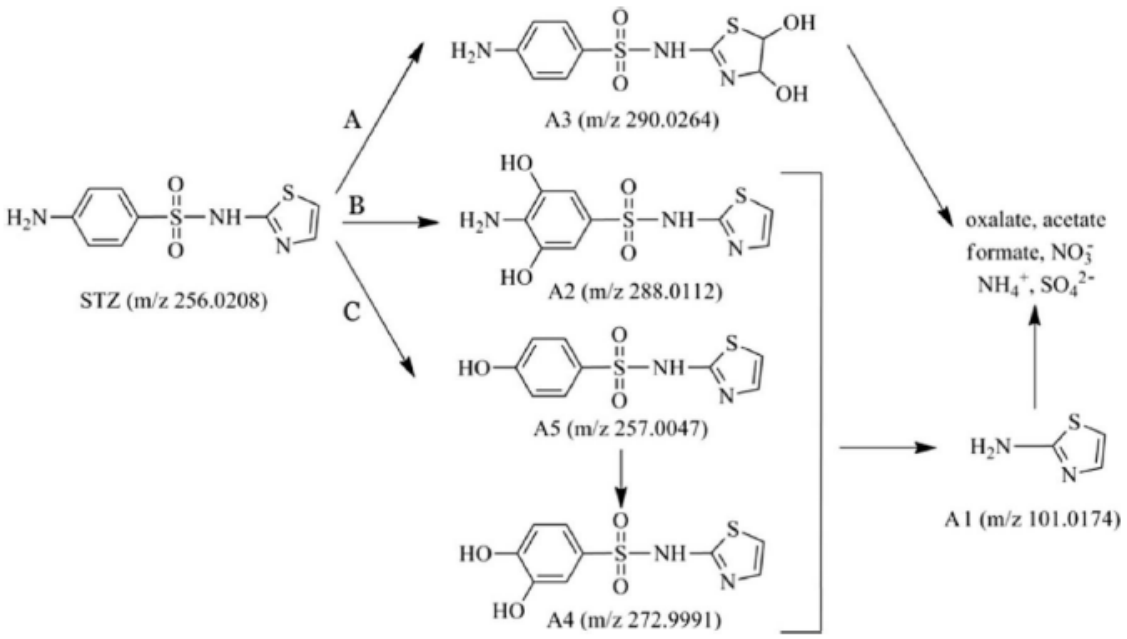

Figure A.2: Proposed degradation pathways for STZ [97]. A1 – A4 are intermediate molecular structures with molecular weights shown as m/z.

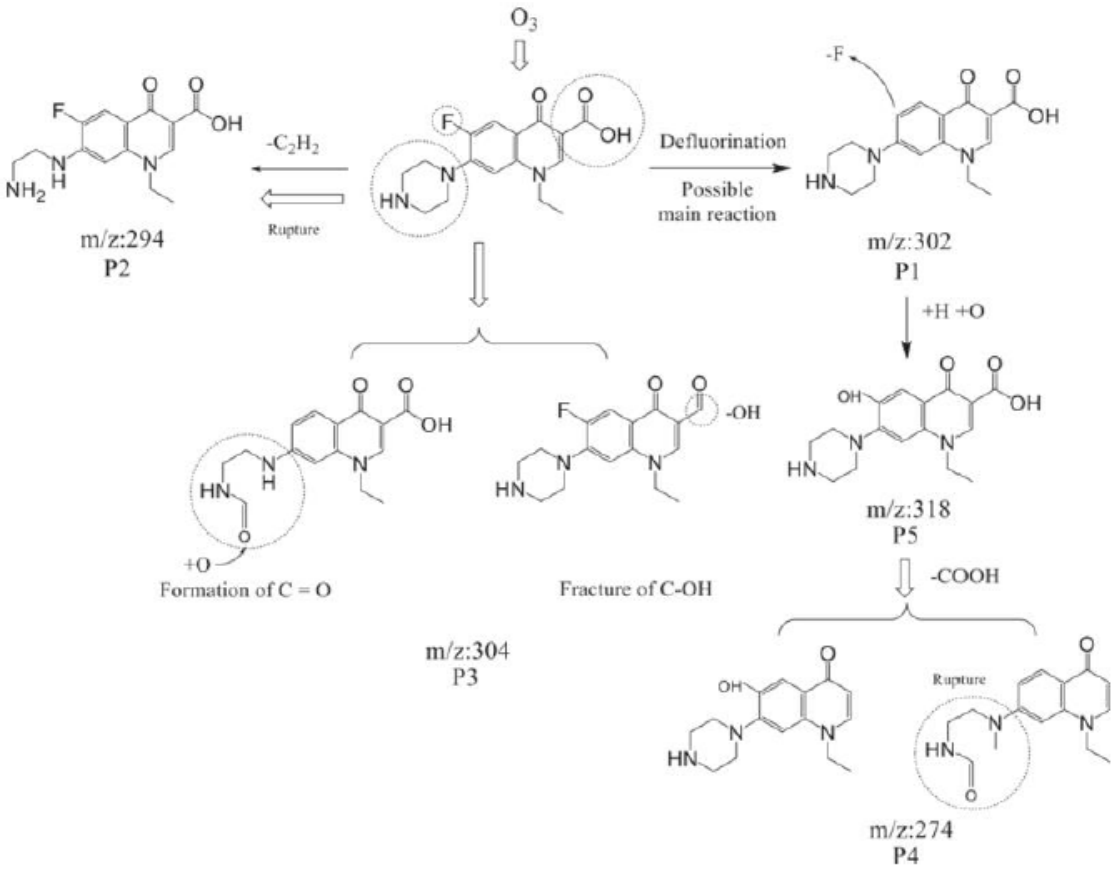

Figure A.3: Possible degradation pathways for NOR [113]. m/z represents the molecular weights of the intermediate structures which are denoted by P1 to P5.